Shock wave loading of a magnetic guide

The cover is explained in the summary (page 108).

Nanophotonics
Debye Institute for Nanomaterials Science
Departement Natuur- en Sterrenkunde
Faculteit Bètawetenschappen
Universiteit Utrecht

Printed by WHRMANN PRINT SERVICE, Zutphen
ISBN: 978-90-393-5663-0

Shock wave loading of a magnetic guide

Schokgolf laden van een magnetisch val

(met een samenvatting in het Nederlands)

Proefschrift

ter verkrijging van de graad van doctor aan de Universiteit Utrecht op gezag van de rector magnificus, prof.dr. G.J. van der Zwaan, ingevolge het besluit van het college voor promoties in het openbaar te verdedigen op vrijdag 21 oktober 2011 des middags te 4.15 uur

door

Louise Kindt

geboren op 6 juni 1979
te Silkeborg, Denemarken

Promotor: Prof. dr. P. van der Straten
Co-promotor: Dr. ir. J.M.Vogels

The work in this thesis was financially supported by NWO through the Innovational Research Incentives Scheme (VIDI grant).

In memory of
Peter Kindt

I wish to thank Professor Peter van der Straten and Dr. Ir. Johnny Vogels for excellent supervision and inspirational talk. I acknowledge all work done by the students. A big thank to friends and family for making me laugh every day.

Contents

CHAPTER 1

Introduction

The optical laser has revolutionized the field of optics. In 1960 both the continuous laser and the pulsed laser were created for the first time. At that time they where thought of as a physical curiosity, but today they are used in an enormous range of scientific and technological applications, due to their high intensity and their ability to emit light in an extremely narrow range of wavelengths. For everyday people they have become a part of everyday life.

The atom laser has long been a holy grail within atom physics and with the creation of an atom laser we hope to bring a similar revolution in to the field of atom optics. With the creation of the Bose-Einstein Condensate (BEC) in 1995 the path to an atom laser was initiated. In a Bose condensate all the atoms occupy the same quantum state and can be described by the same wavefunction. A continuous beam of Bose condensed atoms is an atom laser.
With an atom laser the De Broglie wavelength of atoms can be much smaller than the wavelength of light. Due to the ultimate control over the atoms the atom laser is very interesting for atom optics, lithography, metrology, etching and deposition of atoms on a surface.
All previous atom lasers have been created from atoms coupled out from an existing Bose-Einstein Condensate. The phase of the atom laser remains the same if the atoms laser is created from the same BEC. There are different approaches but common to them all is that the duration of the output of the atom laser is limited by the size of the initial BEC.
In 1997 the group of Ketterle, MIT, Boston [1] (see Fig. 1.1(a)) created the first pulsed atom laser by flipping part of the condensed atoms out of a magnetic trap. These atoms were no longer confined and propagated as a coherent matter wave accelerated by gravity. Every five ms, a new pulse was created leading to a train of pulses. Each small packet of atoms would spread out due to the

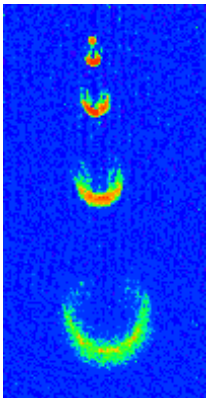

(a) Pulsed atom laser MIT. Each puls has a duration of 5 ms

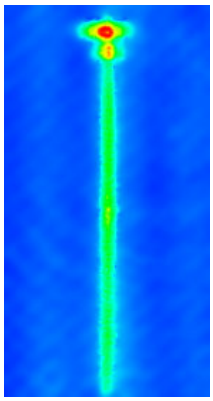

(b) Continuous atom laser Munich. Highly collimated with a duration of 100 ms

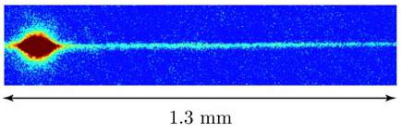

(c) Horizontal atom laser, Paris. The de Broglie wave length can be controlled and is here 1.3 mm.

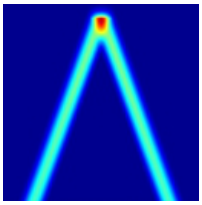

(d) Double atom laser ACQAO. Measured an accuracy of 10^{-9} g.

Figure 1.1: Atom laser gallery. Common for all is that the duration of the atom laser is absolutely depended on the initial size of the BEC

repulsive force between the atoms.

In 1999 the group of Esslinger (see Fig. 1.1(b))[2] produced the first continuous atom laser with an identical experimental setup as Ketterle . By combining a weak rf field with the magnetic trap the condensate output of atoms forms a collimated atomic beam of 100 ms.

In 2006 the group of Aspect, CNRS, Paris [3, 4] managed to out couple a BEC into a horizontal optical guide allowing for a controlled propagation of the atom laser and thus a controlled de Broglie wavelength. In Fig. 1.1(c) the de Broglie wavelength measures 1.3 mm.

In 2010 the group of Close, ACQAO, Brisbane outcoupled a dual atom laser from a double optical guide [5] (see Fig. 1.1(d)) producing an interferometric experiment. The two beams interfere creating an interferometric pattern that with a single shot accuracy of 10^{-9} g for a free fall time of 100 ms.

Common for all these experiments is that the duration of the experiment is limited by the initial number of atoms of the BEC. Thus all these atom lasers have a low flux. This leaves the quest to build a continuous high flux atom laser.

An alternative approach to a continuous BEC beam is to channel a continuous ultra cold atomic beam into a magnetic guide and then cool this beam down to degeneracy. Cooling down a continuous beam of atoms faces three large problems: The collision rate has to be large enough for effective rethermalization, evaporative cooling in 2D is not as effective as in 3D and a large thermal conductivity due to atoms with a high angular momentum causes heating downstream in the guide.

From 2000 to 2007 David Guéry-Odelin ran an experiment in Paris at CNRS. They build an experiment that should have produced the first continuous high flux atom laser. It was a rubidium cold atom experiment using already know experimental tools such as laser cooling, magneto-optical-trapping (MOT) and

molasses cooling. They transported in a pulsed scheme [6] large amounts of cold atoms into an uphill magnetic guide of 1.7 meter and then a horizontal magnetic guide of 2.6 meter. Each atomic packet contained 1.3×10^9 particles and was injected with a rate of 6 Hz overlapping after 50 cm into a continuous beam with a flux of $\Phi = 7.9 \times 10^9$ atoms/s, a mean velocity of 0.9 m/s at the top of the hill, and a temperature of 500 μK. At this velocity the beam is supersonic. The collision rate was not large enough to have an effective 2D cooling, producing a degenerate atomic beam. A conveyor belt was implemented and the atom beam was put into small packets and slowed down, but due to the short length of the magnetic guide efficient RF-cooling was still not possible [7].

In this project we plan to build a continuous atom laser based on the experimental setup from CNRS, but with a larger flux and much lower mean velocity, such that the collision rate will increase. We will use rubidium and transport atoms into a magnetic guide with the pulsed scheme [6]. The large difference between the CNRS and this experiment is the slope of the magnetic guide. The magnetic guide at CNRS had a uphill slope where our magnetic guide will have a downhill slope. We create an atomic beam in the guide with a high collision rate by slowing the beam down to subsonic velocities. Here we slow down and compress the thermal beam using a shock wave. Combined with gravitational compression and evaporative cooling the collision rate increase by more than one order of magnitude, leading to an increase of the number of collisions by two orders of magnitude. This results is an 3 meter long thermal cloud, which can be cooled to degeneracy. However, to have effective evaporative cooling and to overcome the thermal conductivity problem, part of the beam is loaded into a smaller 3D trap, where evaporative cooling is applied and Bose-Einstein condensation is reached.
The generation of the slow dense atomic beam and the possibility to reach degeneracy is the first step in the process towards the atom laser. In the future the 3D trap will be exchanged by a conveyor belt where continuous cooling is preformed and thus a continuous atom laser can be produced.

This thesis contains 6 chapters. Combined they describe the experimental setup of the atom laser and the realization of the 3 meter long thermal cloud where part of the atoms are cooled to BEC. The setup consist of a large atom number Magneto-Optical-Trap (MOT) and a 4 meter magnetic guide, designed to guide the atoms. We plan to have a dense continuous ultra-cold atomic beam in the guide, but this means that the atoms have to be loaded at a large rate in the MOT and transferred into the guide.
The second chapter describes how we create the large number MOT. State-of-the-art oven, Zeeman slower and lasers are described in detail.
The third chapter describes how we transfer these atoms into the magnetic guide. The transfer has to be adiabatic and fast, otherwise we can not create a continuous beam is created in the guide. The transfer rate of 6 Hz is enough to have a continuous beam in the magnetic guide.
The atomic beam is at supersonic velocities and we want to slow the beam down to subsonic velocities. With a large cloud of atoms we can extract part of cold atoms into another magnetic trap. An interesting physical phenomenon is created when the atom beam velocity is lowered from supersonic to subsonic velocity: A shock wave is created. The development and movement of the shock

wave is described in detail in chapter four. In chapter five we show the observations of the shock wave in the magnetic guide.
After the supersonic atomic beam has been converted into a subsonic atomic beam, the density is large and the collision rate is large enough for effective rethermalization. In chapter six we describe in detail how the change of trap configuration has a large impact on the effect of the number of collisions needed for effective evaporative cooling. We also describe, how part of the dense subsonic beam is extracted into a 40 cm hybrid trap and thereafter cooled to condensation. The number of condensed atoms is larger than any other known ^{87}Rb BEC.

CHAPTER 2

Experimental setup

The goal of the experimental setup is to generate a continuous cold atomic beam, with a density that matches normal Magneto-Optical-Trap (MOT) densities (10^{10} atoms) [8, 9]. This is the first important step towards the continuous atom laser. A MOT is a large collection of ultra cold atoms. The creations of the continuous beam is archived by creating multiple MOT's and lead them into the guide, where the will merge together and form the atomic beam. A 4 meter magnetic guide has been build, that will provide guidance for the atomic beam. This setup must deal with very stringent requirements.

- The beam should be isolated from the environment so that no atoms are lost to background residual gasses.
- The flux of atom beam should be as large as possible, so that many collision occur, while propagating through the setup. This will provide a high density.
- The beam velocity should be low, such that the length of the setup is manageable.
- The atoms should be launched into the guide at a high frequency rate, such that each MOT overlap in the guide creating a continuous beam.

The continuity of the atom laser beam depends on whether we are able to make a large atom number MOT in a short time. For this purpose we have constructed several components that are state-of-the-art, namely an oven with a large flux, a highly collimated Zeeman slower, a larger atom number MOT and a vertical launch into the 4 meter horizontal guide. The guide is held in ultra high vacuum below 2.5×10^{-11} mbar.
Each ultra-cold atom cloud will be transferred into a 4 meter magnetic guide

and in doing so each cloud will have an elongated shape that will spread out in the longitudinal direction due to its velocity distribution. These ultra cold thermal clouds will merge together while being further compressed and slowed down by various processes, generating a dense high flux atom beam. If we are not able to create and launch a MOT fast enough, the clouds will not overlap each other and a continuous atom beam can not be made.
In this chapter we will describe how we have created this large atom number MOT. The launching of the atoms and the creation of the continuous atomic beam is described in chapter 3.
First we describe the laser setup. The lasers are used to cool ^{87}Rb to micro Kelvin and to launch these atoms into the guide. Second, the vacuum chamber with the magnetic coils design is described. The magnetic coils must trap and lead the atoms into the guide. Third, we experimentally investigate the number of atoms in the MOT. Fourth, we make a Bose-Einstein Condensate from the MOT. This is thought of as an experimental verification of standards. Finally, we describe the experimental setup of the 4 meter magnetic guide.

2.1 Rubidium

Many ultra cold experiments uses ^{87}Rb [5, 10]. The cooling transition of ^{87}Rb atoms from the ground state S to the exited state P is at 780 nm. A stable laser source that produces this wavelength is a diode laser. They are simple to build, cheap and have a low maintenance.

^{87}Rb has two hyperfine ground states: $|F_g = 1\rangle$ and $|F_g = 2\rangle$ (see Fig. 2.1). Atoms can be in either ground states, but the closed cooling transition is from the $|F_g = 2\rangle \rightarrow |F_e = 3\rangle$ state. Since the linewidth of the laser locked on the cooling cycle transition is in the order of a few MHz and the energy gap between the two ground states is 6.8 GHz, the atoms can get lost from the cooling cycle. To be able to manipulate the atoms independent of their state we need two lasers. One laser producing the $|F_g = 2\rangle \rightarrow |F_e = 3\rangle$ cycling transition and one laser for the $|F_g = 1\rangle \rightarrow |F_e = 2\rangle$ transition. The first laser is called the cooling laser and the second laser is called the repump laser. Atoms pumped to the $|F_e = 2\rangle$ can decay back to the $|F_g = 2\rangle$ and from then on be cooled by the cooling laser. These two lasers are used for the control and cooling of the atoms in the MOT chamber. We build another two lasers for the Zeeman slower: one slowing laser and one repump laser. We build a fifth laser for observation. This laser is called the probe laser and we can change the frequency depending on the state of the atoms, that we want to observe: $|F_g = 1\rangle$ or $|F_g = 2\rangle$.

2.1.1 Optical table

Figure 2.2 shows the laser setup. The five lasers build are on a separate optical table to avoid ambient light disturbances and to increase the stability of the locking process. The AlGaAs diode laser are controlled by a MOGlab control box, which control the current, temperature and the angle of the grating through a piezo actuator. When the light exits each of the diodes it is ellipsoidal in shape and linear in polarization. The shape is cleaned up with isomorphic

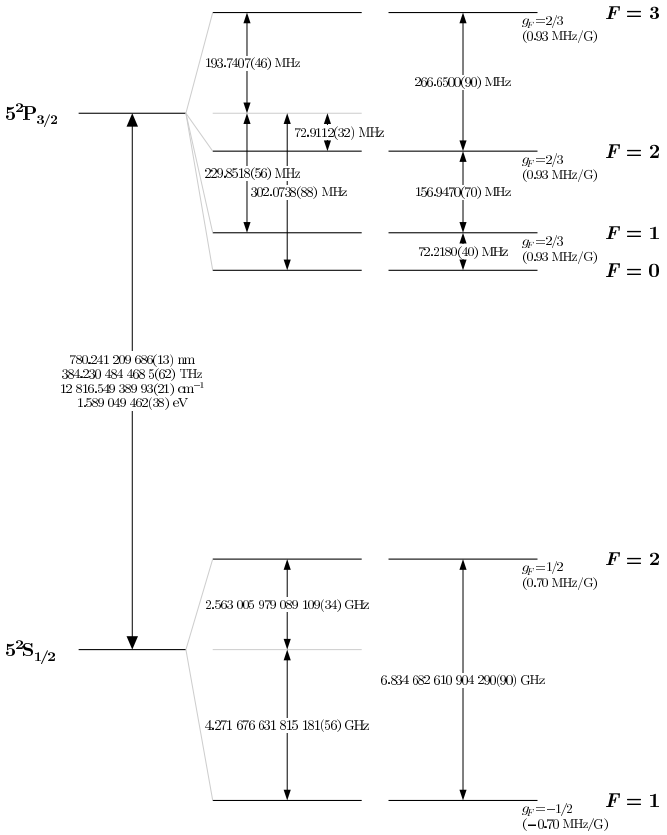

Figure 2.1: The atomic structure of ^{87}Rb [11]. The cooling transition is $|F_g = 2\rangle \rightarrow |F_e = 3\rangle$ state. The closeness of the two exited states $|F_e = 2\rangle, |F_e = 3\rangle$ can lead to a loss into the $|F_g = 1\rangle$. With a repump laser $|F_g = 1\rangle \rightarrow |F_e = 2\rangle$ the atoms are transferred back into $|F_g = 2\rangle$ ground state.

prisms. A optical isolator is installed to prevent reflected light returning onto the diode and thereby knocking the laser out of lock. Part of the beam (1 %) is split off with a beam splitter. This beam is used for saturation absorption spectrometry through a 10 cm long Rb glass cell and an AOM. A reduced absorption is observed when atoms with a velocity are resonant with the laser beam from both directions or the cross-over frequencies. The lasers are frequently modulated using the AOM at 100 kHz. This provides a locking signal with both the resonant frequencies and the cross-over frequencies. All lasers have been found to be stably locked through the whole day.
We use several AOMs to turn the lasers on and off and to shift the light to the appropriate frequencies. All lasers have a mechanical shutter to turn off stray light. The shutters are made out of old hard disc drives and have a shutter time of 7 ms. All light is transferred from the laser table through optical fibers. The optical path of each laser is now described (see Fig 2.2).
The repump laser (Fig. 2.2(a)) and the probe laser (Fig. 2.2(b)) are coupled directly into single-mode optical fibers. The Zeeman slowing and Zeeman repump laser (Fig.2.2(d)) beams are overlapped and amplified through a tapered

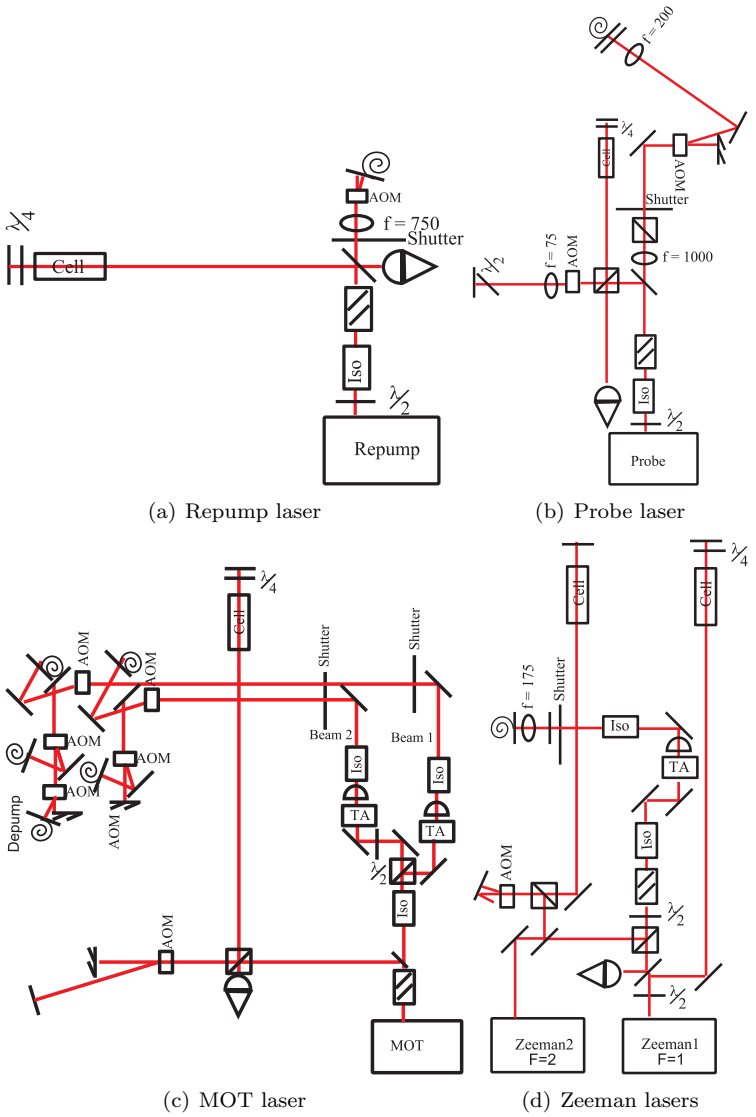

(a) Repump laser (b) Probe laser

(c) MOT laser (d) Zeeman lasers

Figure 2.2: The laser setup.
AOM: Acoustical optical modulator.
ISO: Optical isolator. Preventing back reflected light entering the laser again.
TA: Tapered amplifier. Amplifies the power of the laser.
$\lambda/2$ and $\lambda/4$: Quartz plates that controls the polarization of the light.
f: Focus length of lens.
Cell: ^{87}Rb cell.
Shutter: Mechanical shutter. Prevents stray light from entering the fibers.
Spiral: optical fibers. Guides the light from the laser table to the MOT table.

amplifier producing a laser power of 200 mW. The beam is then coupled into a single-mode optical fiber. The MOT cooling laser (Fig.2.2(c)) is split into two and then both beams are amplified through a tapered amplifier (beam 1 and beam 2). Beam 1 is the MOT cooling laser perpendicular to the guide axes (See Fig. 2.4 x-axes). Beam 1 is split on two AOM. The +1st order is coupled through an optical single-mode fiber. Beam 2 is the MOT cooling laser along the guide axes (See Fig. 2.3). Beam 2 is split on two AOM. These AOMs are shifted in frequency, when we launch the atoms. The +1st order is coupled through optical single-mode fiber. The 0th order beam is split again on a AOM. Here the -1st order is coupled out and this is the de-pump laser.

When the beams exits the optical fibers at the MOT chamber, the polarization is cleaned with a $\lambda/2$ plate and a beam cube. The two MOT beams from beam 2 is again split into two on the MOT table. All six beams are circular polarized and enlarged in diameter to the width of the window. All six beams cross each other in the center of the MOT chamber and have a laser power of 13 mW.

2.1.2 Imaging

For a majority of the experiments described in this thesis, absorption imaging has been employed. Absorption imaging relies on the resonant scattering of light from the atoms of the probe beam. The intensity decays exponentially through the atom cloud $I = I_0 \exp(-OD)$. The optical depth (OD) is the column density of the atoms along the probe direction $OD(r) = \int n(r,z)\sigma_0 dz$ for the light scattering cross section σ_0 and the density $n(r,z)$.
In the experiment three pictures are taken in order to determine the absorption of an atom cloud. The first picture (I_{atoms}) is taken of the shadow created by the atoms. The second picture determines the scattered light from the probe beam (I_{light}) and is evaluated by taking a picture with only the probe light on. This light will be the dominant light compared to any other light that might be present in the lab. A third picture determines the imperfections of the CCD chip (I_{dark}) and is evaluated by taking a picture without any light present. The optical depth is then given by

$$OD = -\ln\left(\frac{I_{atoms} - I_{dark}}{I_{light} - I_{dark}}\right). \tag{2.1}$$

Discussion

Five lasers are built. Two for the Zeeman slower, one for cooling the atoms, one for repumping the atoms into the cooling state and one for imaging.

2.2 MOT generation setup

The surrounding hardware provides the environment for the atoms to propagate in. Since the atoms have a magnetic dipole we can guide and trap the atoms with coils, that provide a minimum for the atoms to follow. Here the oven, Zeeman slower, the MOT chamber and the coils for leading and trapping are described. The whole setup is held under ultra high vacuum in order not to loose atoms to collisions with residual background atoms.

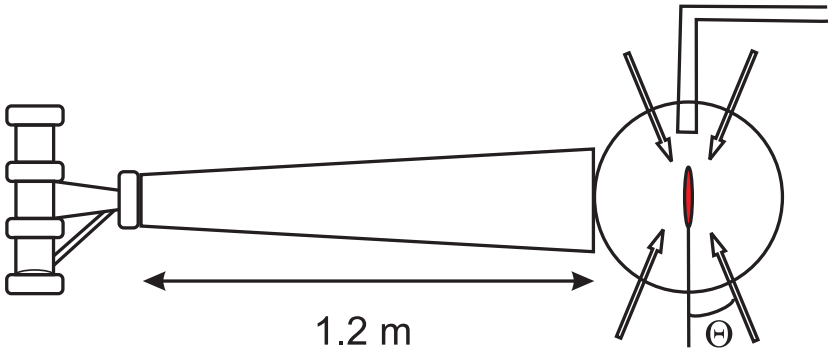

Figure 2.3: From the left is the ^{87}Rb oven, the Zeeman slower, the MOT chamber with the laser light directions at $\theta \pm 45°$ and the entrance to the 4 meter magnetic guide.

2.2.1 The vacuum table

Figure 2.3 shows the MOT generation setup. In the oven 25 gram of Rb is placed. The oven is a vertical vacuum tube of steal NW 40 CF and is heated with 4 heat rings to a temperature of at least 165°C. At the beginning of the beam line a 6 mm diaphragm is placed and 8 cm further a 1 cm diaphragm is placed, each heated to 70°C in order to prevent clogging. Running from the second opening to the bottom of the oven is a recirculating tube. This gives a practically infinite life-time for the oven ($>$ 4 years). The oven is pumped with two ion pumps, a Ti-sublimation pump and two cold plates kept at -15°C that provide a vapor pressure below 3×10^{-10} mbar. Through Doppler absorption spectroscopy the flux of the oven is measured to be $\mathcal{F}_{oven} = 1.25 \times 10^{14}$ atoms/s, a diameter of 2 cm, a velocity of 400 m/s and a 3D density of $n_{3D} = 9.9 \times 10^{14}$ atoms/m^3. The atom beam from the oven is highly collimated and continues through the Zeeman slower.

The atoms have a magnetic dipole that couples to the magnetic field if present. This is the Zeeman effect and is used to reduce the atoms velocity. This is done in the Zeeman slower. The Zeeman slower has an increasing amount of windings going towards the MOT chamber. At the end of the Zeeman slower there is a compensation coil that cancels the longitudinal magnetic field from the Zeeman slower in the MOT chamber. Along the axial direction the Zeeman light is hitting the atomic beam from the oven. The Zeeman light consist of both slowing and repump light. When the atoms travel through the increasing magnetic field they shift into resonance due to the Zeeman effect. At the end of the Zeeman slower the flux of the slowed atoms is measured to be $\mathcal{F} = 5.3 \times 10^{11}$ atoms/s. The diameter is 3.6 cm and has a velocity of 27 m/s, which the MOT can effectively capture. Some atoms are lost due to transverse spreading in the slowing down process and the 3D density has decreased to $n_{3D} = 1.88 \times 10^{13}$atoms /m^3.

The MOT chamber is a spherical steel vacuum chamber with 14 ports. The vacuum is maintained by an 50 liter/s ion pump and two titanium sublimation pumps. Two dual-stage cold plates held at -47°C, providing a vapor pressure

below 2×10^{-11} mbar. Combining the pumps with the cold plates a vacuum pressure of 10^{-11} mbar can be obtained.

2.2.2 Lasers at the vacuum table

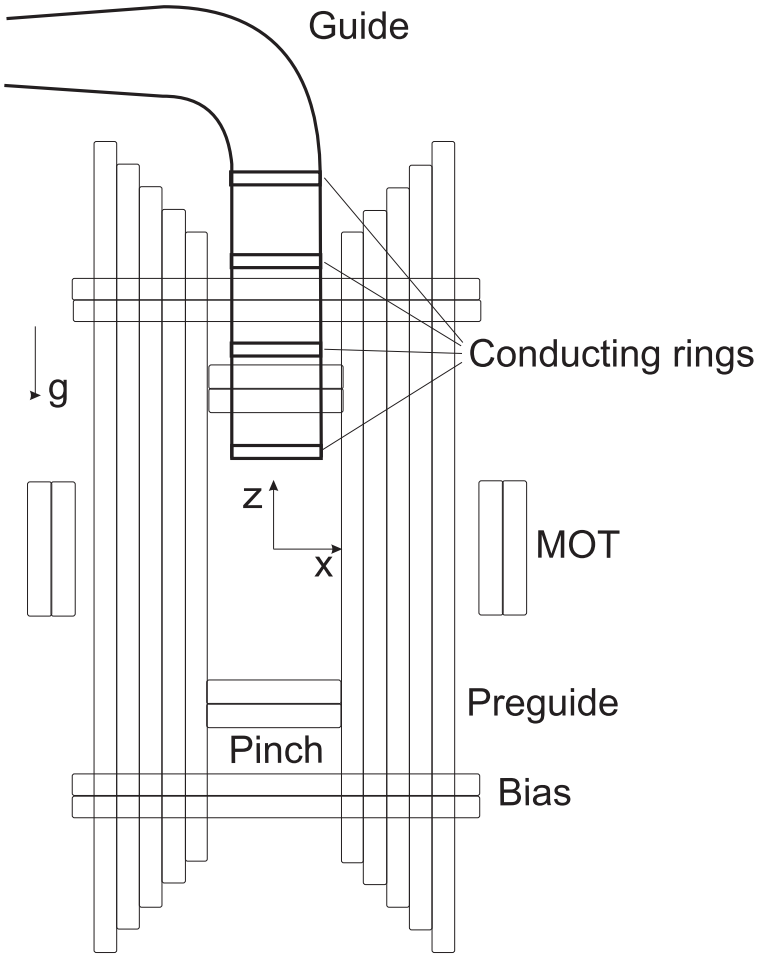

Figure 2.4: Schematic of the magnetic fields. The preguide and the guide is a quadrupole trap both placed vertically. The entrance of the guide starts 4 cm away from the MOT region. The four guide tubes are held together at the beginning of the guide by 4 conducting rings separated at 3 cm distance. The guide bends 90 degrees and the distance between guide wires decreases to 7.8 mm over a length of 20 cm leaving a spacing of 2 mm. For each ring the gradient increases step-wise with a factor of 1.5 whereas with the spacing of the wires the increase is continues with the total increase of a factor 4.2.

The Zeeman effect splits all states according to there magnetic dipole moment. For ^{87}Rb the $|F_g, m_f\rangle = |1, -1\rangle$ is a low field seeker and can be trapped in a pure magnetic trap.

The MOT setup is designed with the six cooling lasers held on the transition $|F_g = 2\rangle \rightarrow |F_e = 3\rangle$: two horizontal σ_+ beam and four $\theta\pm45°$ vertical σ_- beams (see Fig. 2.3). All six beams have a diameter corresponding to the entrance window of 3.6 cm and cross each other in the center of the MOT chamber.

On one of the horizontal σ_+ beam a repump laser $|F_g = 1\rangle \rightarrow |F_e = 2\rangle$ overlaps. The repump laser ensures that all $|F_g = 1\rangle$ atoms are pumped into the desired $|F_g = 2\rangle$ where cooling is possible. In the direction opposite to the repumper a depumper is installed. This is used to pump the atoms into state $|F_g, m_f\rangle = |1, -1\rangle$ after molasses cooling, after which the atoms can be trapped in the magnetic trap.

2.2.3 Magnetic coils

Each set of the magnetic are described here (see Fig 2.4). The MOT coils, the pinch coils and the bias coils are in a set of two coils. The preguide are a set of four coils and the Earth coils are a set of six coils (not shown in Fig 2.4). The MOT operates alone and are design to trap the Zeeman slowed atoms. The preguide operates with the bias coils and are designed to lead the trapped atoms from the MOT into the guide. This configuration provides a harmonic 2D potential for the atoms the follow. The pinch coils operates with the bias coils and the preguide to create a 3D harmonic potential for the atoms to be trapped and cooled to degeneracy (see Sec. 2.4).
The entrance of the guide is placed 4 cm away from the MOT center and in between the two top $\theta\pm45°$ vertical σ_- beams.
The magnetic trap, in the MOT is made by a set of two anti-Helmholtz coils of 4×5 windings located around the horizontal beam axes (x-axes) and at equidistance of 7 cm away from the MOT center.
In the frame of the setup at an equidistance of 50 cm 6 Earth-coils are placed, two for each direction. These compensate for the Earth magnetic field, gravity and any other permanent stray magnetic field that might be in the laboratory. Since they compensate for permanent magnetic fields the coils are placed in Helmholtz configuration.
In the horizontal direction a 4 meter guide is placed with a 90° bend of the entrance of the guide. The entrance of the guide is situated 4 cm away from the MOT center. The entrance of the guide is designed such that the magnetic field gradient increases with distance. After 10 cm the guide bends 90°. This will be explained in detail in chapter 3.
In the longitudinal direction four preguide coils are placed. They are able to produce a magnetic field gradient of up to 320 Gauss/cm at 410 A. They have 20 windings in an elongated shape and are wound with a decreasing magnetic field at the end. They are 30 cm long and overlap the guide until the bend. The two counter imposing decreasing and increasing magnetic fields from the preguide and the guide, counteract each other and provide an adiabatic transfer of the atoms from the MOT to the preguide to the guide.
Around the preguide a small set of Hemholtz coils are placed to create a bias field. In the direction of the preguide a set of Hemholtz pinch coils are situated at a distance of 10 cm away from the MOT center. They do not generate a homogenous field because their diameter is smaller than their mutual distance.

They have 2×5 windings and are in combination with the preguide coils and the bias coils used as a standard Ioff-Pritchard trap. In this trap a standard BEC is created.

Magnetic trapping

The principle of magnetic trapping is based on the interaction between the magnetic dipole moment of the atom μ and the magnetic field B. The hyperfine state $|F, m_F >= |1, -1 >$ is a low field seeker for ^{87}Rb and can be trapped in a pure magnetic trap. The atoms will be trapped in the minimum of the potential $dU/dy = 0$. The potential for an Ioff-Pritchard trap in the gravitational field reads

$$U = mgy + \frac{\mu_B}{2}\sqrt{\left(B_z + \frac{1}{2}z^2 B_z''\right)^2 + \left(B_\rho'\rho\right)^2} \tag{2.2}$$

with $\rho = \sqrt{x^2 + y^2}$ is the radial direction and z is the axial direction and m is the mass of the ^{87}Rb atom.
With the earth coils the contribution from any permanent magnetic fields can be neglected and the axial and radial trap frequencies are found to be

$$\omega_z^2 = \frac{\mu_B}{2m}B_z'' \tag{2.3}$$

$$\omega_\rho^2 = \frac{\mu_B B_\rho'^2}{2mB_0}. \tag{2.4}$$

Here B' is the magnetic field gradient and B'' is the magnetic field curvature. B_0 is a combination of the field from the bias coils and the pinch coils. The trap frequencies determine the width of the atom cloud.

Discussion

We have created a large flux source of slowed atoms with a state-of-the-art hardware: an oven, a Zeeman slower and magnetic coils all held in ultra high vacuum. The coils are placed such that they can be used as a trapping potential. With the lasers we are able to create a MOT of 3.5×10^{10} ultra cold atoms.

2.3 Load and losses of atoms from the MOT

The properties of the MOT is described in this section. The properties are the loss rate, the lifetime and number of atoms. The loss rate and the life time of the MOT is important for a stable MOT. In this experiment we are interested in a large atom number MOT. The density of the MOT is not important since the atoms are loaded into the magnetic guide and manipulated to large densities.

Atoms entering the capture zone of the MOT with a low enough velocity will be loaded into the MOT. After a certain period of time, an equilibrium between the load of atoms and loss of atoms due to collisions is reached. The evolution

of the number of atoms N in the MOT is described by the differential equation

$$\frac{dN(t)}{dt} = L - AN(t) - BN(t)^2, \tag{2.5}$$

where L is the load rate and A is the linear loss rate, stated as $A = A_{thermal} + A_{back}$. $A_{thermal}$ is the loss rate from collisions with the thermal atomic beam with the flux $\mathcal{F}$ and A_{back} is the loss rate from the background collision. B is the loss rate due to cold collision where atoms within the MOT colliding with each other.
The physical steady state solution of Eq. (2.5) is

$$N_0 = \frac{-A + \sqrt{A^2 + 4BL}}{2B} \tag{2.6}$$

Previous work [12] has shown that the cold collisions are negligible within a MOT of $N_0 = 10^5$ atoms. However, in this work we have 10^{10} atoms.

2.3.1 MOT decay

To determine the influence of cold collisions we detect the MOT decay. The load L from the oven is turned off and Eq. (2.5) under these conditions becomes

$$\frac{dN(t)}{dt} = -A'N(t) - BN(t)^2 \tag{2.7}$$

The solution to this differential equation is

$$N(t) = \frac{N_0}{\left(1 + \frac{BN_0}{A'}\right)\exp(A't) - \frac{BN_0}{A'}} \tag{2.8}$$

Here $A' = A_{back}$, the loss rate from the oven load. $A_{thermal}$ is no longer present. Figure 2.5 shows the decay of a MOT where the atom source have been turned off. The red curve is the fit of Eq. (2.8). Plotting the data on a logarithmic scale clearly shows the quadratic term. The linear loss from the background atoms is found to be $A' = 0.05\ \mathrm{s}^{-1}$. Initially the decay is fast, this is due to two-body collisions $B = 3 \times 10^{-11}\ \mathrm{s}^{-1}$. The lifetime for low density is $\tau = 20$ s.

2.3.2 MOT load

During the loading of the MOT the number of atoms is given by

$$N(t) = N_0\left(1 - \frac{1}{\left(1 + \frac{BN_0}{A}\right)\exp(At) - \frac{BN_0}{A}}\right) \tag{2.9}$$

Figure 2.6 shows the load of a MOT and the fit of Eq. (2.9). At $t = 0$ the magnetic field and all the laser light (the Zeeman light, the repump laser and the MOT cooling laser) are turned on.
The number of atoms rises to a saturation level of 3.5×10^{10} atoms after a load time of 300 ms. The cold collisions are in the same order as the decay. The linear loss rate is fitted to be A of $8.1\ \mathrm{s}^{-1}$. This gives a load rate L of 3.7×10^9

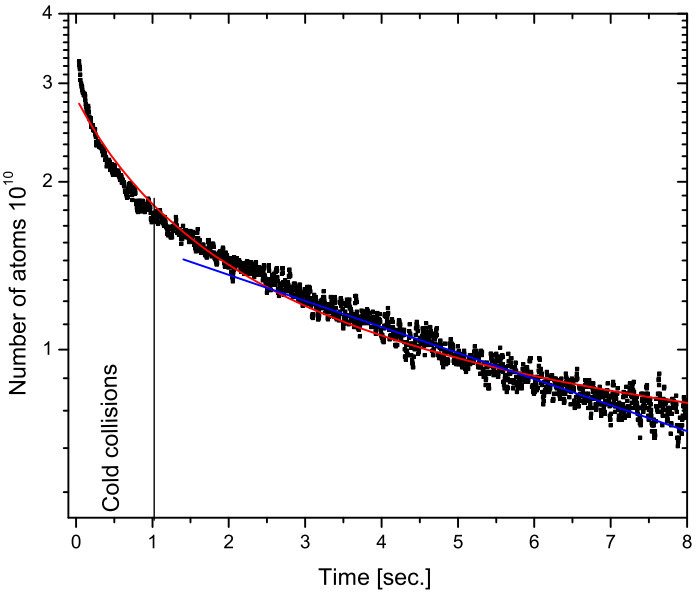

Figure 2.5: MOT decay. Initially the decay is dominated by cold collisions after 1 sec. the linear loss is dominating. The lifetime is 20 sec. A straight line is plotted through the linear decay indicating where it is dominant.

atoms/s. The atomic level reaches 50 % after 80 ms and this is set to be the load time of the MOT with the Zeeman slower load.
The lifetime of the low density MOT is 20 s, but in the experiment we only use 45 ms to lead the atoms into the guide. This is a short time span where losses from the background gas collisions and the cold collisions are negligible.
There are 2 orders of magnitude between the two linear loss rates (A and A'). This indicates that the contribution from the load atomic thermal beam is the dominating factor in the load procedure. Therefore in the MOT load sequence the load from the Zeeman slower is turned off after 80 ms but the load of the MOT continues for another 35 ms to increase the load and minimize the loss.

Discussion

A MOT with 3.5×10^{10} atoms are loaded in 300 ms. However, for the continuity of the next stage of the experiment we load the MOT for 80 ms.

2.4 Bose-Einstein condensation

The stationary large atom number MOT was used for cooling to degeneracy. The BEC created was never used for any experiments but was merely thought of as an experimental verification of standards. It must be noted that initially

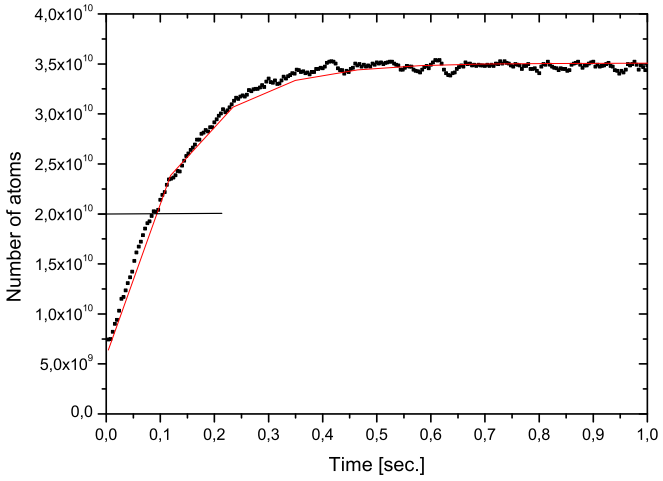

Figure 2.6: MOT load. The MOT has a load rate of $L = 3.7 \times 10^9$ atoms/s and is fully saturated after 300 ms. After 80 ms the MOT is halfway full and in the launch sequence the MOT load with atoms from the Zeeman slower is stopped.

the MOT chamber was rotated 90°, so that the preguide coils where horizontal. We compensate the sag from gravity with the bias coils.

2.4.1 Observing a BEC

When atoms start to condense into BEC from a thermal cloud the density distribution of the cloud changes from a Gaussian distribution into a bi-modular distribution

$$n_{bi}(\rho, z) \quad = \quad (1-\beta)n_{th}(\rho, z) + \beta n_{TF}(\rho, z) \tag{2.10}$$

where β is the fraction of Bose condensed atoms n_{th} is the thermal distribution and n_{TF} is the Thomas-Fermi distribution. In Ref. [13] it is shown that a BEC in a harmonic trap will have a sharp density distribution in the central region of the trap. The Gaussian distribution and the bimodal distribution are two distinctly different profiles and from the obtained density distribution of the cloud we can directly confirm Bose-condensation. We look for a large increase in density and a bimodal space distribution.
The coils used for the magnetic trap are the preguide, the pinch coils and the bias coils (see Fig. 2.4). Due to the geometry of our magnetic coils the atoms cloud will be an ellipsoid, with a symmetrical radial direction $\rho = \sqrt{x^2 + y^2}$ and an axial direction z.
By simply observing the change of spatial distribution we are able to identify a BEC. A thermal cloud has a Gaussian spatial distribution and for the projection

in the x-z-plane is written as [14]

$$n_{th}(\rho, z) = A_{th} \exp\left(\left(\frac{x - x0}{\rho_{th}}\right)^2 + \left(\frac{z - z0}{z_{th}}\right)^2\right) \tag{2.11}$$

where A_{th} is given by the optical density observed and ρ_{th} and z_{th} is the width of the thermal cloud in the radial and axial direction. A BEC has a distinct bi-modular distribution

$$n_{TF}(\rho, z) = A_{TF}\left(1 - \frac{x^2}{\rho_{BEC}^2} - \frac{z^2}{z_{BEC}^2}\right)^{3/2} \tag{2.12}$$

here A_{TF} is the optical density for the BEC. The width of the cloud is found through Time-Of-Flight. By releasing the cloud from the magnetic trap the cloud will expand ballistically accordingly to

$$r = r_0\sqrt{1 + \omega^2\tau^2} \tag{2.13}$$

where τ is the expansion time, ω is the trap frequency and r is the chosen observable radius of either ρ or z.
From the width and the absorbtion of each distinct profile we can determine the number of atoms and the temperature. The number of atoms is given by

$$N_{BEC} = \frac{2\pi}{5}\left(\frac{A_{BEC}}{\sigma_0}\right)\rho_{BEC}z_{BEC} \tag{2.14}$$

$$N_{th} = 2\pi\left(\frac{A_{th}}{\sigma_0}\right)\rho_{th}z_{th} \tag{2.15}$$

where $\sigma_0 = \frac{3\lambda^2}{2\pi}C_{ge}$ with C_{ge} being the coupling strength.
The temperature in the radial direction is given by $k_BT_\rho = m\omega_\rho^2\rho^2$ and likewise for the axial direction. Measuring the width of the cloud is a direct measure of the temperature, as long as we know the trap frequency and the time of flight time.

To properly evaluate a BEC, we need to first measure the trap frequencies and then estimate the absorption coefficient via absorption imaging and the radius of the cloud.

2.4.2 Measuring trap frequency

The setup has several windows where direct observation of the thermal cloud is possible. Therefore the oscillation of the cloud can be measured directly. The atoms are trapped in the magnetic trap and an additional magnetic field is used to temporally shift the minimum of the trap to a higher point of the original potential. Turning off the extra magnetic field accelerate the thermal towards the original trap minimum and thereby creating an oscillation of the thermal cloud around the trap minimum. This oscillation can be measured directly for both the axial direction and the radial direction. The contribution from gravity is cancelled by the earth coils and for small energy shifts the oscillation follows a harmonic potential. The radial trap frequency is found $\omega_\rho/2\pi = 29$ Hz and

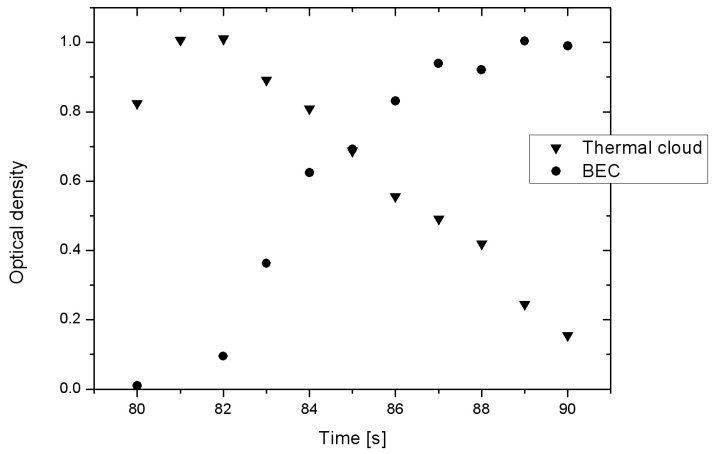

Figure 2.7: Optical density of thermal atoms and Bose condensed atoms as a function of evaporation time.

the axial trap frequency $\omega_z/2\pi = 16$ Hz.

The radial trap frequencies are relevant for the guiding of atoms into the guide, whereas the axial trap frequencies are only relevant for the stationary BEC. The pinch coils not used in the launching procedure and only used for the creation of this BEC in the MOT chamber.

2.4.3 BEC in the MOT chamber

A normal MOT of 10^{10} atoms/cm is loaded (1 mK) and molasses cooled to 60 μK. The atoms are transferred into the purely magnetic state $|F, m_f\rangle \rightarrow |1, -1\rangle$ via the depumper. Three cm from the center of the MOT inside the vacuum is a single wounded RF antenna. The evaporation curve follows Eq. (6.6) for $\alpha^T = 3$ (to be explained in detail in Sec. 6.3) and cools from 100 MHz to 200 kHz above the trap minimum at $t_0 = 120$ s. Figure 2.7 shows the optical density of thermal atoms and Bose condensed atoms as a function of evaporation time. The number of Bose condensed atoms is found with Eq. (2.14) from absorption imaging and with the given trap frequencies. The BEC created consists of 6×10^6 condensed atoms at a temperature of 150 nK.

Discussion

The BEC presented is a large Rubidium BEC compared to other BEC Ref.[15, 5]. The BEC created was never used for any experiments but was merely thought of as a experimental verification of standards, which have been met.

It would be interesting to launch the BEC into the guide and observe how a BEC would evolve in a magnetic guide, where the BEC is left to expand freely in the axial direction. This would be a difficult task since the launching procedure would excite the BEC.

2.5 The guide

The transfer of atoms into the guide is described in the next chapter. Here the magnetic guide is described (see Fig.2.8). The guide is 4 meters long and consists of four 6 mm hollow copper tubes with a spacing of 2 mm. The copper tubes are water cooled with a pressure of 10 bar. The copper tubes are level out on the 10 μm scale. The tubes are held together with non conducting ceramic claps separated at 20 cm. The end of the guide is feed through swagelock mounted on a ceramic plate. Both current and water are connected outside of the vacuum. The operational current is 2×550A. Spanned underneath the guide is a NEG-Strip. The strips contains a getter that helps maintaining a vacuum below 10^{-11} mbar. The lifetime of the atomic beam in the guide is measured to be $\tau = 400$ s. The entrance of the guide is vertical and 20 cm long. At the entrance the tubes diverges into a separation of 2 cm and is held together with 3 conducting rings. Each ring has a resistance such that 1/3 of the current is lead through the ring, creating a diverging magnetic gradient. The end conducting piece is hollow to let water circulate and has a centered opening of 3 mm. This is where the atoms are launched through from the MOT region. In the entrance a glass tube 12 cm long and 3 mm in diameter is placed to have differential pumping between the MOT chamber and the guide. In this way the pressure in the MOT chamber can be significantly larger than the pressure in the guide. This is preferable, since the loading of the MOT by the Zeeman slowed beam increases the pressure in the MOT chamber considerably. The increasing magnetic gradient from the guide entrance in combination with the preguide configuration leads to an adiabatic transfer of the atoms into the guide. The end of the guide is placed on a mount that can be manually lowered from horizontal down to a maximum of 7 cm.

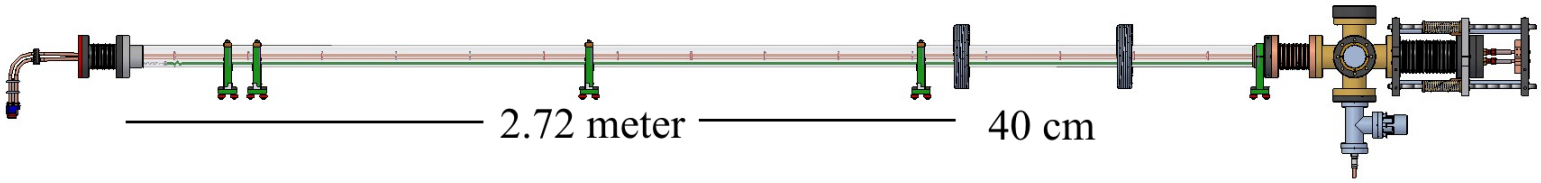

(a) The 4 meter magnetic guide. The first coil is placed 2.72 meter down from the bend in the guide. This coil acts as a barrier, that the atoms can not pass. A second coil is placed 40 cm after the first coil and combined they act as a 3D trap with the guide.

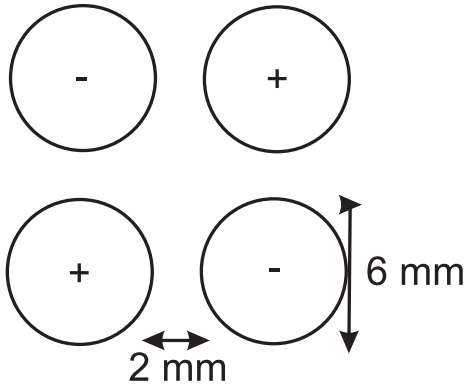

(b) Cross section of the four conducting tube of the guide. The spacing between each tube is 2 mm and held there by ceramic plates. The diameter of each tube is 6 mm. All tubes carries water and current. The current in such a configuration that there is a minimum field in between the tubes.

Figure 2.8: Schematics of the 4 meter magnetic guide and cross section of the copper tubes.

2.6 Resume

In this chapter we have described how a larger atom number MOT is created in the experiment. We have described how the state-of-the-art oven with a flux of $\mathcal{F}_{oven} = 1.25 \times 10^{14}$ atoms/s and the Zeeman slower with a flux of $\mathcal{F} = 5.3 \times 10^{11}$ atoms/s work. The lasers for cooling and slowing down the atoms are described and so are the magnetic coils and ultra high vacuum. All combined ensures perfect conditions for the 3.5×10^{10} atoms collected in the MOT. We used this large MOT to cool to BEC. This provides us with a large ^{87}Rb BEC of 6×10^6 condensed atoms.

CHAPTER 3

Launch

From the MOT we transfer the atoms into the guide and further cool the atoms to degeneracy. For the cooling, we must create a continuous atom beam with a larger flux, a lower mean velocity and a large enough collision rate to cool to degeneracy.
Atoms in the MOT are transferred away from MOT region to the magnetic guide. Another MOT is created and then moved quickly into the magnetic guide, thus creating a continuous atom beam. This launching process is described in this chapter. The launch velocity is so large that it is at supersonic velocities.

To lead the atoms from the MOT into the guide there is a preguide. In this chapter, first the setup of the preguide and the guide is described. The preguide is initially a harmonic trap and the guide is a linear trap. Secondly, the transfer of atoms between these two trap shapes are investigated. We are interested in minimizing the loss of phase-space density and the increase of temperature. Thirdly, the vertical launching of an atom packet is simulated and fourth investigated experimentally. Finally, the simulation of the continuous beam is explained.

3.1 Experimental setup.

The entrance of the guide is situated 4 cm away from the MOT region and to transfer the atoms from the MOT into the guide we have a preguide. The preguide overlap geometrically the MOT coils and the entrance of the guide (see Fig. 2.4).

3.1.1 Preguide

The preguide is a magnetic quadrupole field which is created by four rectangular, elongated coils located in the planes $x = \pm$ 5 cm and $y = \pm$ 5 cm, where the symmetry axis is at $x = 0$ and $y = 0$. The current in the coils facing each other have opposite sign, with the resulting field given by

$$B = (-B'x, B'y, 0) \tag{3.1}$$

where B' is the magnetic field gradient. The field is zero along the z-axis and the transverse gradient can be varied. By adding a longitudinal bias field B_0 the magnetic field is nonzero everywhere in space.

3.1.2 Guide

The magnetic field gradient from the guide and the preguide overlap. The entrance of the guide starts 4 cm away from the MOT region. The four copper tubes of the guide are parallel and their centers are spaced 16 mm. The four tubes are held together at the beginning of the guide by 4 conducting rings separated at 3 cm distance. The total distance the atoms have to travel vertically is 20 cm. After that the guide bends 90 degrees and the distance between guide tubes decreases to 7.8 mm over a length of 20 cm leaving a spacing of 2 mm. Both the conducting rings and the increase in distance between the guide tubes creates an increase of the magnetic filed gradient. For each ring the gradient increases step-wise with a factor of 1.5, whereas with the spacing of the tubes the increase is continuous with the total increase of a factor 4.2. The preguide fully overlap the first three conducting rings adding an extra magnetic gradient. In Fig. 3.1 the magnetic field gradient in the radial direction is shown at the beginning of the guide. The stepwise increase is caused by the conducting rings holding the 4 copper tubes together and the shape of the preguide being decreasing just before the bend in the guide ensures a smooth transfer from the preguide to the guide and a close to adiabatic transfer between the magnetic traps. Two power supplies generate the current through the guide. A magnetic field minimum is generated in the center of the guide, where the atoms will travel in the same manner as the preguide with an extra bias field B_0. In fact, the 4 meter long guide is a very long Ioffe-Pritchard trap. The magnetic field gradient can be as strong as 20 T/m, when the guide is running at maximum current.
The black curve is where the preguide is ramped up to 1.78 T/m and the magnetic gradient of the guide is held at 13.5 T/m. High transfer efficiency was found to be here. The preguide can be run at a maximum gradient of 3.56 T/m for a current of 200 A and the guide can run at max gradient of 20 T/m for a current of 800 A. A more stable system or a larger increase in atom numbers was not found using higher operational values.

3.1.3 Minimum and maximum launch velocity

The atom cloud has to travel 20 cm vertically upward where the guide bends into horizontal. To overcome the gravitational potential a minimum launch velocity

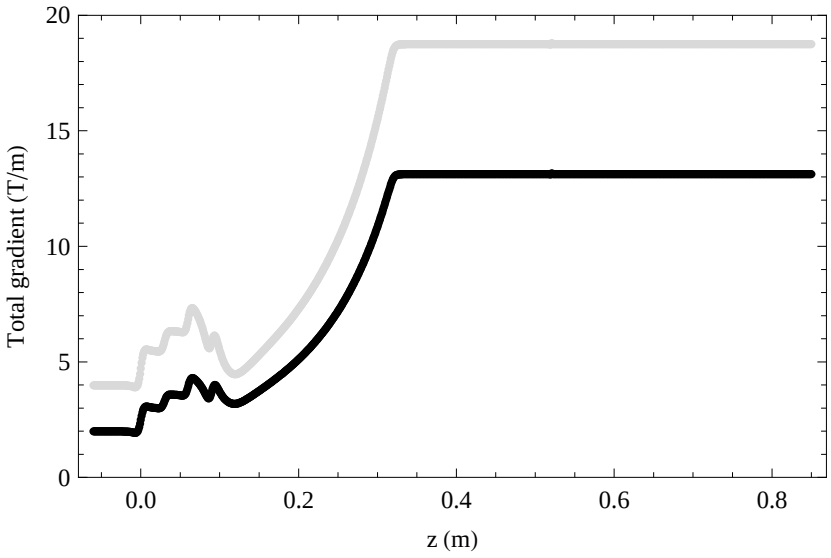

Figure 3.1: The magnetic field gradient from the guide overlapped with the preguide. At $z = 0$ is the entrance of the guide. The black curve represents the operational value (550 A), whereas the gray curve represents the maximum value (800 A). There is no change of magnetic field gradient in the bend.

of 2.0 m/s is needed. The maximum launch velocity v_{max} is determined by the strength of the magnetic field gradient in the bend of the guide and the gravitational potential. The maximum value of the velocity v_{bend} in the bend is found by equating the centrifugal force with the magnetic force:

$$\frac{mv_{bend}^2}{R} = \frac{1}{2}\mu_B B'. \tag{3.2}$$

With a magnetic field gradient of 3 T/m in the bend (see Fig. 3.1) the maximum velocity v_{bend} is found to be 3.1 m/s. Which gives a maximum launch velocity of $v_{max} = 3.7$ m/s.

Discussion

The preguide and the guide is described. The preguide overlap the MOT coils and the guide providing a guiding magnetic minimum for the atoms to follow.

3.2 Transfer of atoms from the MOT into the guide.

The transfer of atoms from the MOT into the guide has to be as subtle as possible. The preguide overlapping with the entrance of the guide is designed such that the transfer is as adiabatic as possible. The increase from the four conducting rings gives a gentle increase of the magnetic field gradient that the

atoms experiences in contract to a single conducting ring where the increase of the magnetic field gradient is very sudden [6]. Initially the preguide is kept at a weak magnetic field gradient, but as the atoms propagate along the preguide towards the guide the strength is increased into a linear guide, thus overlapping the shape of the guide. The increase and change of the shape will lead to a temperature and phase-space density increase. Here the conditions for adiabatic transfer is investigated and the change of temperature and phase-space density.

3.2.1 Adiabatic transfer

In order to have an adiabatic transfer of atoms from the preguide into the guide the conditions of the guide entrance have to be matched with the preguide. However, the initial trapping conditions of the MOT do not match the guide conditions and the atoms are loaded in to a weak trap in the preguide. This is governed by the current in the coils. The strength of the preguide is increased, until the guide entrance condition are met. This process has to be adiabatic to conserve phase-space density, but the adiabatic process is by definition slow. A fast reliable adiabatic transfer can be achieved by stepping the trap frequency. Ref. [16] shows a shortcut to adiabaticity in a time depended harmonic trap. To go from an initial trap frequency ω_0 to a final trap frequency ω_f fast an intermediate trap frequency ω_1 is used in a two step process, where ω_1 is the geometric average $\omega_1 = \sqrt{\omega_0 \omega_f}$. The initial trap frequency is immediately raised to ω_1, where it is held at a quarter of the corresponding oscillation period $t_f = \frac{\pi}{2\omega_1}$, before stepping the frequency to the final trap frequency ω_f.
Another issue for the transfer is the atoms passing the stepwise increase of magnetic confinement at the guide entrance. For each of the four rings at the entrance of the guide the current through the guide changes suddenly and thereby also the magnetic field gradient. This may alter the adiabaticity, depending on the velocity of the atoms passing the rings.
The stepwise increase of the magnetic field gradient adds an additional transverse compression. If the increase is done slow enough the phase-space density is conserved and thereby adiabatic. To compress slow enough means that the atom will make many transverse oscillations, while being compressed in the radial direction. If the time used for the atom to pass the ring t_{pass} is much larger than the time it takes to make one oscillation t_{osc}, then the compression is adiabatic: $\frac{t_{pass}}{t_{osc}} \gg 1$. The time it takes to pass a ring is given by $t_{pas} = \ell / v_z$, where ℓ is the length of the region where the compression is performed. The length ℓ is assumed small and therefore the velocity v_z does not change during the pass even though the passing is vertical.
The time for one oscillation in the harmonic potential is found to be $t_{osc} = \frac{2\sqrt{2mk_BT}}{\mu_B B'}$. The adiabatic condition resolves into

$$\frac{2\sqrt{2mk_BT}v_z}{\mu_B B' \ell} \ll 1 \tag{3.3}$$

At the entrance of the guide v_z is the largest and with a length of $\ell = 2$ cm, the temperature can not be higher than 5 mK to meet the condition from Eq. (3.3) at experimental operational values, namely $v_z = 1.9$ m/s and $B' = 1.78$ T/m.

3.2.2 Change of temperature in the confinement

When atoms are transferred from one trap to another, the two traps differ in strength and shape. Due to the change the temperature and phase-space density will change. In our system the atoms move from a harmonic trap into a linear trap. To estimate how much the temperature changes in this process the number of states is evaluated and the energy difference of the total system is calculated. A trap has a number of states with index $\mathcal{S}$ and a total energy of

$$\varepsilon_{tot} = \int_0^\infty f(\mathcal{S})\varepsilon(\mathcal{S})d. \tag{3.4}$$

where the state S has the energy $\varepsilon(\mathcal{S})$ and the distribution is a Maxwell-Boltzmann distribution describing the system in equilibrium and is given by

$$f(\mathcal{S}) = f_0 \exp\left(\frac{-\varepsilon(\mathcal{S})}{k_B T}\right). \tag{3.5}$$

Here the number of states has to be evaluated and can be done so from the density of states:

$$\mathcal{S} = \int_0^{\varepsilon(\mathcal{S})} \mathcal{D}(\varepsilon')d\varepsilon' \tag{3.6}$$

For the atoms entering the guide the transverse and the longitudinal directions are completely separate. With the density of states per unit area in two dimensions being $\frac{m}{2\pi\hbar^2}$, the density of state in a trap is written as

$$\mathcal{D}_{2D}(\varepsilon) = \frac{m}{2\pi\hbar^2}\int_{U_\perp(\rho)<\varepsilon} 2\pi\rho d\rho \tag{3.7}$$

where the integral over the surface is restricted to energies, and $U_\perp(\rho) < \varepsilon$ is the transverse potential.
For a linear guide $U_\perp(\rho) = \lambda\rho$ and thus $\rho_{max} = \varepsilon/\lambda$. For a linear guide the density of states becomes

$$D_{2D,\ell}(\epsilon) = \frac{m\varepsilon^2}{2\hbar^2\lambda^2} \tag{3.8}$$

and $\varepsilon_\ell(\mathcal{S}) = \left(\frac{6\mathcal{S}\lambda^2\hbar^2}{m}\right)^{1/3}$ from Eq. (3.6). The total energy Eq. (3.4) can be written as $\varepsilon_{tot,\ell} = 3k_BTN$ where N is the number of atoms in the trap.
For a harmonic trap $U_\perp(\rho) = \frac{1}{2}m\omega^2\rho^2$, thus the maximum radius is $\rho_{max} = \sqrt{\frac{2\varepsilon}{m\omega^2}}$. Therefore, the density of states becomes

$$D_{2D,h}(\epsilon) = \frac{\varepsilon}{\hbar^2\omega^2} \tag{3.9}$$

and $\varepsilon_h(\mathcal{S}) = \sqrt{2\mathcal{S}}\omega\hbar$ from Eq. (3.6). The total energy from Eq. (3.4) can be written as $\varepsilon_{tot,h} = 2k_BTN$.
It is now possible to express how much the temperature changes as the strength and the shape of the trap changes. With Eq. (3.5) the initial distribution $f(\mathcal{S})$ will remain the same in the new trap with energy $\varepsilon(\mathcal{S})$, since the transfer is

adiabatic. This will result in an energy difference. The energy difference in the three scenarios are: from harmonic to harmonic and from linear to linear:

$$T_f = T_i \frac{\omega_f}{\omega_i} \qquad T_f = T_i \left(\frac{\lambda_f}{\lambda_i}\right)^{2/3} \tag{3.10}$$

and from harmonic to linear trap

$$k_B T_\ell = \Gamma \left(\frac{8}{3}\right) \left(\frac{\lambda^2 k_B^2 T_h^2}{9m\omega^2}\right)^{1/3}. \tag{3.11}$$

Initially the MOT has a trap frequency of $\omega_{int}/2\pi = 11.3$ Hz at a temperature of T_i =70 μK as determined by TOF measurements. With the launching of the atoms the strength of the preguide increases until it overlaps the magnetic field gradient of the entrance of the guide. Thereafter the strength of the magnetic field gradient of the guide increases due to its design to 13.5 T/m. With Eq. (3.11) this gives a final temperature of $T_f = 900$ μK.
In the experiment a rise of temperature from 70 μK from the molasses to 1.2 mK is measured in the beginning of the horizontal guide, concluding that we do not have a perfect adiabatic transfer.

The increase of phase-space density can be found from the number of atoms which is given by

$$N = \int_0^\infty D(\varepsilon) \exp\left(-\frac{(\varepsilon - \mu)}{k_B T}\right) d\varepsilon \tag{3.12}$$

where μ is the chemical potential. For a linear trap the number of atoms are found to be

$$N_\ell = \frac{8m\varrho_\ell}{(\hbar\lambda)^2 (k_B T)^3} \tag{3.13}$$

and for the harmonic trap the number of atoms are found to be

$$N_h = \frac{8\varrho_h}{(\hbar\omega k_B T)^2} \tag{3.14}$$

where $\varrho = e^{\mu/k_B T}$ is the phase-space density.
With no loss of atom number the phase-space density will remain the same if the shape of the trap is the same. However, in the transfer between harmonic and linear trap there is an increase of phase-space density of $\varrho_\ell = 2.64\varrho_h$. This is preferred since we want a larger phase-space density. As described in Ref. [17] the change of trap shape can help for reaching degeneracy. If for some reason the phase-space density is not high enough in a harmonic trap, changing the trap shape into a linear trap can increase the phase-space density.

Discussion

To have a transfer of atoms that is fast and adiabatic we need in the preguide a quarter of a trap frequency t_f of the intermediate frequency ω_1. In the passing of the stepwise increase of the magnetic field gradient in the guide, a pass time

t_{pass} has to be larger than one oscillation. This condition is met at $\frac{\sqrt{T}v_z}{B'\ell} \ll 2.3$ $\sqrt{K}$/s T.
With a stepwise increase of the trap frequency and the relation between the launch velocity and magnetic field gradient the design of the preguide overlapping with the guide provides as close to adiabatic transfer. The change of the trap strength and shape causes an increase of the temperature and the phase-space density.

3.3 Calculation of the launching of the atom cloud.

The launching of atoms is in the vertical direction against gravity. The atoms start with a Gaussian velocity and spatial distribution, but when transported in the preguide and the guide, the spatial distribution becomes wider in the longitudinal direction and smaller in the transverse direction due to the magnetic confinement. The cloud becomes dilute in the longitudinal direction. A simulation that illustrates the launch of the atoms in the longitudinal direction is described here.

The initial distribution in a trap with frequency ω launched vertically up with a velocity v_0 is given by

$$f(z, v, t = 0) = f_0 \exp\left(-\frac{m\omega^2 z^2 + m(v - v_0)^2}{2k_B T}\right) \tag{3.15}$$

The atoms travel vertically upwards and the position and velocity change accordingly to

$$z(t) = -\frac{1}{2}gt^2 + v_0 t + z_0 \tag{3.16}$$

$$v(t) = -gt + v_0 \tag{3.17}$$

A boundary condition representing the bend of the guide is added. All atoms with an energy larger than the gravitational potential mgh are cut away, where $h = 20$ cm is the distance to the bend of the guide.

If the atoms do not have enough energy to enter the guide, the atoms will return to the MOT chamber. The return of the atoms cloud is observed at $z = 0$, *e.g.*, at the MOT position. The atoms cloud is launched towards the guide with an initial velocity v_i and returns due to gravity at a time t. When the atom packet returns it has expanded in width, where the initial width is determined by the initial temperature only.
Figure 3.2 shows the result of the simulation of returning atoms as a function of time. Five different initial velocities v_i are shown. Notice that at low velocities not all atoms leave the MOT region. This makes is difficult to distinguish these atoms from atoms returning from the launch and at larger launch velocities the returning cloud stretches out and the signal becomes smaller. At large launch velocities the atoms do not return since they have an energy that exceeds the gravitational potential of $h = 20$ cm, representing atoms entering the horizontal

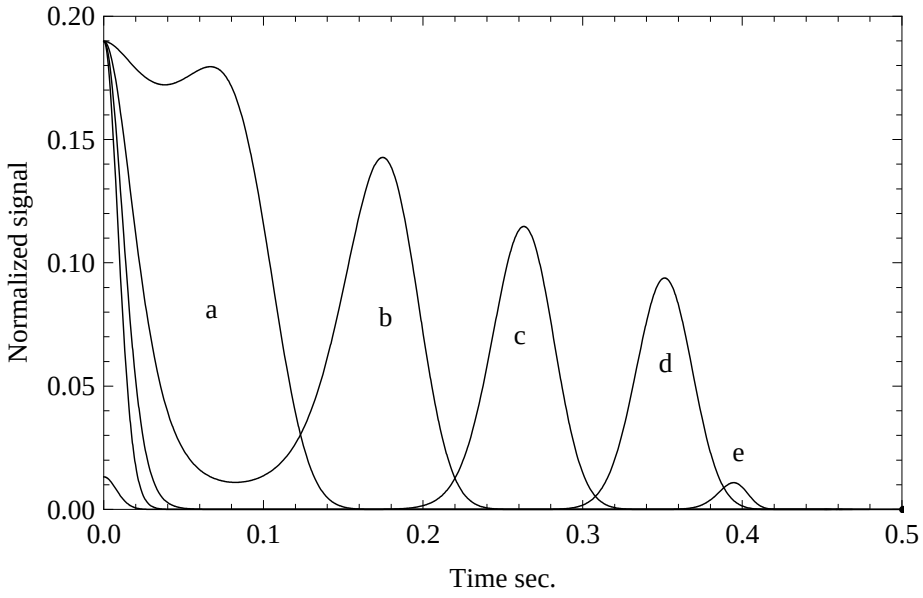

Figure 3.2: Simulation of normalized atoms distribution returning from a throw vertical and only influenced by gravity. The initial velocities are $v_i = 0.35$ m/s, 0.88 m/s, 1.32 m/s, 1.76 m/s and 2.1 m/s.

guide.

Figure 3.3 shows the width of the distribution of returning atom. Notice how the width increases with launch velocity in a linear way. Initially the spatial width of the atom cloud is ~ 1 cm, but after the launch the cloud expands to several centimeter. At low velocities the width can not be determined properly, since it is hard to distinguish between atoms staying in the MOT region and atoms that have been launched. At large launch velocities the energetic atoms are removed and therefore the width of the distribution of the returning atoms is smaller.

The signal decreases with launch velocity and the width increases with launch velocity. Figure 3.4 shows the number of returning atoms as a function of launch velocity determined through a Gaussian fit. Notice how the number of atoms stays constant except for small velocities and large velocities for the same reason as previous explained.

3.4 Launching the atom cloud experimentally

In order to produce a high-flux, low velocity cold atomic beam propagating in the guide we use a pulsed injection scheme. The sequence is 168 ms long and is used to inject one packet of atoms into the guide. For a measurement the sequence is repeated at a rate of 6 Hz.

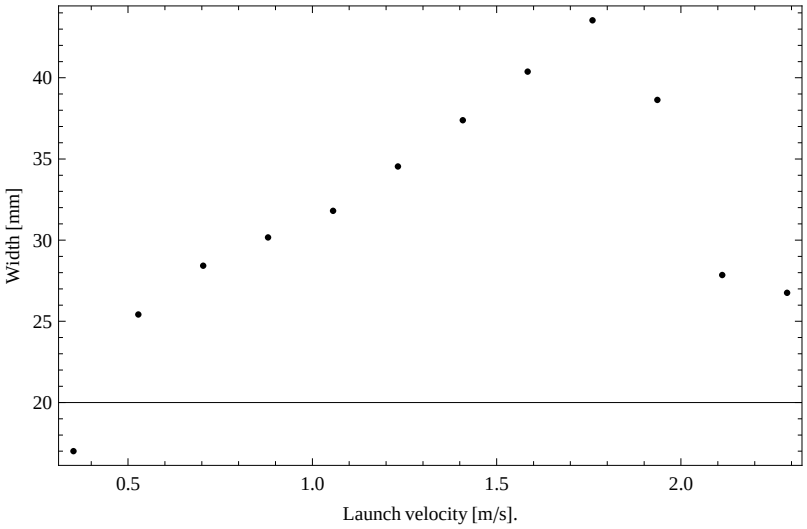

Figure 3.3: Simulation of the width of the distribution of the returning atom

Figure 3.5 shows the time line of the sequence, to illustrate the changes in the magnetic fields and detuning of the light. A time of 8 ms is used to open the mechanical shutters for the Zeeman, MOT and repump light, followed by a full load of the MOT in 80 ms. After the MOT load the Zeeman slower is turned off and the MOT and repump light continue for another 35 ms. Meanwhile the preguide is turned on to a magnetic field gradient of 0.4 T/m. This compresses the atoms and ensures that the MOT and the preguide overlap after the launch and the molasses cooling. The shape of the atomic cloud is slightly cigar shaped. The MOT is fully loaded to 10^{10} atoms and is launched in about 15 ms by accelerating the atoms. The launching velocity Ref. [18] is controlled by shifting the frequencies of the 4 $\pm\theta$=45° beams according to

$$v = \frac{\delta}{k\cos(\theta)}. \tag{3.18}$$

A small frequency offset δ is applied between the front and the rear pairs of the MOT beams lying in the vertical plan. The atoms have to travel 20 cm upwards before entering the horizontal guide. Therefore typical launch velocities are 2.1 m/s. We found that more atoms are launched if we initially accelerate the atoms away from the guide and then accelerate the atoms towards the guide. The reason for this is that the atoms are exactly in the center of the laser beams again when the acceleration toward the guide is stopped. We can at that point perform co-moving molasses cooling for 3 ms. For the cooling the magnetic fields are switched off and the detuning of the cooling lasers is increased to -60 MHz leading to a temperature of the cloud is 70 μK. The atoms are pumped into the $|F_g, m_f\rangle = |1, -1\rangle$ state. The magnetic trap is initially switched on at a gradient of 0.4 T/m corresponding to a harmonic trap frequency of $\omega_0/2\pi$ = 76.5 Hz. In order to transfer the cloud fast and adiabatic into the 1.78 T/m harmonic trap the stepwise scheme is used. Initially the trap frequency ω_0 is mode-matched to the MOT. The trap frequency is increased over a time of 5

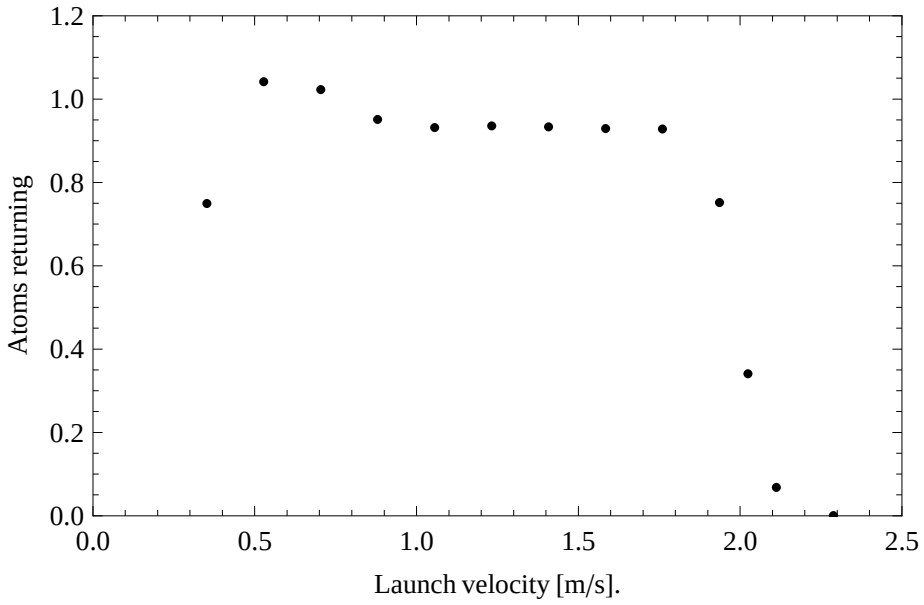

Figure 3.4: Number of returning atoms as a function of launch velocity, fitted through a Gaussian fit.

ms to the intermediate frequency ω_1. The cloud shrinks and after $t_f = 8$ ms the cloud is as small as possible, after which the final frequency ω_f is immediately set. The final trap frequency is mode-matched to the guide conditions. The cloud then propagates for another 18 ms. When the atoms are launched with a velocity of 2.1 m/s, they travel 6 cm before the preguide is fully ramped up. The entrance of the guide is placed 4 cm away from the MOT region and therefore the atoms have reached the second ring of the guide before the preguide is fully ramped up. A time of 24 ms is used to turn on the Zeeman magnetic fields. It takes 10 ms, before the magnetic fields are stable. Turning on the Zeeman slower has no effect on the atoms propagating in the preguide or the guide, since the contribution from the longitudinal magnetic field gradient and the bias of the Zeeman slower is cancelled out with a compensation coil. Due to the compression caused by the ramping up of the preguide the atom cloud is compressed and squeezed into a cigar shape. The bias field is turned on at the same time as the preguide to improve mode-matching.

Figure 3.6 shows data from launching the atoms. The atom pack has been launch upwards in the gravitational field and is returning due to gravity. The curves represent the data fitted with a Gaussian distribution. For the red curves the guide is not on and for the blue curves the guide is on. With a launch velocity less that 1 m/s the atom packet does not reach the guide and is therefore not affected by the guide gradient. At low velocity ($v_i = 0.35$ m/s) the returning atoms are difficult to distinguish from the atoms that are not launched and an accurate fit can not preformed. At $v_i = 0.7$ m/s the launched atoms do not reach the entrance of the guide and are therefore not affected by the magnetic

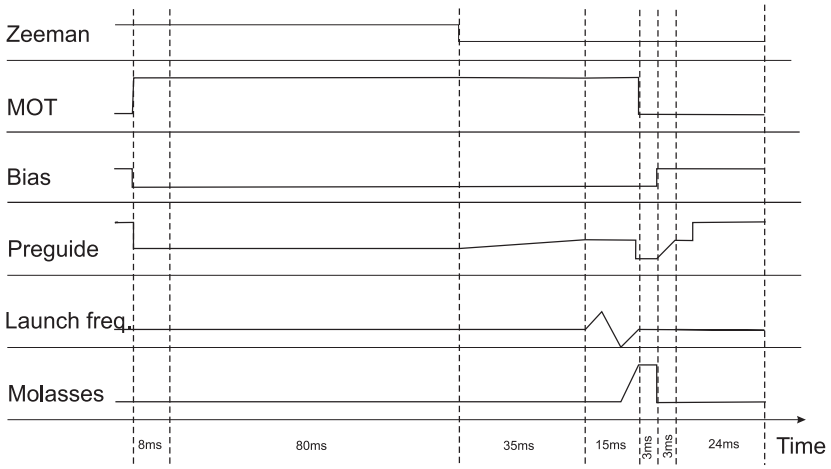

Figure 3.5: The time sequence for the launch of one atom packet into the guide. The scheme for both the Zeeman and the MOT, is controlling the light and magnetic fields at the same time. The bias and preguide is only magnetic fields. The launch frequency and the the molasses are both shifting of the detuning of the light.

field gradient present. The returning atoms are fitted with a Gaussian profile and the number of atoms and the width are determined.
When launching at 1 m/s the atom packet does reach the guide and is affected. For a launch velocity of 1 m/s results both with and without the guide on are shown. With the guide off the returning atoms show a Gaussian profile and this indicates that the entrance of the guide is hit spot on. However, with the guide on a double peak occurs. The first peak is from atoms returning on the confinement created by the magnetic field of the guide, whereas the second peak is from the atoms returning from gravity. The slowest atoms get affected by the transverse force from the sudden increase of the magnetic field gradient from the guide, they come to a halt and return.
At larger velocities ($v_i = 1.4$ m/s and 1.75 m/s) all atoms enters the guide and the confinement is not strong enough to return on. Notice how the shape does not follow the Gaussian profile anymore. This is caused by atoms lingering in the bend or entering the guide but are returned on the extra confinement after the bend. The last curve is at a velocity of $v_i = 1.9$ m/s. Here a large part of the atoms have a velocity large enough to enter the bend of the guide and subsequential enter the 4 meter guide. From the simulation in Fig. 3.2 we would expect a sudden cutoff for the fastest atoms. However, we detect an almost linear decrease of atoms. This is due to lingering atoms in the bend and in the horizontal confinement. The atoms are returning on the increasing confinement of the guide after the bend. A weak second peak from atoms returning on the increasing confinement after the bend has also been observed (not shown here). At a velocity of 2.1 m/s no atoms return from the launch and all atoms have entered the guide.

Figure 3.7 shows the change of width of the atom distribution as a function

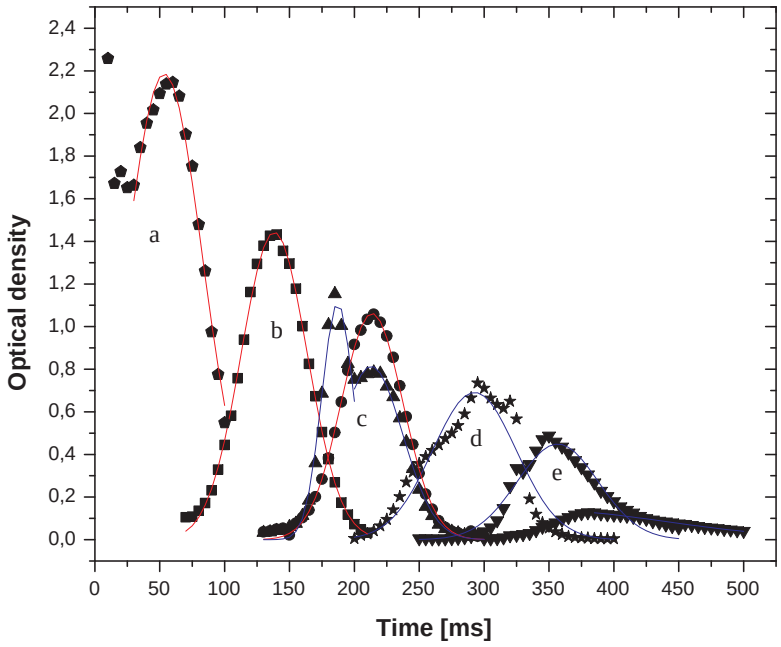

Figure 3.6: Atoms returning from the launch. The launch velocity are (v_i = 0.35 m/s, 0.7 m/s, 1 m/s, 1.4 m/s, 1.75 m/s and 1.9 m/s). The red curves are atoms that are not launched into the guide whereas the blue curve are atoms that have been in the guide. They are fitted with a Gaussian function. The low velocities shows a clear return of the atoms and a clear Gaussian distribution. When the atoms enters the guide the width becomes wider due to lingering atoms from the confinements.

of launch velocity. As can be seen the width increases with launch velocity as expected from the simulation (see Fig. 3.3). However, at the largest velocity the width is much larger, which is a clear sign of lingering atoms in the bend and at the horizontal confinement. The increase of the width and thus the expansion of the packet in the longitudinal direction is beneficial, since we want to have a continuous atom beam and therefore each atom packet has to overlap with the previously launched packet.

Figure 3.8 shows the number of atoms returning from the launch as a function of launch velocity. The average value of the number of returning atoms is 1.8×10^{10} atoms. Since the number of atoms returning stays nearly constant indicating that the launching is effective. If the number of atoms drops suddenly for a certain launch velocity it indicates that the transfer is not adiabatic, *e.g*, the atoms are heated out of the trap, or that the atoms have hit the guide tubes or

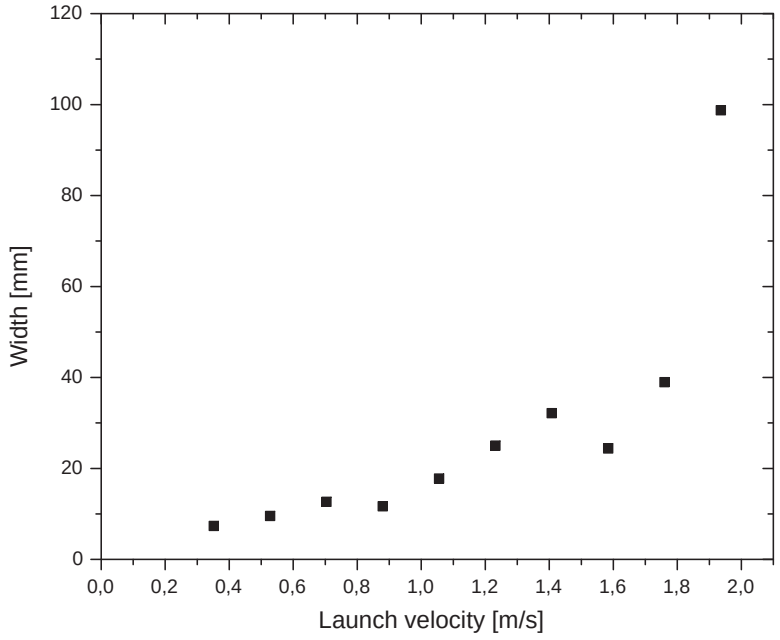

Figure 3.7: Measured width of the atom distribution returning from the launch. The strong increase is due to lingering atoms returning later that expected.

guide entrance and therefore had an inefficient launch.
Launching at a velocity larger than 2.1 m/s yields a launch efficiency of 50% from the MOT number of atoms, producing 1.8×10^{10} atoms per MOT cycle in the horizontal guide. Dispersion stretches the cloud in the longitudinal direction to 7 cm and the cloud has a mean velocity of 0.7 m/s at the top of the guide. Measurements show that increasing the launch velocity does not help in the final goal, since launching faster does not show a significant improvement of efficiency. The faster velocity only produces a more supersonic atom beam velocity, which is not beneficial for a slow continuous beam.

Discussion

We have simulated the launch of one atom cloud. We fully understand how the atoms cloud expand with the initial launch velocity. We have verified this experimentally and understand how the increase of the magnetic field gradient causes the slower atoms to return to the MOT chamber. A minimum launch velocity of 2.1 m/s is required so that a dominant fraction of atoms are launched into the guide.

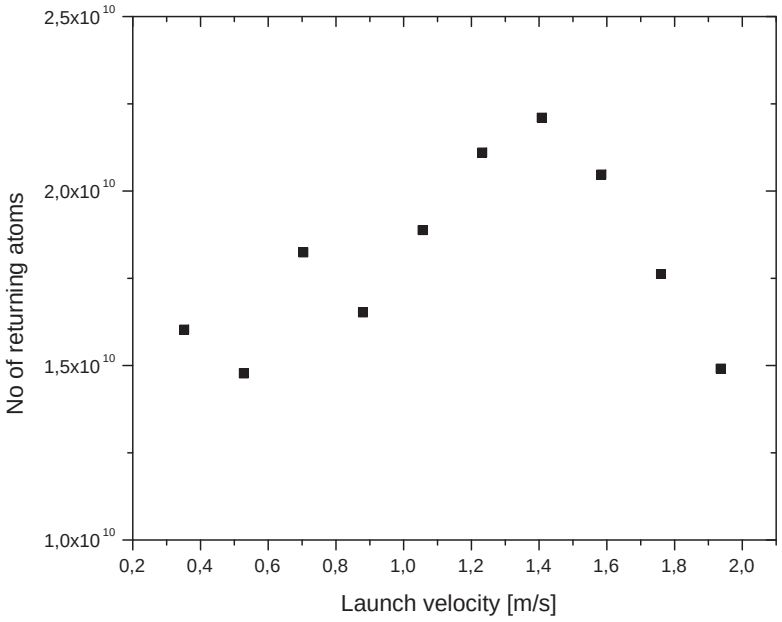

Figure 3.8: Number of atoms returning from the launch

3.5 The continuous atom beam

The width of each cloud increases with distance in the guide. With several clouds launched after each other the clouds will overlap leading to a continuous atom beam. When the beam can be considered continuous is investigated here. The conservation of energy can be used, where $\delta\overline{v}$ is the width of the distribution centered around $\overline{v}$

$$\frac{1}{2}m\overline{v}_i^2 - mgh = \frac{1}{2}m\overline{v}_f^2 \tag{3.19}$$

$$\frac{1}{2}m\left(\overline{v}_i + \delta\overline{v}_i\right)^2 - mgh = \frac{1}{2}m\left(\overline{v}_f + \delta\overline{v}_f\right)^2 \tag{3.20}$$

From Eq. (3.19) and (3.20) the final deviation from the mean velocity is expressed as $\delta\overline{v}_f = \delta\overline{v}_i\frac{\overline{v}_i}{\overline{v}_f}$, thus the velocity width increases due to the slowing of the beam.

Figure 3.9 shows the simulation of three atom packets at the bend. With a launch sequence of 168 ms we can have a launch rate of 6 Hz. With an initial launch velocity of 2.1 m/s the thermal cloud has slowed down to 0.7 m/s at the bend of the guide. The cloud has expanded to 7 cm due to the width $\delta\overline{v}_f = 0.32$ m/s and the distance between two packets in the vertical launch is 11 cm. The atom beam is continuous in the horizontal guide after 10 cm. Experimentally we observe a continuous beam 50 cm after the bend with a flux of 1.2×10^{11}

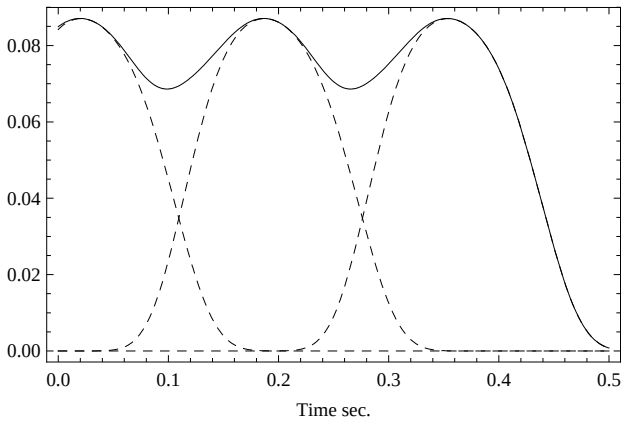

Figure 3.9: Three packets of cold atoms at 20 cm after the bend with a launch rate of 6 Hz. The beam is close to being continuous.

atoms/sec, a temperature of 1.4 mK and a beam velocity of 1 m/s.

3.6 Scattering

In usual cold experiment only s-wave scattering is considered, since in stationary experiments the atoms has a low kinetic energy. However, the atoms do not have a low kinetic energy in the guide and therefore the scattering in the guide is not isotropic. The atoms enter the horizontal guide with a longitudinal velocity of 0.7 m/s and collide with returning atoms from the end coil, which are initially at a velocity of 0.7 m/s. The scattering is therefore no longer just in the s-wave regime at but may also have larger angular momentum contributions and the scattering distributions changes from the usual scenario.

The scattering distribution $W(\theta)$ is directly proportional to the differential elastic cross section. For two identical bosons it reads

$$\sigma(\theta) \quad = \quad 2\pi|f(\theta) + f(\pi - \theta)|^2. \tag{3.21}$$

Here the Bose-symmetrized scattering amplitude is given by a summation over the even partial waves,

$$f(\theta) + f(\pi - \theta) \quad = \quad \frac{2}{k} \sum_{l=even} (2l+1) e^{i\eta_l} P_l(\cos\theta) \sin\eta_l, \tag{3.22}$$

where $P_l(\cos\theta)$ is the Legendre polynomial of order l and η_l is the partial wave phase shift. Only even l are allowed since odd partial waves are forbidden by the argument of complete symmetric wave functions for identical bosons. The l'th term represents particles having orbital angular momentum $l\hbar$.

The phase shift can be evaluated since the radial wave function corresponding to scattering of different low collision energies and different angular momenta

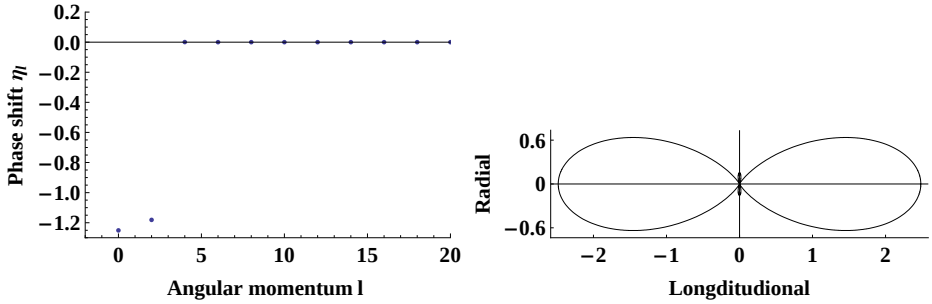

(a) Low velocity (0.32 m/s)

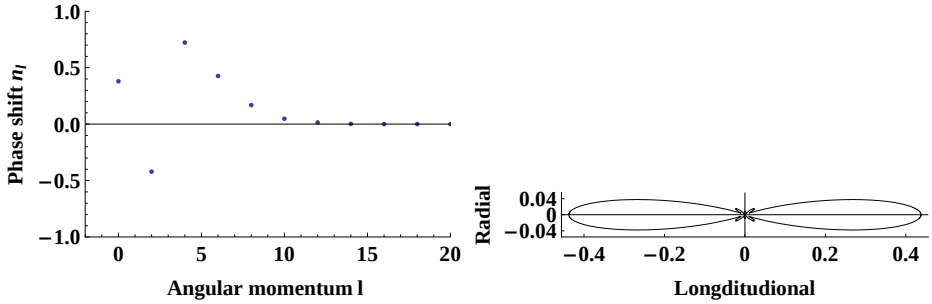

(b) High velocity (2 m/s)

Figure 3.10: Phase shift as a function of increasing angular momenta and the differential cross section, at low and a high velocity in our experiment.

should all be in phase at small distances 20 a_0. The accumulated phase shift is given by

$$\Phi(r) \quad = \quad \mathcal{K}(r) \left(\frac{\partial \ln \psi(r)}{\partial r} \right)^{-1}, \tag{3.23}$$

where $\psi(r)$ is the radial wave function and $\mathcal{K}(r)$ is the wave vector of the atoms with $V(r) = -\frac{C_6}{r^6}$ being the Van der Waals potential

$$\mathcal{K}(r)^2 \quad = \quad \frac{\mu(E - V(r))}{\hbar^2} - \frac{l(l+1)}{r^2}. \tag{3.24}$$

The accumulated phase shift can be determined from the scattering length a_0. Fig. 3.10 shows the change of phase shift as a function of increasing angular momentum at a low center of mass velocity (0.32 m/s) and at high center of mass velocity (2 m/s). As can be seen the relevance of the larger angular momenta drops of but for larger relative velocities, more angular momenta become relevant. For velocities of 2 m/s we have to take into account the contribution from all even waves until the $l = 8$.
With a higher relative velocity the phase-shifts varies between positive and negative lowering the total scattering cross section as seen in Fig. 3.10(b). The scattering is mostly in the longitudinal direction and is more of the glancing kind than the head on collisions, which causes large scattering angles.

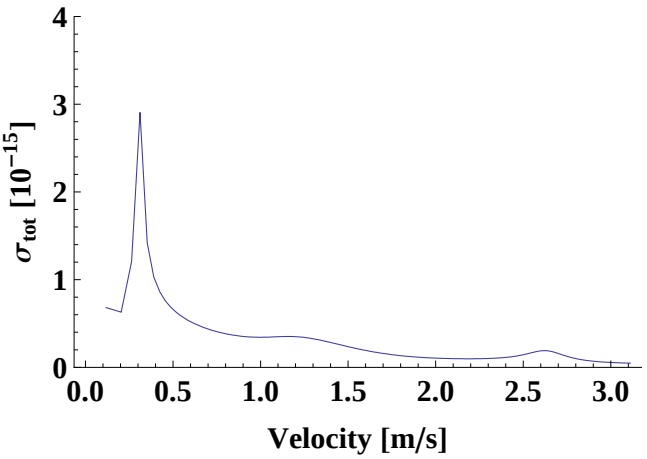

Figure 3.11: The total cross section as a function of the relative velocity of two colliding particles. The largest cross section is at the d-wave resonance

The total cross section as a function of the relative velocity is depended on the scattering angle.

$$\sigma_{tot} = \int_0^{2\pi} \sigma(\theta) \sin\theta d\theta \tag{3.25}$$

As can be seen in Fig. 3.11 initially with a high relative velocity the cross section is not large. This is because there are more destructive interferences between the phases (see Fig 3.10(b)). In our experiment we have a center of mass velocity of 1.4 m/s. This corresponds to a cross section of 2×10^{-16}. But still our experimental results shows that there are enough collisions for the atoms to slow down. Moreover, when the atoms slow down the cross section increases and become more effective than s-wave scattering. In all our simulations we always assume s-wave scattering, since this is possible to work with.

3.7 Measurement of density and temperature in the guide.

When the atoms have entered the guide, the atomic beam is supersonic. But at the end of the guide is a magnetic coil that acts as impassable barrier for the atoms and the supersonic beam returns and creates a subsonic beam through collisions. Between the two velocity regimes a shockwave will occur naturally. This process is described in chapter 4. With a shock wave we should be able to observe a sudden increase of both density and temperature.
In the experiment it is possible to measure the density and temperature directly. By aligned the probe beam vertically to the guide tubes the change of temperature and density can be measure over radial distance. The scattering cross section changes according to the magnetic field and the polarization of the

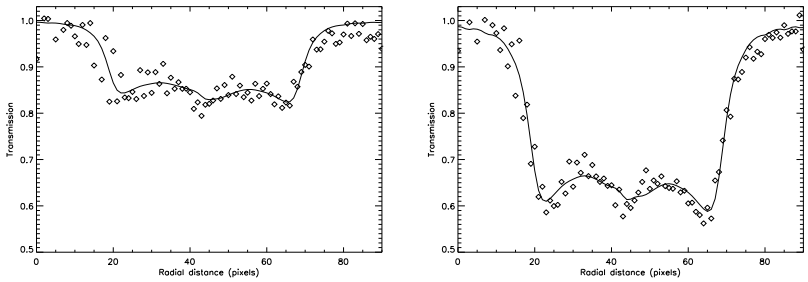

(a) The supersonic beam (b) The subsonic beam

Figure 3.12: The measured transition with a fixed polarization

probe beam and is given by [19]

$$\sigma_0 = \sum_e \frac{3\lambda^2}{2\pi} C_{ge} \frac{1}{1+\left(\frac{2\delta_{ge}}{\gamma}\right)^2} f_{ge}, \tag{3.26}$$

where the summation is taken over all possible transitions of the magnetic ground states. C_{ge} is the coupling strength and f_{ge} is the fraction of the laser light available to drive the π- or σ- transition. The fraction of light depends on the magnetic field and the detuning δ_{ge} is given by the Zeeman offset: $\delta_{ge} = \delta_{\Delta|F,m_f>} + \delta_0$. This can be determined through the interaction Hamiltonian, since the orientation of the polarization changes with respect to the magnetic field. Figure 3.12 shows the measured transition with a fixed polarization of the supersonic (Fig. 3.12(a)) and subsonic (Fig. 3.12(a)) beam as a function of the radial distance, *e.g*, the magnetic field. The line is the theory and the transition value is the absorption with respect to the other regions where no atoms are present. When comparing Fig. 3.12(a) and Fig. 3.12(b) a stronger absorption is observed in subsonic beam when the end coil is turned on indicating an increase of density.

When fixing the polarization, the density and temperature can be measured as the shock wave moves past a certain point in the guide. Figures 3.13 and 3.14 show the temperature and the density of a shock wave moving past a point situation $z = 50$ cm from the bend of the guide. Initially the beam is supersonic and the temperature is measured to be 1.14 mK and a linear density of $n_{1D} = 1.8 \times 10^{10}$ atoms/m. After the end coil is turned on at time $t = 0$ the temperature rises to 1.8 mK and the linear density starts to increase. Notice that for $t > 10$ s the temperature decreases whereas the density continues to increase. This is due to evaporative cooling on the guide tubes. Evaporative cooling is explained in details in chapter 6

3.8 Resume

The transfer of atoms from the MOT region to the preguide has been investigated and explained. The overlap between the preguide and the design of the guide entrance ensures an adiabatic transfer. The preguide is initially considered as being a harmonic trap, but with the increase of the magnetic field gradient

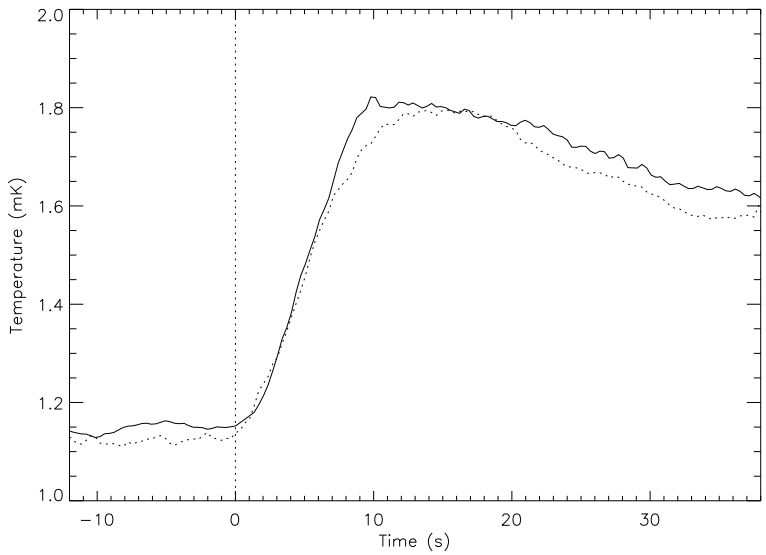

Figure 3.13: Temperature in the guide at a fixed position 50 cm after the bend of the guide. At $t = 0$ the coil is turned on.

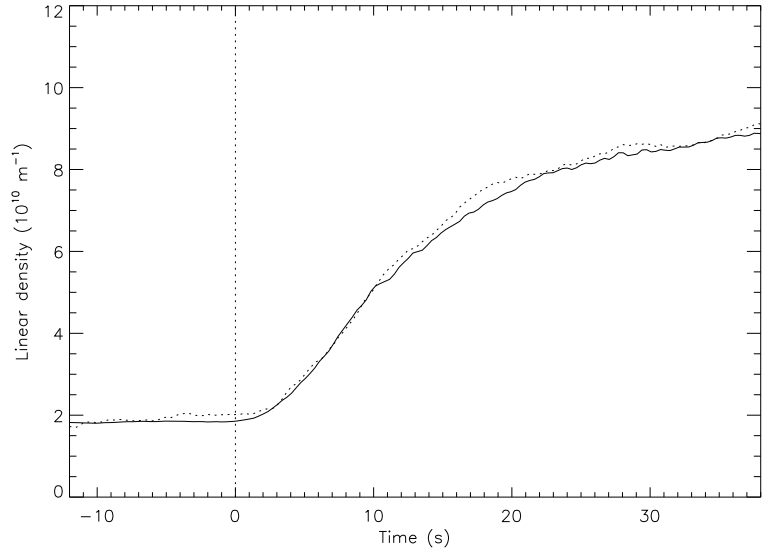

Figure 3.14: Linear density in the guide at a fixed position 50 cm after the bend of the guide. At $t = 0$ the coil is turned on.

the trap becomes linear, which overlaps the guide magnetic field gradient. This causes an increase in temperature as well as in phase-space density, which only works at our advantage. When the cloud is launched the cloud will expand in the longitudinal direction and the atoms will return to the MOT chamber, if the launch velocity is not larger than 2.1 m/s. When the atoms are in the guide the cloud has expanded and with a launch rate of 6 Hz the atom clouds overlap each other into a continuous beam. The beam is measured to be continuous 50 cm into the guide with a flux of 1.2×10^{11} atoms/s, a temperature of 1.14 mK and a supersonic beam velocity of 0.7 m/s. We have noted that we do not have s-wave scattering, but that the scattering is dependent on the center of mass velocity and that the cross section increases with slower center of mass velocities.

CHAPTER 4

Shock wave

When the continuous beam has formed in the magnetic guide the density of the beam is $\sim 2\times10^{10}$ atoms/m and the velocity is 0.7 m/s. In order to manipulate as many atoms as possible in a controlled way, we slow the beam velocity down to zero. This provides a continuous source of ultra cold atoms with a density close to $\sim 10^{11}$ atoms/m, which are normal MOT atom numbers. The slow down of atoms can be done in two ways: either by a decelerating potential or through collisions.
A magnetic coil is placed 3 meter down the magnetic guide. This coil acts as a potential barrier. The potential is so large that atoms can not pass it and incoming atoms will return on the barrier. Initially the beam is supersonic but is slowed down to subsonic velocities on the rising potential from the barrier or through collisions. In the region between the supersonic beam and the subsonic beam a shock wave will be created. After its generation close to the barrier the shock wave moves upstream in the guide generating a dense beam in its wake. The shock wave stabilizes in the beginning of the guide, where the confinement is weakened. If enough collisions occurs in the beam a shock wave is generated regardless of the potential, which can be upwards, downwards and horizontal. The density increase after the shock wave depends on the potential. With an upwards potential the density increase is less than with a downward slope. If the shockwave is on a downward slope another physical effect happens: gravitational compression. The weight of the upstream atoms simply increases the pressure on the downstream beam.
In this chapter the generation of the subsonic atom beam through a shock wave is discussed in detail. The hydrodynamical equations describe the system completely, but to get a deeper understanding of the process we first look at a simplified system.
The first approach is to discuss a system of two atomic beams colliding and

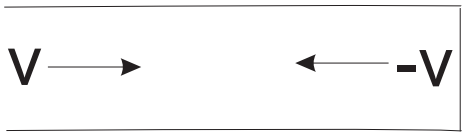

Figure 4.1: A confinement closed off at time $t = 0$ with a beam of particles with velocity v returning at the barrier in opposite direction with a velocity $-v$.

observe how the density increases, independent of the original beam velocity and the potential used.
Second, a flow continuity model is presented. This is the ideal case of the shock wave, where the properties of the supersonic beam and the subsonic beam are evaluated separately. It is shown that in order to change from one velocity regime to another, a shock wave must occur.
Third, the Boltzmann transport equation is used to describe the system. Two beams of supersonic velocity are set to collide with a controlled collision strength. The difference of collision strength is investigated and the scenario where a region with collisions become collisionless. This will create a stabilization of the shock wave.
Fourth, the hydrodynamical equations are used to describe the system fully. With a supersonic beam entering the linear trap confinement from the left, the beam slows down on the barrier to subsonic velocity. Subsequently the supersonic beam hits the subsonic beam creating a moving shock wave from the right. The collision strength is governed by thermal conductivity and viscosity. These are two important parameters when addressing flow and are evaluated in the relevant trap configurations, both the harmonic trap and the linear guide.

4.1 Filling up the bucket

A simple way of understanding the motion of the atoms in the guide is by looking at how a 1D horizontal "bucket" is filled up. Here it is shown how filling up a bucket creates a density increase with a distinct edge.

A beam of particles moves from the left with a certain velocity v and density n_0. We assume that there is only particle conservation and no external forces, no temperature dependency or no damping processes between the particles. The beam moves in a confinement that at $t = 0$ is closed off at one end (see Fig. 4.1). We assume that the atoms return from the end barrier with a velocity $-v$. If the particles do not collide the density in the confinement will increase with a factor of two (see Fig. 4.2 dashed line). However, depending on the cross section σ and density n of the particles the atoms will collide. Now, we assume that if two particles collide they will both stop. Let this be scenario a. Furthermore, we assume that if an atom with a velocity $+v$ collides with a particle that stands still, they both have zero velocity after the collision. Let this be scenario b. Thus, in the last case there is no momentum conservation.

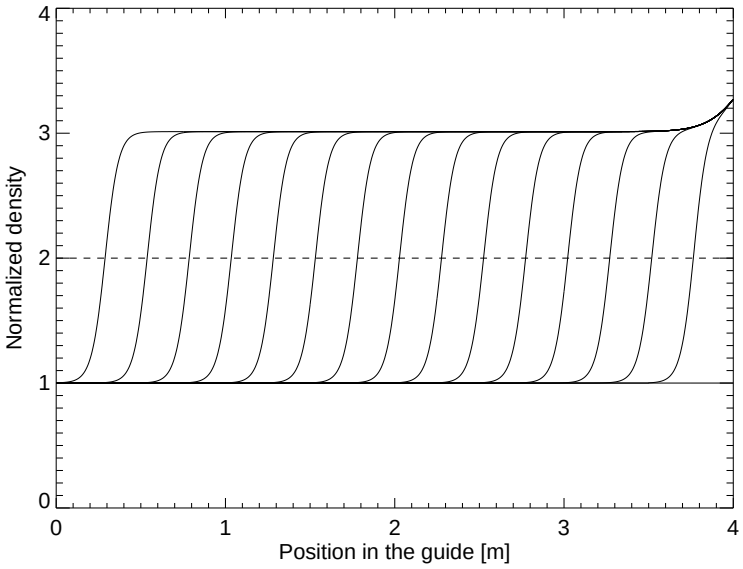

Figure 4.2: The "pile-up" wave created from a beam of particles returning from the barrier colliding with the incoming beam. The "pile-up" wave moves in time from the right to the left.

The time evolution of the atoms at rest is thus given by

$$\frac{dn_0}{dt} = \sigma_a n_+ n_- + \sigma_b \left(n_+ n_0 + n_- n_0\right) \tag{4.1}$$

with $\sigma_{(a,b)}$ being the cross section for each scenario.

Figure 4.2 shows the result for $\sigma_a = \sigma_b$. At $t = 0$ the particles will start to pile up at the end of the confinement. A "pile-up" wave will start to travel from the right to the left, leaving behind a stand still beam with a density of n_{tot}. In this case the edge of the "pile-up" wave is very sharp and moves with a velocity of $v_{beam} = v/3$. Initially the density is more than three times higher, since there is a contribution from n_0, n_+ and n_-. After some time the particles n_- is depleted and only atoms from n_0 will contribute from the left side of the "pile-up" wave, leaving only a contribution from n_0, replicating the "pile-up" wave as it is filled up from the left side. The "pile-up" wave then moves from the right to the left.

In Fig. 4.2 the edge of the "pile-up" wave is very sharp due to the effect that the cross section is set very high. However, if the cross section decreases, the edge will have a finite width. Figure 4.3 shows 3 cases at a certain time t, where the cross sections are from one figure to the next decreased with a factor 10. It can be seen that the width of the edge is direct correlation to the cross section.

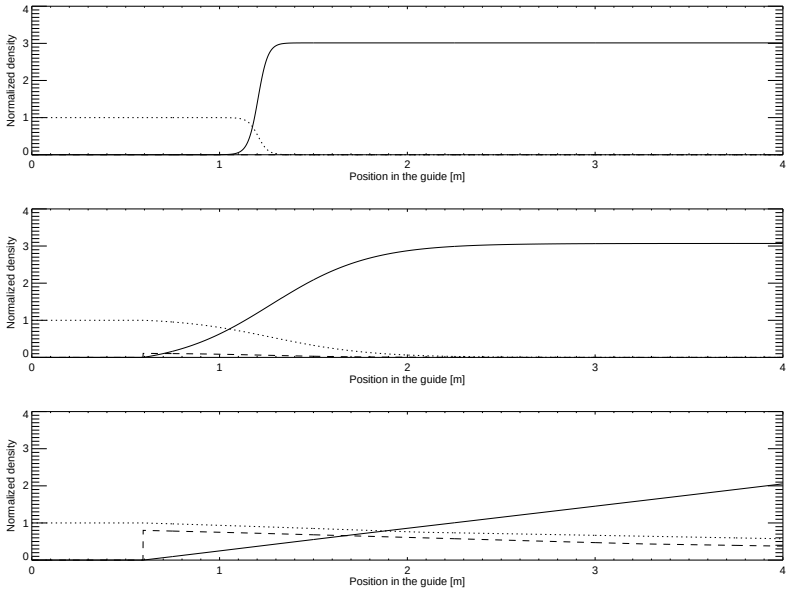

Figure 4.3: Change of cross section with a factor 10 decrease. The solid line is the stand still beam, the dotted line is the beam from the left (v), the dashed line is the beam from right ($-v$).

Discussion

This simple and crude model shows that in this configuration with collisions between two atomic beams an increase of the density larger than two is observed and that this increase moves towards the source. In this model the width of the "pile-up" wave depends on ratio between σ_a and σ_b. In Sec. (4.4) this is related to thermal conductivity and viscosity in the hydrodynamical model.

4.2 Flow continuity model

Depending on the average velocity of the particles, the beam is either in the supersonic velocity regime or in the subsonic velocity regime. In each regime the flow is different. Here it is shown that the transition between the two regimes has to be done through a shock wave.

Subsonic flow

Sound is a wave travelling through a medium. When this wave travels through the medium it exerts a small change of pressure. A small disturbance travels through a medium with a maximum velocity of the speed of sound. So if a medium has a velocity less than the speed of sound, information can travel throughout the system. Changes downstream will have an impact upstream. If there is an object in the path of the beam, a stagnation pressure builds up and this can bring the fluid to a standstill.

Supersonic flow

Flow travelling at a speed larger than the speed of sound is supersonic flow. In supersonic flow information can not travel through the system. What happens downstream of the system has no impact upstream. When a supersonic flow hits an object the properties of the temperature, pressure and density can change. This is done through an irreversible process called a shock wave.

Shock wave

A shock wave is an abrupt and discontinuous change of the characteristics of the medium, such as pressure, temperature and density. It carries energy and can propagate through the medium (BEC [20], solid, liquid, gas or plasma).
The relation between the speed of sound and the beam velocity is the Mach number: $\mathcal{M} = v_b/v_s$. The sound velocity is given by $v_s = \sqrt{\frac{c_p}{c_v}\frac{k_B T}{M}}$. Here $c_p = \frac{5}{2} + \frac{2}{\gamma}$ and $c_v = \frac{3}{2} + \frac{2}{\gamma}$, where γ is the exponent of the radial confinement of the potential $U_\rho = \lambda\rho^\gamma$. If $\mathcal{M} > 1$ the beam is supersonic and if $\mathcal{M} < 1$ the atom beam is subsonic. Initially in the guide the atoms have supersonic velocities, but we are interested in slowing the atoms down to subsonic velocities. If the atoms are slowed down almost to a standstill, the density of the atom beam can be much larger causing the mean free path to decreases significantly. When the atoms go from supersonic to subsonic speed a shock wave occurs, with a discontinuity in temperature and density. The temperature will increase, but more importantly the density will increase even more.

4.2.1 Continuity equations

The flow of a beam can be expressed by the linear density $n(z)$, the velocity $u(z)$ and the temperature $T(z)$ in an external potential $V(z)$. In a closed stationary ideal system there is conservation of particles flux and phase-space density. With the only external force from a potential $V(z)$ there is enthalpy flux conservation. This allows us to write down the conservation laws of the number of particle flux, enthalpy flux and phase-space density.
Conservation of particles flux

$$n(z)u(z) \quad = \quad Const \tag{4.2}$$

Conservation of enthalpy flux

$$n(z)u(z)\left(c_p k_B T(z) + \frac{1}{2}Mu^2(z) + V(z)\right) \quad = \quad Const \tag{4.3}$$

Conservation of phase-space-density

$$\frac{1}{k_B T(z)^{3/2}}\frac{n(z)}{(k_B T(z))^{2/\gamma}} \quad = \quad Const \tag{4.4}$$

This set of equations for the flow has two real solutions for the velocity $u(z)$: the supersonic and the subsonic solution.
Figure 4.4 shows the Mach number as a function of potential. The characteristics of the graphs is determined by the density, phase-space density and the

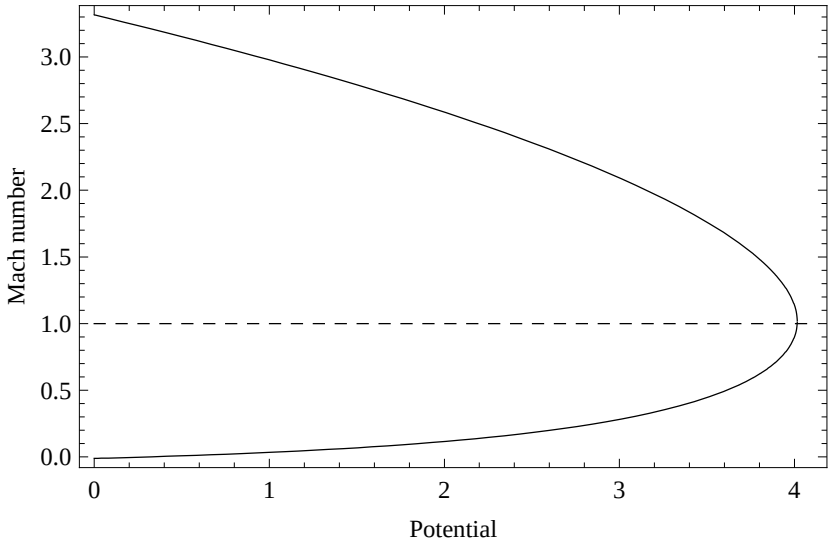

Figure 4.4: The two velocity classes as a function of potential. The super sonic velocity branch is the top curve. The lower curve is the subsonic branch.

enthalpy through Eq. (4.2)-(4.4). The upper curve is the supersonic branch and the lower is the subsonic branch. At the connection point the Mach number is one. Notice that particles travelling in a rising potential with supersonic velocity will reach a point where the velocity has slowed down to subsonic velocity, from then on the particle will follow the subsonic branch travelling down the potential again.

Between the two solutions a shock wave occur. At the shock wave phase-space conservation no longer holds but particle flux conservation Eq. (4.2), momentum flux conservation and enthalpy flux conservation Eq. (4.3) does.
Momentum flux conservation is given by

$$n_1 \left(k_B T_1 + M u_1^2\right) \quad = \quad n_2 \left(k_B T_2 + M u_2^2\right) \tag{4.5}$$

Here the index indicates particles on each side of the shock wave. Eq. (4.5) with Eq. (4.2) and Eq. (4.3) has two solutions, a trivial and the physical solution given by

$$n_2 \quad = \quad \frac{8 M n_1 u_1^2}{9 k_B T_1 + M u_1^2} \tag{4.6}$$

$$u_2 \quad = \quad \frac{9 k_B T_1 M u_1^2}{8 M u_1} \tag{4.7}$$

$$k_B T_2 \quad = \quad \frac{-9 k_B T_1^2 + 62 M k_B T_1 u_1^2 + 7 M^2 u_1^4}{64 M u_1^2}. \tag{4.8}$$

Figure 4.5 shows the phase-space density as a function of $\mathcal{M}$. It can be seen that if $\mathcal{M} < 1$ before the shock wave the phase-space density increases dramatically. A transition from a subsonic beam to a supersonic beam through

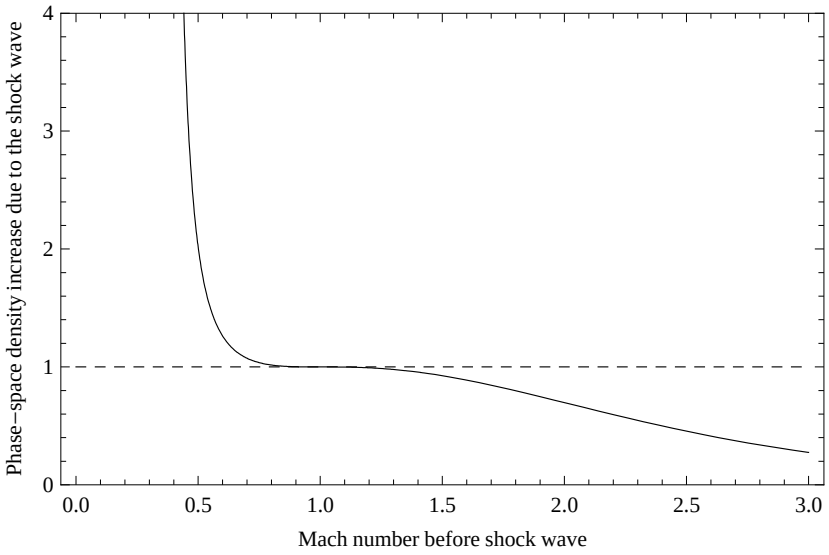

Figure 4.5: Phase-space density as a function of $\mathcal{M}$.

a shock wave is forbidden since the entropy of the closed system can no decrease. For $\mathcal{M} > 1$ the phase-space density remains constant. For large $\mathcal{M}$ the the phase-space density decreases. This not not desirable, since a large phase-space density is needed to reach degeneracy. This shows that we want to have a shockwave transition from a supersonic beam to a subsonic beam close to $\mathcal{M}$=1.

Figure 4.6 shows the change in density, velocity and temperature given by Eq. (4.6)-(4.8). The larger the $\mathcal{M}$ before the shockwave the larger the density increase will be. Notice though that the increase of temperature is not as large. This means that the gain of density compared to the temperature increase is large. However the phase-space ratio is still decreasing. Also note that the decrease in velocity is significant at larger $\mathcal{M}$.

4.2.2 The calculation

This model is an ideal case and can be used to describe what happens in the experiment. Equations (4.2)-(4.4) give two solutions for the flow. The first is the supersonic solution, the second is the subsonic solution. Both solutions are dependent on the external potential $V(z)$.
The external potential resembling the magnetic guide with an end coil is expressed as

$$\begin{aligned} V(z) &= mgh\left(1-\frac{1}{z_{max}}\right)+ \\ &\quad \frac{\mu_0 I N r^2}{W_{coil}}\int \frac{1}{2\left((z-z_{max}-z_{coil})^2+r^2\right)^{3/2}}dz_{coil}. \end{aligned} \tag{4.9}$$

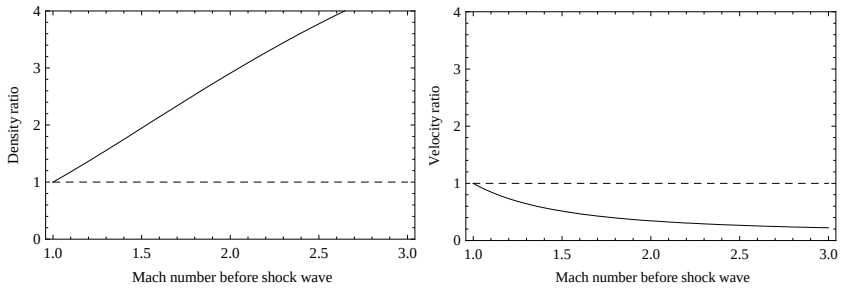

(a) Density. (b) Velocity.

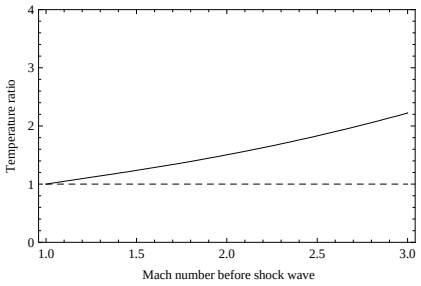

(c) Temperature.

Figure 4.6: Ration after the shock wave for the density, velocity and temperature as a function of the Mach number before the shock wave.

where W_{coil} is the width of the coil, z_{max} is the length of the guide and z_{coil} is the position of the coil. The initial conditions are set to be experimentally realistic values. The guide is $z_{max} = 4$ m and has a coil at $z_{coil} = 3$ m. With a current of $I = 70$ A and with 55 windings, a radius of 6.4 cm and a W_{coil} of 3.7 cm the coil works as an impassable barrier. The density is set at $n_0 = 1 \times 10^{10}$ atom/s., with a temperature of $T_0 = 1.4$ mK and a velocity of $u_0 = 0.7$ m/s corresponding to a Mach number of $\mathcal{M} = 1.7$, which is well into the supersonic regime.
The calculation is done where the shock wave is already created. For the calculation the shock wave is chosen at $z_{shock} = 1.7$ meter and described by Eq. (4.6)-(4.8).

First, a horizontal guide is used. Figure 4.7 shows the calculation at the initial conditions. The shape of the potential is shown as a reference. The shock wave is step-wise which is due to the lack of damping processes. The density ratio is 2.4 and the Mach number ratio is 1.7 and both remain constant as long as the potential does not change. The calculation on the right side of the barrier has no interest, since this part is strongly governed by the boundary conditions.

Figure 4.8 shows the calculation with a sloped guide. Here the elevation is set to 10 cm. In the experiment the maximum elevation is 7 cm and is usually not more than 2 cm while running the experiment. The large elevation is chosen to show the effect of the elevation. The initial conditions are the same as previous. In the supersonic case the atomic beam is accelerated, thus the density decreases and the Mach number increases. This is due to the increase of velocity

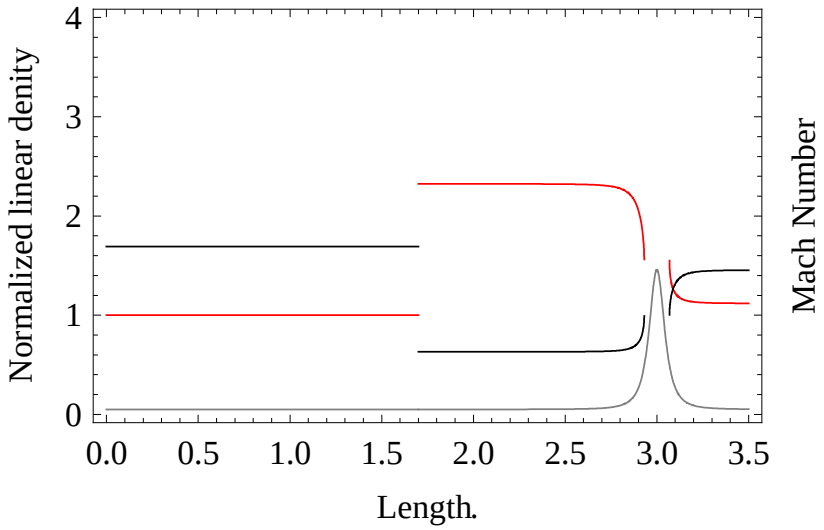

Figure 4.7: Ideal shock wave in a horizontal guide. The gray curve is the potential. The black curve is the Mach number and the red curve is the density.

and the temperature remains nearly constant. After the shock wave the Mach number decreases below 1 into the subsonic regime and the density increases stepwise with a ratio of 2.73. The temperature increases slightly but the velocity decreases more. The atoms pile up against the end barrier and continue to slow down while travelling downstream. The density goes up since there is a pile up of atoms at the foot of the barrier. If the shock wave is placed higher up the stream the density increase from the potential will be larger. This is gravitational compression. Gravitational compression is caused by the weight of atoms accumulating at higher elevation

Discussion

The continuity model shows that if there is a supersonic regime and a subsonic regime, the transition between the supersonic regime and the subsonic regime happens through a shock wave. Over this shock wave the temperature will increase but more importantly so will the density. The increase of density of more than a factor of 2 and the step wise increase is so significant that it is observable in the experiment. With a downward slope a larger increase is observed due to gravitational compression.

4.3 Boltzmann collision model

To simulate the change of density through collisions at supersonic velocities, we produce two beams of opposite velocity. These will collide and interact through collisions and a shock wave will occur. This is described through the Boltzmann transport equation. This simulation is based on the interaction

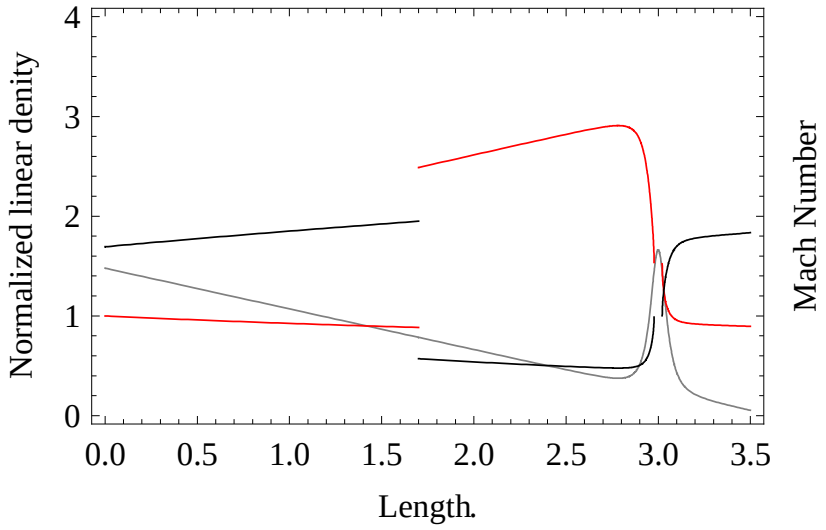

Figure 4.8: Ideal shock wave in a sloped guide, $h = 0.1$ meter. The gray curve is the potential. The black curve is the Mach number and the red curve is the density.

between distribution which makes it difficult to describe the evolution of density n, velocity u and temperature T under different situations. However a good clear picture of the development of a shock wave can be described in this model. To describe the motion of the beam, it has to be evaluated if the beam is collisionless or not, both in the axial direction and in the radial direction. The mean free path is the average distance travelled by an atom between collisions. If the mean free path is longer than the size of the thermal cloud, in general no collisions will occur during one oscillation. However, if the mean free path is shorter than the thermal cloud, many collisions will occur during one oscillation and the behavior of the atoms is dominated by the interaction. This is the hydrodynamical regime.
The mean free path is given by $l_{mfp} = \frac{1}{\sigma n}$. For s-wave scattering, the isotropic cross section of two identical bosons is $\sigma = 8\pi a^2$ where a is the scattering length and n is the effective density of the trapped thermal atoms. The mean free path in a linear guide can be written as [21]

$$l_{mfp} = \frac{32\pi k_B^2 T(z)^2}{n_{1D}(z)\mu_B^2 B'^2 \sigma}.$$

Inserting realistic values for $T = 1.4$ mK, $B' = 13.5$ T/m and $n_{1D} = 2.5 \times 10^{10}$ atoms/m, yields a mean free path of 13.5 cm. Since our guide is 2 mm wide and 3 meter long, the radial direction is nearly collisionless, but the 3 meter axial direction is fully hydrodynamical.
In the experiment, the guide design is such that after the bend of the guide the distance between the guide wires decreases from 7.8 mm to 2 mm. This decreases the collision rate. This simulation will allow to change the collision rate causing the shape of the shock wave to change. Also it is shown that if the

collision is removed in a region in front of the shock wave, the shock wave will stabilize.

4.3.1 The Boltzmann transport equation

The transport process are described by Boltzmann transport equation and is written as

$$\left[\frac{\partial}{\partial t} + v \cdot \frac{\partial}{\partial r} - \frac{1}{M}\frac{\partial U}{\partial r} \cdot \frac{\partial}{\partial v}\right] f(r, v, t) \quad = \quad I_{coll}(f) \tag{4.10}$$

where U is the external potential and $I_{coll}(f)$ is the collision integral.
The distortion of the distribution function $f(v, r, t)$ can be described as a function of the coefficients $\alpha_{ijk}(r, t)$ that determines all properties of the system:

$$f(v, r, t) \quad = \quad f_0(v, r) \sum_{ijk} \alpha_{ijk} E_{\perp}^{i} L^{2j} v_z^k \tag{4.11}$$

where $E_{\perp}$ is the transverse energy and L is the angular momentum. The function $f_0(v, r)$ is the equilibrium Maxwell distribution function, given by

$$f_0 \quad = \quad \frac{M^2 \Gamma_{coll}}{2\sqrt{2}\pi\sigma(k_B T)^2} e^{\frac{-E}{k_B T}}. \tag{4.12}$$

where Γ_{coll} is the collision rate, σ is the cross section and E is the total energy.
Starting from the Boltzmann transport equation (Eq. (4.10)), the evolution of the distribution function reads

$$\begin{aligned} \frac{\partial f(v, r, t)}{\partial t} \quad = \quad & -v\frac{\partial f(v, r, t)}{\partial r} + \frac{dU}{Mdr} \cdot \frac{\partial f(v, r, t)}{\partial v} \\ & - \int\int \frac{\sigma}{4\pi} |v - v_2| \left(f(v, r, t) f(v, r_2, t) - f(v_3, r, t) f(v_4, r, t)\right) d\Omega_{34} dv_2 \end{aligned} \tag{4.13}$$

The term on the left is the time evolution term, on the right is first the convection term, then the acceleration term, and last the collision term. The collisions are assumed to be in the s-wave regime, where the cross section σ is constant and isotropic. Ω_{34} is the direction of v_3 with respect to the center of mass v_{cm} determined by v and v_2.

With the use of the bi-linear property of collision term, Eq. (4.13) can be rewritten with Eq. (4.11) by the use of cylindrical coordinates in real space and spherical in velocity space and integrated over v and ρ:

$$\mathbf{A}\frac{\partial \alpha}{\partial t} \quad = \quad \mathbf{B}\frac{\partial \alpha}{\partial z} + \mathbf{C}\alpha\frac{dU}{dz} + (\mathbf{J}\alpha)\,\alpha. \tag{4.14}$$

Here $\mathbf{J}$ is a collision tensor and $\mathbf{A}, \mathbf{B}, \mathbf{C}$ are matrices that can be determined, as described in [22]. Due to the radially collisionlessness, there is no radial dependency and α is a vector as a function of z.

4.3.2 The simulation

The change of density for two opposing supersonic beams moving through each other can be simulated with Eq. (4.14). The density is the integral of the

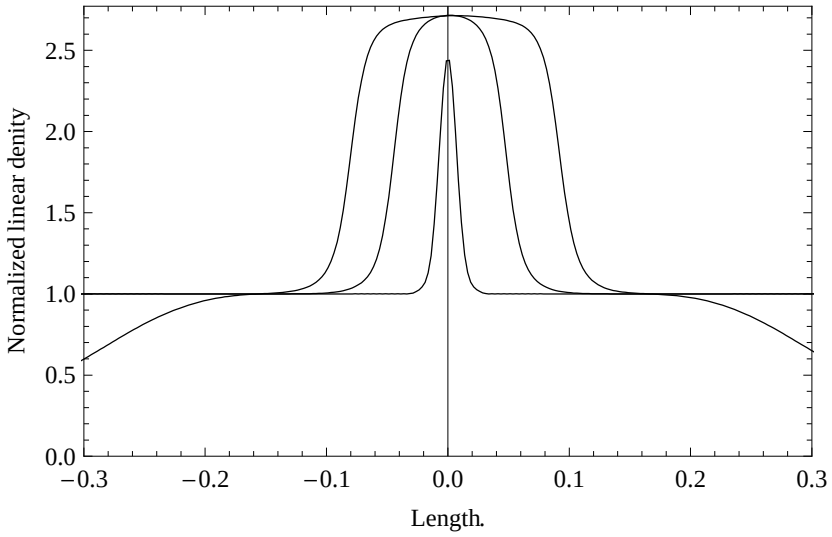

Figure 4.9: Two thermal clouds collide and a shock wave occur and atoms pile up behind the shock wave. Each line is at time step on 50 ms.

distribution function with the linear confinement set at $\gamma = 1$. Knowing the matrices $\mathbf{A}, \mathbf{B}, \mathbf{C}$ and $\mathbf{J}$ from ref.[22] the vector α from Eq. (4.14) can be evaluated as a function of distance r and time t.

Figure 4.9 shows the density of the two beams of atoms in a linear guide colliding. Initially the beam velocity is supersonic. The interaction between the atoms slows the atoms down to a standstill thus creating a shock wave between the supersonic region and the subsonic region, leaving behind a slow dense cloud of atoms. For each time step the shock wave moves away from the center. In a co-moving frame the Mach number of the incoming beam is $\mathcal{M} = 2.0$. This lead to an density increase according to the ideal case of 2.7 (see Sec. 4.2).

Figure 4.10 shows the difference in collision rate. Notice how the shape of the shock wave changes with collisions strength. With less collisions the shock wave becomes wider and the density increase is slower. As long as there are collisions the density increase will remain the same, but the time used is longer.

Figure 4.11 show the normalized density growth at the position slightly away from the center of the collision region ($z = 0.02$ m). The blue curve is the Boltzmann collision simulation where the collision term J is set to zero. The wiggles are due to a break down of the simulation accuracy. The density increases less without collisions as the beams just pass through each other. In the collisionless regime the maximum increase of density is a factor of 2.

The black curves is with increasingly stronger collision rates. Initially only atoms moving to the right are observed and the density does not increase. After a time the atoms from the left arrive, but some of the atoms may be stopped by collisions and arrive later. However, with the piling up of the atoms the density increases more that expected without collisions.

Figure 4.12 shows the normalized density growth for different initial velocities. In the co-moving frame of the shock wave, the Mach number of the incoming

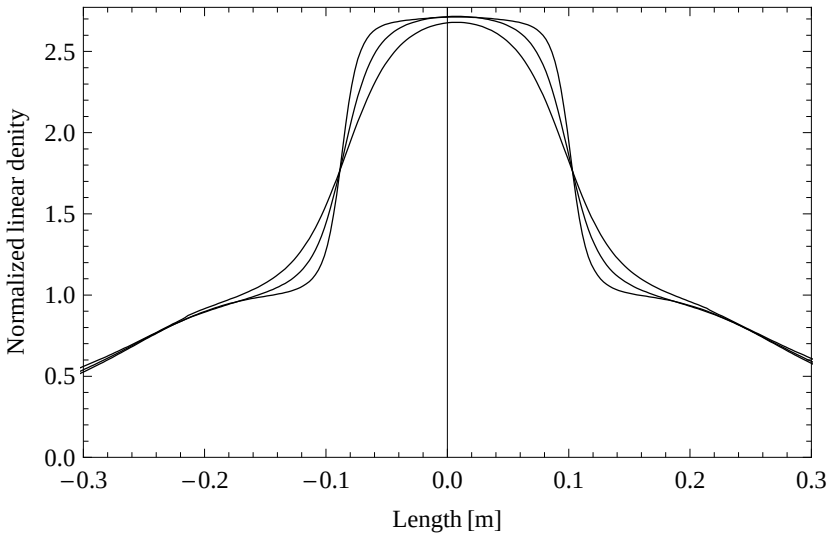

Figure 4.10: Difference in collision rate. The stepped curve is no collisions and each step is the velocity class. The oscillation is due a break down of the simulation that could be solved by increasing the accuracy.

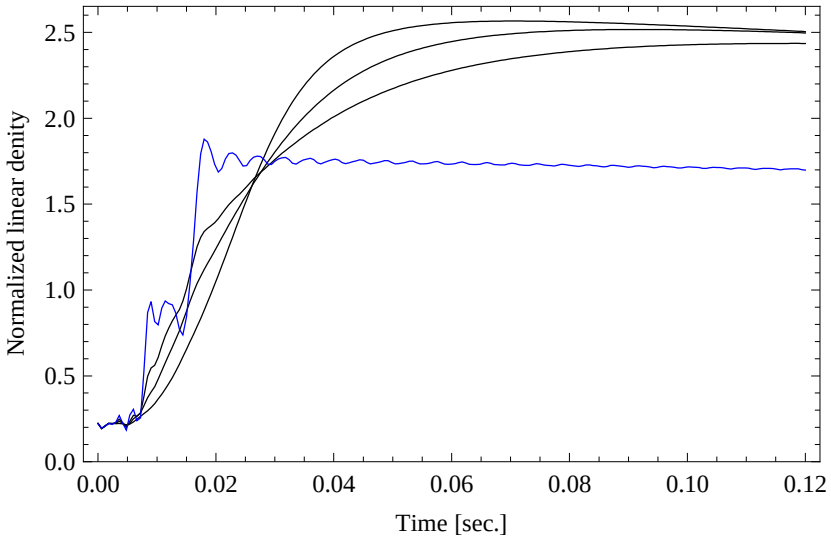

Figure 4.11: Increase of density for stronger collision interactions (black curve), The blue curve is no interaction.

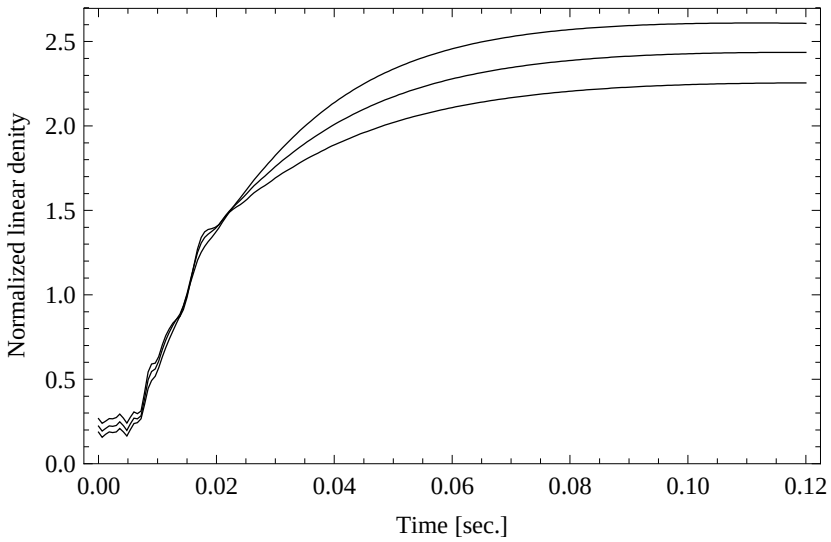

Figure 4.12: Increase of density for different initial velocities. There is a 10% velocity increase for each curve. All initial velocities are supersonic.

beam is $\mathcal{M} = 1.45, 2.0, 2.32$, respectively. The smallest density increase is for the lowest initial velocity. The density increase is larger with larger initial velocity, supporting the model from Sec. 4.2. The density increase follows Fig. 4.6(a). Notice how the slope of the shock wave does not change. This shows that the velocity and collision rate are independent.

Figure 4.13 shows the situation where collisions only occur within a certain region. This represents the shock wave generated at the guide entrance. This can be considered for the following reason: At the guide entrance the diverging geometry of the guide wires would normally destabilize the shock wave in a fully hydrodynamical system. However, here, the diverging wires can also cause a critical weakening of the collisions. In this situation the shock wave will stabilize at the edge of the collision region. When this happens, atoms will leak from the subsonic region through the incoming beam. But notice how the density in the center increases even more, than when the collisions are everywhere. This is because of the stabilization of the momentum flux. Momentum flux is a better way to describe pressure in the collisionless region. The momentum or recoil of the escaping atoms causes a larger pressure in the guide and hence a larger density in the center.

Discussion

The Boltzmann collision model shows that a subsonic cloud will emerge between two supersonic beams due to the collisions. Not only can we show that the density increase of the subsonic beam is larger than a factor of 2 but also how the density is dependent on the initial velocity and independent of the collision rate. Moreover, the shape of the shock wave is only dependent on the collision

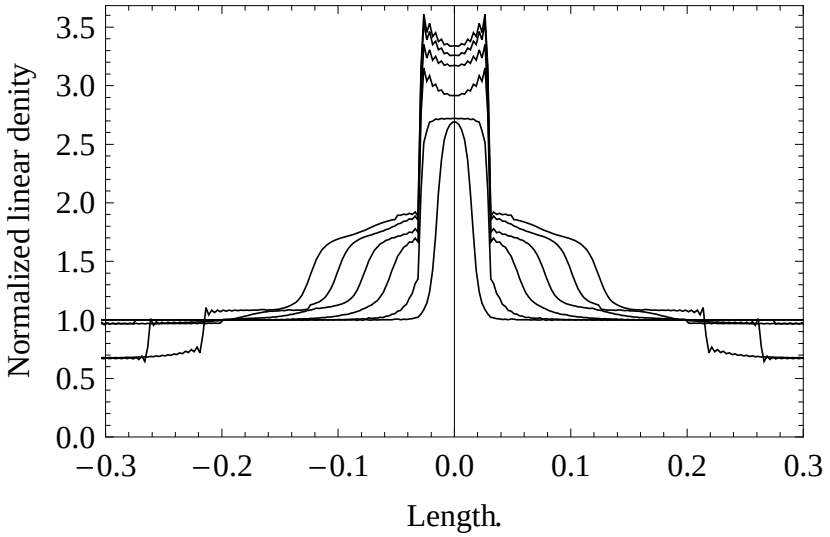

Figure 4.13: Collision within a restricted collision region. Notice how the density is larger. This is due to the stabilization of the momentum flux.

rate and not on the initial velocity. Finally, it is seen that stabilizing the shock wave between a region with collisions and a region without collisions provides an even larger density increase.

4.4 Hydrodynamical model

The Boltzmann model deals with distributions. When using distributions it is difficult to describe the evolution of density n, velocity u and temperature T under different situations, like damping process and losses. If the system is hydrodynamic, we can describe the system with the hydrodynamical model. Since the system is fully hydrodynamical is the axial direction and fully collisionless in the radial direction the system can establish a local thermal equilibrium specified by linear density n, velocity u and the local temperature T. Radially, the system is in good thermal equilibrium. The density n, the velocity u and the temperature T are all independent of each other and we can use the hydrodynamical model in the axial direction. The hydrodynamical model describes the evolution of n, u and T. This is three parameters and easier to work with than distributions. In the hydrodynamical model we can also include factors such as damping processes and loss.

4.4.1 Hydrodynamical equations

Since the beam is fully hydrodynamical in the longitudinal direction we can get a clear pictures of the shock waves development in the guide potential using the hydrodynamical equations. The hydrodynamical equations describes the propagation of the shock wave in the system. Setting up the hydrodynamical equations reflects the conservation of particles, momentum and energy.

The evolution of n, u and T can be derived from Boltzmann Equation Ref. [23] by multiplying on both sides of Eq. (4.10) by 1, to get the particle conservation, by u to get the momentum conservation and by the energy $E = \left(c_v k_B T(z,t) + \frac{1}{2} M u(z,t)^2 + V(z,t)\right)$ to get the energy conservation, and then integrated in cylindrical coordinates over radial space and velocity . The system is radial collisionless, thus u and T are independent of the radial distance ρ but $n(\rho)$ depends on the radial potential $V(\rho)$. However, the potential $V(\rho)$ is constant throughout the guide and therefore $n(\rho)$ remains constant. To include loss processes due to inelastic collisions, collision with background atoms and evaporation on the guide tubes we ad-hoc include a loss rate Γ in the equations. The generalized hydrodynamical equations can be given by the linear density $n(z,t)$, the velocity $u(z,t)$, the temperature $T(z,t)$ and the external potential $V(z)$ given by Eq. (4.9). Including the damping processes which are the viscosity η and κ the thermal conductivity a full set of equations can be written. In all three cases, the integrals over $I_{coll}(f)$ will vanish by the virtue of conservation of atoms, momentum and energy. On the right side of Eq. (4.15)-(4.17) a loss term Γ has been added and the space and time indicator (z,t) has been omitted. The conservation of particle

$$\frac{\partial}{\partial t} n + \frac{\partial}{\partial z}(nu) = -\Gamma n \tag{4.15}$$

The conservation of momentum

$$M\frac{\partial}{\partial t}(nu) + \frac{\partial}{\partial z}\left(n\left(k_B T + M u^2\right) - \eta\frac{\partial}{\partial z} u\right) + n\frac{\partial}{\partial z} V = -M\Gamma n u \tag{4.16}$$

The conservation of energy

$$\frac{\partial}{\partial t}(nE) + \frac{\partial}{\partial z}\left(u\left(n\left(E + k_B T\right) - \left(\eta\frac{\partial}{\partial z} u\right)\right)\right) - \frac{\partial}{\partial z}\left(\kappa\frac{\partial}{\partial z} k_B T\right) = -\Gamma n E \tag{4.17}$$

The viscosity can be defined as [23]

$$\eta = \eta_0 \Sigma M \sqrt{\pi}\sqrt{\frac{k_B T}{M}}\frac{1}{\sigma} \tag{4.18}$$

and the thermal conductivity as

$$\kappa = \kappa_0 \Sigma \sqrt{\pi}\sqrt{\frac{k_B T}{M}}\frac{1}{\sigma} \tag{4.19}$$

where the surface of the beam Σ is defined as the area, where the density is larger than $1/e$ of the peak density:

$$\Sigma = \pi\left(\frac{k_B T}{\lambda}\right)^{\frac{2}{\gamma}} \tag{4.20}$$

with λ is the gradient of the potential: $V(\rho) = \lambda\rho^{\gamma}$.

γ	Thermal conductivity κ_0	Viscosity η_0
1	99	15.66
2	5.98	1.56
∞	1.2	0.42

Table 4.1: Thermal conductivity and viscosity as a function of confinement.

The initial coefficients η_0 and κ_0 can be found by evaluating Eq. (4.11) through the Chapman-Enskog procedure (see Ref. [24]).
The result can be seen in Tab. 4.1. Here $\gamma = (1, 2, \infty)$ in a linear guide, a harmonic guide and hard wall potential respectively. As can be seen the thermal conductivity and viscosity increases dramatically due to the inhomogeneous distribution. In the linear case, the increase in thermal conductivity is two orders of magnitude. A large thermal conductivity limits the achievable temperature gradient, which is needed to reach degeneracy. For a beam based atom laser it is important that heat does not transfer from upstream, hot atoms to already colder atoms downstream. The hot atoms spiraling around the beam, will travel downstream and eventually collide with much colder atoms, heating them up again. This will lead to a less effective cooling towards degeneracy.
The enhancement of the thermal conductivity and viscosity can be interpreted as an increase of the effective surface of the beam with respect to Σ: $\Sigma_{\kappa,eff} = \kappa\Sigma/\kappa_{\gamma=\infty}$. For a linear confinement, we found $\Sigma_{\kappa,eff} = 82.5\Sigma$, which is surprisingly large. Evaporative cooling on the guide wires will removed these outer spiralling atoms leaving the colder atoms one behind.

The following boundary and initial conditions apply:

$$n(0,t) = n(z,0) = n_0 \qquad u(0,t) = n(z,0) = u_0 \qquad T(0,t) = T(z,0) = T_0$$

$$\frac{\partial}{\partial z}u(z_{max},t) = 0 \qquad \frac{\partial}{\partial z}T(z_{max},t) = 0$$

The atoms are injected from the left at supersonic velocity. They are accelerated on the downward slope (if present) and slowed down to subsonic velocities on the potential barrier created by the magnetic coil situated 3 meter down the guide. At the crossover between the supersonic and subsonic beam is a shock wave. The characteristics of the shock wave, such as width and density increase is determined by the damping processes and the initial Mach number.

4.4.2 The motion of the shock wave

As previous there is an incoming flux of particles from the left moving towards the right with a certain supersonic velocity. The beam direction is reversed at the barrier, which is in this case a magnetic coil. The beam returns and collisions between atoms in the two beams occur resulting in a shock wave that moves from the right to the left.

Figure 4.14 shows the shock wave developing in time and moving from the right to the left in a horizontal guide resembling the experimental setup. As the shock wave propagates through the system the beam velocity drops to an almost zero and the density increases. Note that the density increase is the same

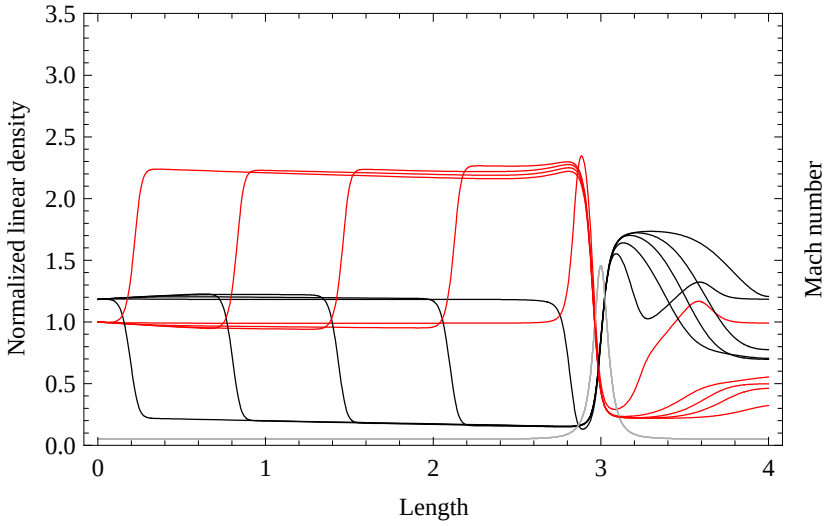

Figure 4.14: The shock wave developing, moving from the right to the left in a horizontal potential

as the density increase of Fig. 4.9, as expected since all simulations starts with the same initial conditions. Close to the barrier the density is slightly larger, which is due to the contribution from atoms rolling back from the barrier. The simulation on the right side of the barrier is not relevant, since this part is strongly governed by the boundary conditions.

In the experiment we set the probe laser at fixed positions on the guide and observe the density increase as a function of time. Fig. 4.15 shows what we should expect as a function of time. Notice how the width of the shock wave does not change as a function of position and that the density stays constant after the shock wave has passed by. The shock wave moves with a constant velocity through the guide with conditions before and after the shock wave, that are independent of position. In the co-moving frame the shock wave does not move and the incoming flux and the outgoing flux obeys the shock wave relations from Eq. (4.6)-(4.8), except for the additional loss rate. Passing the shock wave both the drop in Mach number and increase of density is seen, following Fig. 4.6(a).

By tilting the guide the shock wave occurs as before, but the continuous density increase is due to the gravitational compression from the tilt. Figure 4.16 shows the shock wave for different heights h at the same time t. Notice how the Mach number is the same for all heights of the barrier, but the drop of Mach number over the shock wave is not the same. The lower the external potential the larger acceleration of the supersonic beam and hence larger supersonic Mach number. This gives a larger density increase than with the horizontal guide. Notice how the shape of the shock wave does not change, confirming that the width of the shock wave is independent of the external potential.

Figure 4.17 shows the development of the shock wave at the same time steps as in Fig. 4.14. The shock wave does not propagate as far to the left as in a

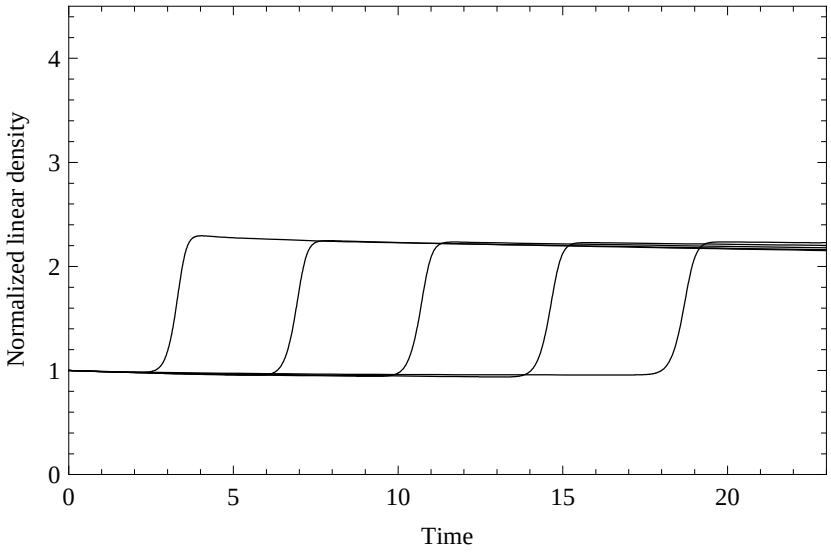

Figure 4.15: Shock wave moving in a horizontal guide. Observed at different positions z=0.5 1 1.5 2 2.5 m.

horizontal guide. This is because atoms pile up at the bottom of the potential and the density increase due to the gravitational compression. Notice how the velocity of the shock wave slows down. The shock wave can come to a standstill if the losses from the beam is large enough. However, this has never been observed in the experiment. Also, initially the density increase is larger, before a density equilibrium point is reached between the pressure from gravity and the pressure from the incoming beam. The extra increase is from atoms returning on the barrier. As can be seen the density increase from the gravitational compression is a much more effective than the density increase from the shock wave.

Figure 4.18 shows the motion of the shock wave at different positions at a fixed height. Again an increase of density due to the shock wave and the gravitational compression is clear observable. However, the density increase from the gravitational compression is continuous but limited by the pressure at the beginning of the guide. Notice how the shape of the shock wave does not changes.

4.4.3 No losses, no damping

The shape of the shock wave will change if the collision cross section changes. The collision cross section is determined by the thermal conductivity and the viscosity. They are both damping processes.

The effect of the damping processes is evaluated at a certain time t. Figure 4.19 shows the hydrodynamical simulation with a sloped guide of 10 cm, no damping process ($\eta = 0$, $\kappa = 0$) and no losses ($\Gamma = 0$). The Mach number resembles an initial velocity $u_0 = 0.7$ m/s and temperature $T_0 = 1.4$ mK and the conditions for the ideal case (see Sec. 4.2). Figure 4.19 overlaps with Fig. 4.8, the ideal case. This shows that the hydrodynamical equations can be used to understand the changes of the system. With a low damping rate it can be seen

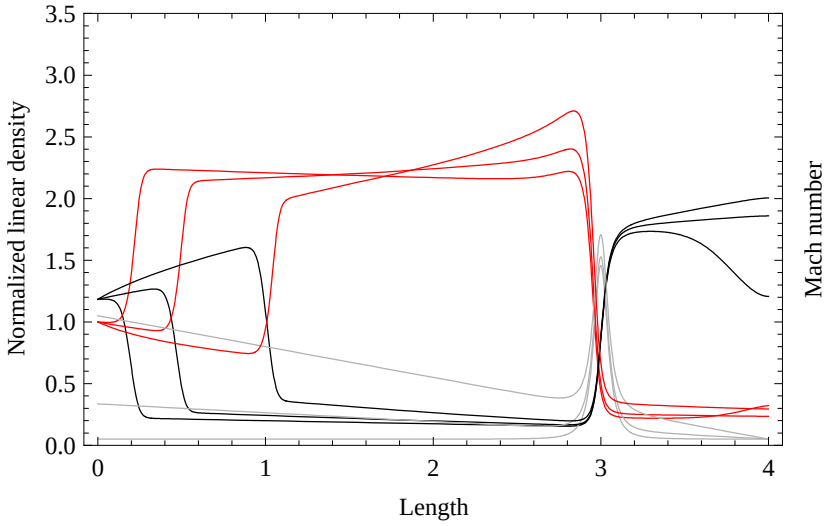

Figure 4.16: The change of potential h=0, 2 cm, 7 cm at a time t. Notice that the density increase from the shock wave is the same, but the final density is larger with a larger compression

that the shock wave become very step and close to stepwise. Initially the beam is supersonic and accelerated down the slope leaving the beam more diluted at the shock wave. The beam changes characteristics and becomes subsonic with an increasing density on the downward slope.

4.4.4 Loss rate

If the loss rate is large enough the shock wave can be stabilized independent of the shape of the potential. Atoms can escape from the guide due to background collisions, evaporative cooling or a finite height of the end barrier. In figure 4.20 the effect of the change of loss rate is shown. Both curves are at the same time step t. Only the density changes, the shape of the shock wave does not. However the gravitational accumulation is affected. If there is no loss the beam velocity will go to zero since there is no place the atoms can escape to.

4.4.5 Damping processes

Figure 4.21 shows the effect of the change of the damping rate at time t. The lower the damping rate the stronger the shock wave becomes. The only property that determines the width of the shockwave is the rate of the damping process. Notice that changing the flux corresponds to the change of damping process rate.

Discussion

To explain the motion of the supersonic atom beam propagating in the 1D magnetic guide the hydrodynamical equations are set up from the Boltzmann trans-

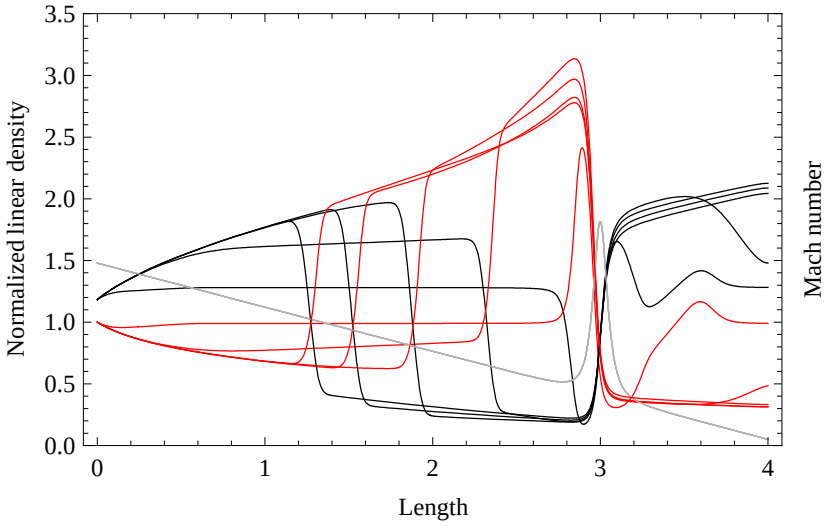

Figure 4.17: Shock wave moving in a sloped guide h=10 cm, at the same time t as the horizontal guide (see Fig. 4.14). Notice how shock wave moves slower due to compression as the guide is filled up.

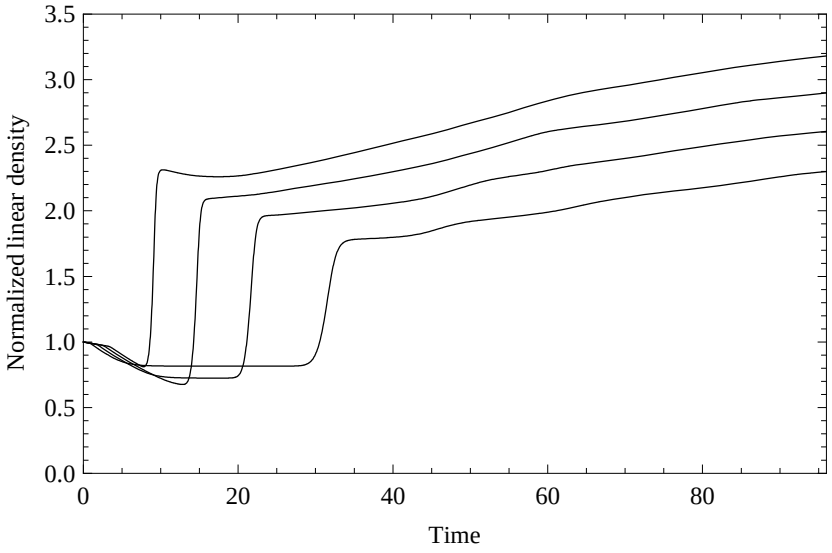

Figure 4.18: Shock weave moving in a sloped guide h=10 cm, observed at different positions z=0.5,1,1.5,2

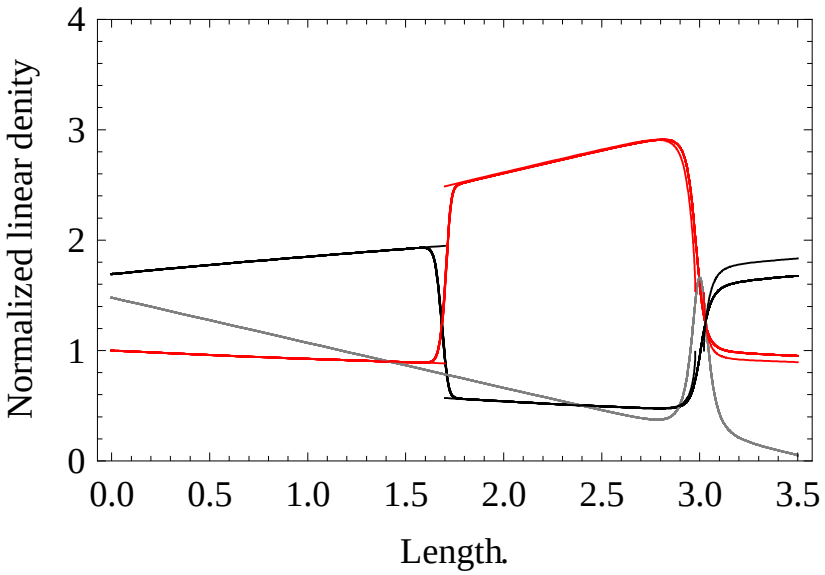

Figure 4.19: Hydrodynamical simulation with no losses and no damping processes, $\eta = 0$ and $\kappa = 0$. The grey curve is the potential. The black curve is the mach number and the red curve is the density. The simulation overlap with flow continuity flow figure 4.8.

port equation. The development of the supersonic beam moving in a returning potential and thus creating a subsonic beam is investigated. The development of the shock wave in the guide is initially because a few atoms slow down to subsonic velocity. Thus creates a shock wave. New incoming supersonic atoms collide with the shock wave/slower atoms and enhances the shock wave, letting it grow. It is shown that the density increases and the Mach number decreases over a shock wave. Further more it is shown that adding a downward slope increases the density after the shock wave. This is due to gravitational compression. Finally it is shown that the shape of the shock wave is independent on the initial velocity and the change of external potential and only dependent on the damping process.

4.5 Resume

Four models have been presented each describing the features of a shock wave. The first model lets us understand how the density increases due to collisions and that a simple pile-up wave will be created that moves towards the source. The second model lets us understand how the transition between supersonic and subsonic flow happens through a shock wave. It is shown that a large density increase through a shock wave can be achieved and a larger density increase can be achieved through gravitational compression. In the third model the collision between two supersonic beams are investigated. It is found that solely through collisions a subsonic beam emerges with a shock wave separating

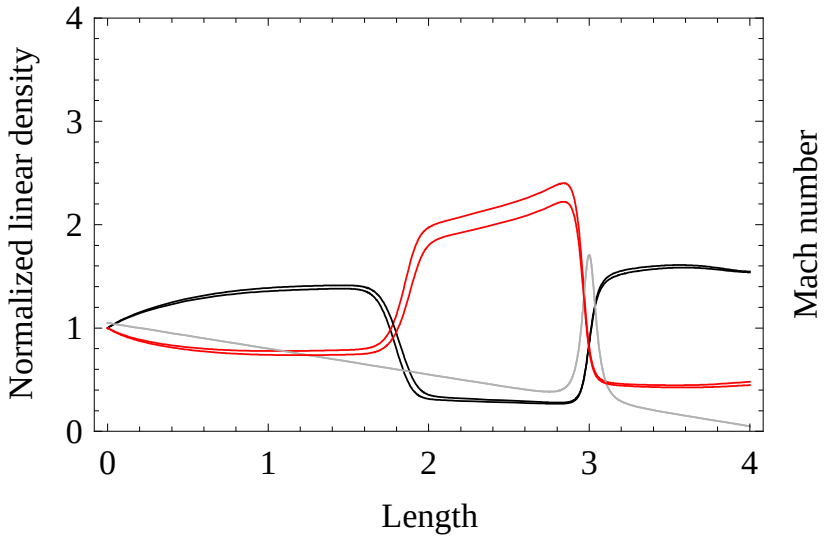

Figure 4.20: Shock wave with and without losses at time t.

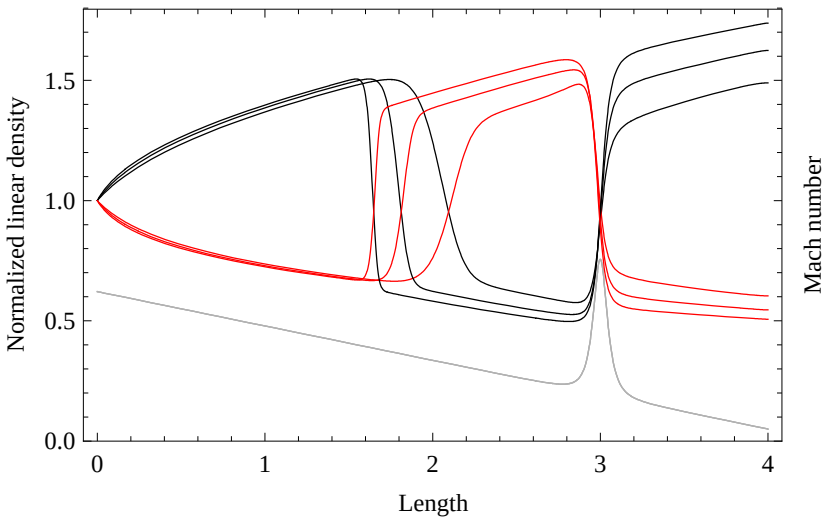

Figure 4.21: Shock wave at damping rates $100\%, 50\%, 25\%$ with losses at time t. The lower the damping rate the stronger the shock wave becomes.

the two regimes. The width of the shock wave is found to be governed by the collision rate and the density increase is governed by the initial velocity. Furthermore it is found that the shock wave can be stabilized by only having collisions in a well-defined area. This only adds to the density increase. In the fourth model the hydrodynamical equations are used to understand the motion of a supersonic beam moving in the potential of the magnetic guide. It is found that a subsonic beam is created from atoms decelerating through an increasing potential or through collisions. The shock wave can be created on any potential. The density increase through the shock wave is larger and is enhanced with gravitational compression. In the guide loss of atoms can occur and it is found that only the density increase is affected by losses. It is found that the guide potential and initial velocity determines the density increase, whereas the damping rate determine the width of the shock wave.

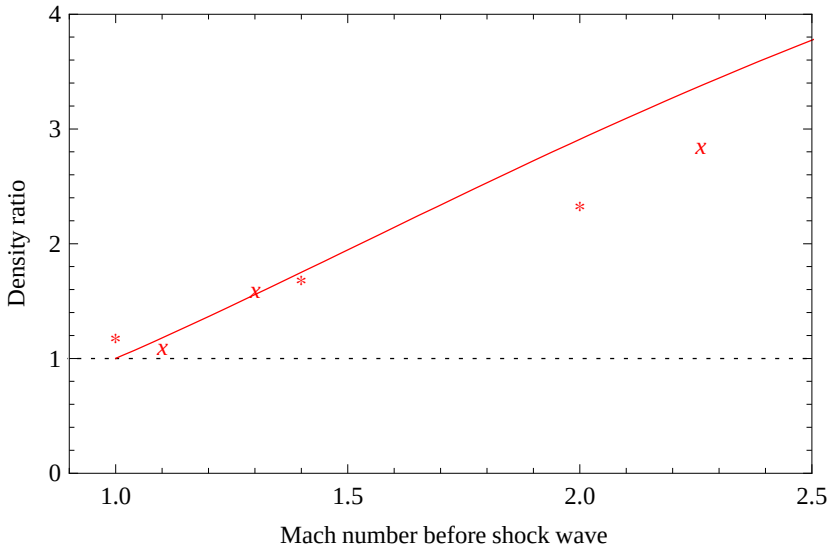

Figure 4.22: Density increase in a horizontal guide as a function of Mach number for the last three models. The solid red line is the density increase from the flow continuity model, the "$*$"'s are from the Boltzmann model and the "x"'s are from the hydrodynamical model.

The last three models simulates the development of the shock wave in the horizontal guide show a density increase. Figure 4.22 shows the density increase for each model. We understand from the theoretical side the evolution of the shock wave.

CHAPTER 5

The shock wave driven atom laser

We have build the experimental setup with a 4 meter magnetic guide. We can load atoms into the guide with a flux of 1.2×10^{11} atoms/s. We have a theoretical understanding of how a shock wave is created in the guide. This chapter describes the experimental verification of the shock wave.

This chapter is based on a publication for Science.
Authors: L. Kindt, P.C. Bons, K. van Aken, P. van der Straten, J. M. Vogels

Abstract
Shock waves are abiquitous in astrophysics, aerodynamics and liquids, when matter moves faster than the speed of sound. Shock waves are utilized to increase the density of a medium, for example in ramjets. Here we demonstrate the use of a shock wave to slow down and compress a magnetically guided, supersonic beam of atoms. Due to the ability of optical absorption techniques to measure the density, velocity and temperature of the atoms, the physics of shock waves in a unique, dilute regime can be studied. After the shock wave the subsonic atomic beam is gravitationally compressed. By extracting the beam in packets we are able to perform evaporative cooling to degeneracy, generating a pulsed atom laser. We expect that all future continuous atom lasers will be based on shock waves.

An atom laser is a beam of Bose condensed atoms, which due to the ultimate control over the atoms is very interesting for atom optics [25], atomic clocks [26], precision measurements of fundamental constants [27, 28], tests of fundamental symmetries [29], and atom lithography [30]. The first atom lasers [1, 31, 2, 32] consisted of atoms coupled out from a cloud of condensed atoms limiting its applicability, since the condensate is rapidly depleted due to the outcoupling. Schemes have been implemented to replenish the condensates during the outcoupling, but these are difficult to implement and only result in small sustained fluxes [33, 34]. An alternative idea is to channel atoms into a magnetic guide, which can be cooled down to degeneracy [35]. This idea has been implemented in several experiments [18, 36, 37, 38]. However, this approach appears futile, since the evaporative cooling to degeneracy requires several hundreds of collisions, where in the most promising experiment only thirty could be achieved [39]. Here we slow down and compress the beam using a shock wave. The shock wave is robust, reproducible, stable, and improves the evaporation efficiency dramatically. Due to the shock wave we can use gravitational compression and combined with the shock wave it leads to an increase of both the collision rate and the traversal time through the cooling section by more than one order of magnitude. This leads to an increase of the number of collisions by two orders of magnitude. The resulting densities and temperatures of the beam are adequate to cool the atoms down to degeneracy using evaporative cooling, but the cooling is restricted due to heat conduction of the hot part of the beam to the cold part. We show that the beam can be cooled to degeneracy by transferring part of the beam periodically out of the subsonic region to an insulated cooling region, which results in a pulsed atom laser. Due to the large increase of the number of collisions we expect that the next generation of continuous atom lasers will rely on the use of shock waves.

A shock wave is a surface of discontinuity in the flow of matter, where the flow abruptly changes from supersonic to subsonic behavior. This is characterized by marked increases in temperature, pressure, and density. In our setup the shock wave is generated due to collisions between two counterpropagating beams of supersonic atoms creating a region of subsonic atoms. The first beam is created by launching atoms supersonically into the guide. The second beam is created by reflecting the first beam at the end of the guide using a magnetic barrier. After the generation of the shock wave near this barrier, atoms hitting the shock wave are slowed down and accumulate in the subsonic region. As a result the density in the subsonic region increases and this pushes the shock wave upstream. It generates a dense, subsonic beam in its wake with an increased density and collision rate and a reduced speed compared to the supersonic beam. The shock wave stabilizes in the beginning of the guide, where the radial confinement is weaker.

The situation for magnetically guided atomic beams is unique, since the beams are hydrodynamic in the axial direction, whereas they are collisionless in the radial direction. Furthermore, in contrast to other cases of hydrodynamic behavior, the microscopic interactions between the particles are well-known and this allows for a complete modelling of the hydrodynamic features. In the usual case the temperature and density after the shock wave are given by their stagnation values, which are mainly determined through the flux conservation of particles, momentum and energy through the shock wave. In our case we can after the shock wave compress the beam above the stagnation density using

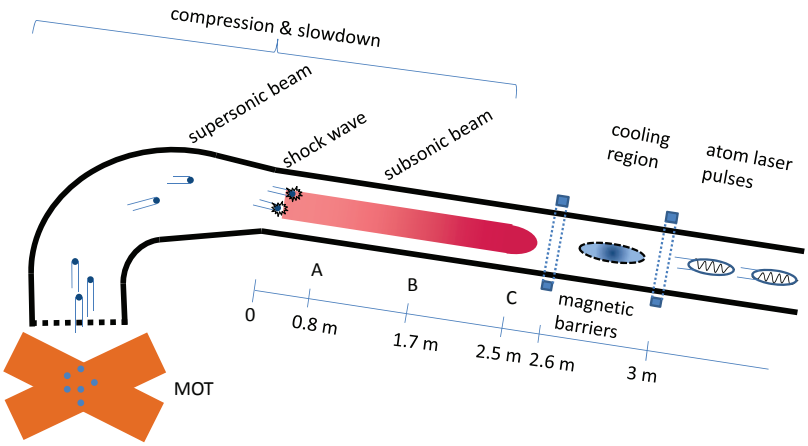

Figure 5.1: Schematic overview of the setup. Atomic packets launched from the MOT at supersonic velocities and hit the shock wave resulting in a reduction of the beam speed to subsonic speeds. Subsequently the beam is gravitationally compressed to obtain sufficient high collision rates for cooling to degeneracy. Beam packets are extracted, cooled to degeneracy using rf-induced evaporative cooling and released from the cooling region.

gravitational compression as well as cool the beam below the stagnation temperature using evaporative cooling. All these features play a crucial role in improving the performance, stability and feasibility for cooling to degeneracy. Due to the well-developed imaging techniques for cold atoms, by which one can study locally and temporally the density, velocity and temperature in the guide, our system allows for a detailed research of the shock wave in this unusual regime. Shock waves in ultra-cold, degenerate matter, where the system is hydrodynamic in all directions, have been observed by several groups [40, 41], but in that case the shock wave only led to heating of the cloud.

The magnetic guide is 4 m long (see Fig. 5.1) and consists of rods carrying currents producing a two-dimensional quadrupole field to guide the atoms. The guide is loaded with ^{87}Rb atoms, which are launched up in packets from a magneto-optical trap (MOT) and enter the horizontal part of the guide with a speed of $v_b = 0.7$ m/s. The flux of the atoms is $1.4 \times 10^{10}/s$ at a temperature of $T = 1.2$ mK. At the beginning of the guide the magnetic field gradient increases gradually by a factor of 13. The slope of the guide is adjustable by tilting the guide. At the end of the guide there are two coils, which can act as a magnetic barrier for the atoms. Under these conditions the speed of sound $c = 0.4$ m/s is below v_b and thus the initial beam is supersonic.

One of the key features of a shock wave is that it converts a supersonic beam into a subsonic beam. In the *supersonic* case $v_b > c$ and atoms are predominantly moving downstream. In the *subsonic* case $v_b < c$ and a significant fraction of the atoms can temporarily move upstream. This can be used to determine the velocity of the beam. Atoms in a certain region are optically pumped to an untrapped state and can no longer be imaged. After a certain time the atoms at the edges are replenished from the upstream and downstream side and from

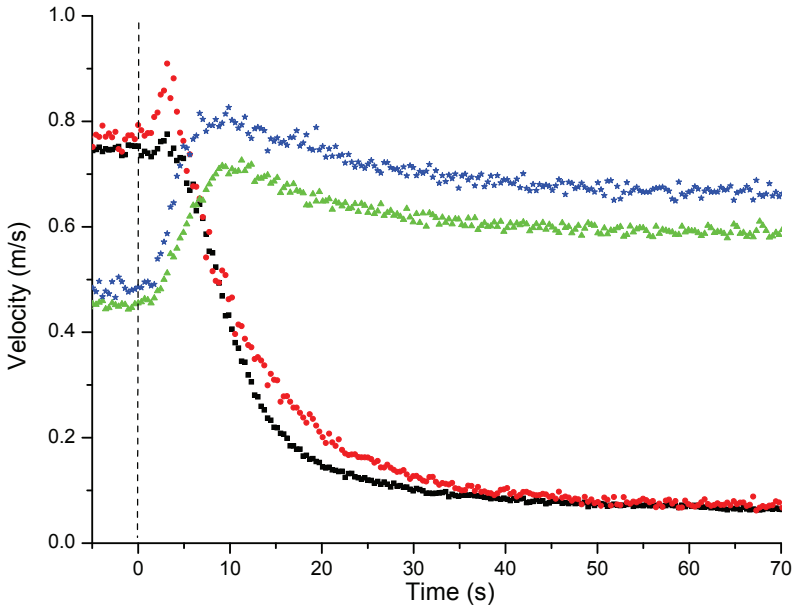

Figure 5.2: Beam velocity v_b and speed of sound c measured at point A as a function of time after the magnetic barrier is turned on at t=0. Results are for full flux (black squares (v_b) and green triangles (c)) and for half flux (red circles (v_b) and blue stars (c)). When the shock wave develops the beam velocity v_b drops below the speed of sound c and the temperature increases. In the case of full flux the shock wave develops faster than the case of half flux, leading to a faster decrease of the beam velocity and a faster rethermalization.

an absorption image of the region we can determine the velocity distribution of the beam. Its center yields the mean velocity and its width is a measure for the temperature of the atoms.

In Fig. 5.2 the beam velocity v_b and speed of sound c measured at point A (see Fig. 5.1) are plotted for different fluxes of the beam, where at $t = 0$ the barrier is switched on. For full flux the beam velocity drops, once the supersonic atoms return from the barrier at $t \approx 5$s. Collisions between atoms from the two counterpropagating beams produce a shock wave, which leaves atoms with subsonic speeds behind. At the same time the axial temperature and therefore the speed of sound increase. The incoming supersonic atoms are further suppressed by collisions with the subsonic atoms, which reduces the beam velocity even further. In the shock wave the atoms are not in thermal equilibrium and when the shock wave develops the axial and radial temperature become more in equilibrium causing a reduction of the axial temperature. The results clearly show that the shock wave converts the incoming beam of supersonic atoms ($v_b > c$) to a beam of subsonic atoms ($v_b < c$). For half flux the situation is comparable to full flux, although relatively more supersonic atoms return from the barrier and they are inadvertently detected as fast moving downstream atoms. This results in an apparent increase of the beam velocity and an apparent stronger initial increase in the temperature. Notice that the reduction of the beam velocity is

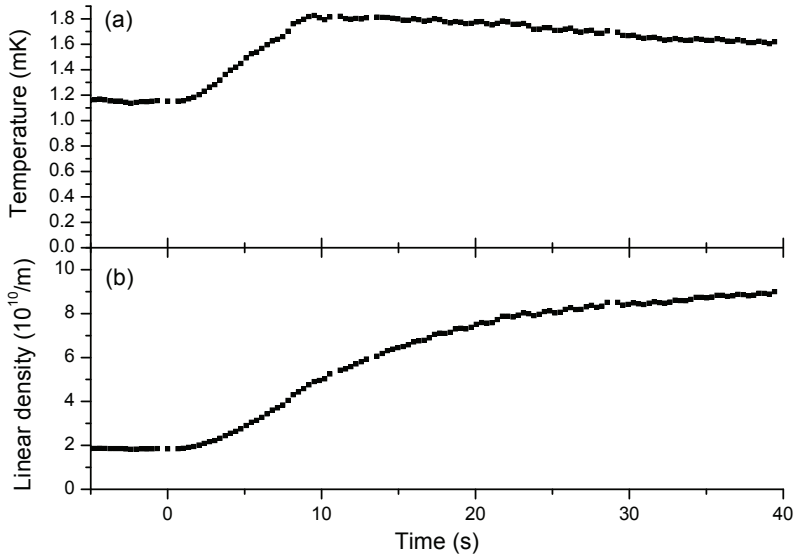

Figure 5.3: Radial temperature (a) and density (b) of the atoms in the beam, as measured using absorption imaging of the beam. At $t = 0$ the barrier is turned on. The increase of the temperature in the period up to $t = 10$ s is due to the shock wave, whereas the decrease for longer times is due to evaporative cooling.

faster for the case of full flux compared to half flux and this is to expected, since the shock wave develops faster under more hydrodynamic conditions. The data shows that our system allows for a detailed observation of the thermodynamic properties during the shock wave, which is not easily achieved in other cases.

Complementary to the measurements of Fig. 5.2 the radial temperature and density are measured again at point A by imaging the absorption of the beam as a function of time (see Fig. 5.3). In order to obtain sufficient accuracy the images are recorded at several detunings and from the combined images the radial temperature and the density of the atoms can be determined (see Supplementary information). After the initial increase of the radial temperature for a period of 10 s, the temperature decreases, which we attribute to evaporative cooling in the guide. The ratio η for the evaporation process between the depth of the guide and the radial temperature reaches a value of $\eta \sim 6$ at $t = 10$ s, which is sufficiently low for the evaporative cooling of the atoms against the guide rods to be effective. The evaporative cooling leads to an inhomogeneous temperature in the guide, where the atoms at the end of the guide have the lowest temperature. The combined effect of the shock wave and the evaporative cooling lead to an increase of the linear density, by a factor $\sim$5 under the circumstances of Fig. 5.3. Note that for collisionless behavior in the guide the increase can not exceed a factor of 2, since after switching on the barrier atoms are also moving upstream instead of only moving downstream. This is another clear signature of the shock wave. The atoms are retained in the guide due to the kinetic pressure of the incoming atoms. If we stop launching the packets of atoms from the MOT, the number of atoms in the guide quickly diminishes.

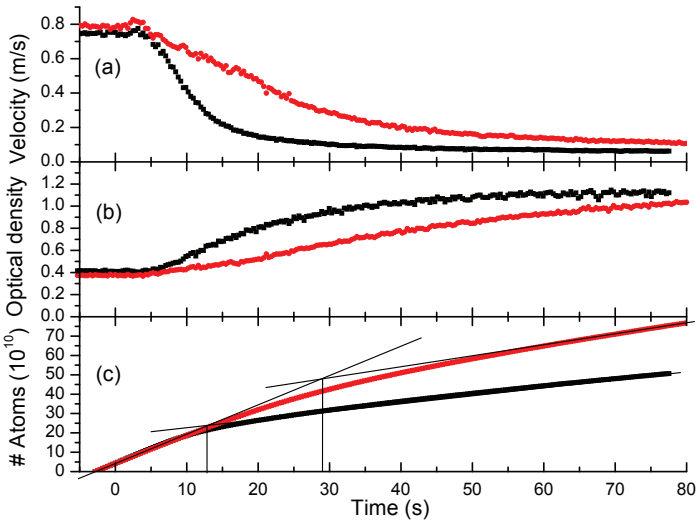

Figure 5.4: Beam velocity (a), optical density (b) and number of atoms (c) for a horizontal guide (black squares) and a guide with a downward slope of 5 mrad (red circles). The barrier is turned on at $t = 0$. The beam velocity and optical density indicate that the shock wave appears later in the tilted guide compared to the horizontal guide. From the beam velocity and optical density we can derive the number of atoms, which pass by the detector at point A. In the tilted guide the accumulation of atoms occurs over a longer period, which leads to a larger accumulation of atoms in the guide compared to the horizontal guide.

Tilting the guide downwards has a dramatic effect on the shock wave. In Fig. 5.4 we compare the beam velocity and optical density at point A for a horizontal guide with the same measurement on a tilted guide. As can be seen from the beam velocity and the optical density, the shock wave appears later when the guide is tilted. From these two parameters we can derive the number of atoms, that have passed the detector at point A and accumulate in the guide. In both cases the initial flux (the slope of the number of atoms) is identical and the loading rate does not depend on the tilt of the guide. However, the growth of the number of atoms in the guide continues longer for the tilted guide compared to the horizontal guide. Thus more atoms accumulate in a tilted guide, which we refer to as gravitational compression. Gravitational compression is caused by the weight of atoms accumulating at higher elevation and works in our guide due to two reasons. First, the gravitational energy of the atoms for a guide that is tilted a few cm downwards is comparable to the thermal energy. Second, the shock wave has converted the supersonic beam into a subsonic beam and gravitational compression on a downward slope only works for subsonic atoms. This has to be contrasted to slowing a supersonic beam on an upward slope [39], where the slowing is limited to the speed of sound. Here we can slow the beam down to arbitrary low velocities. The straight lines indicate the situation for a discrete shock wave in the hydrodynamic limit. The slope of the number of atoms for long times are determined by the loss of atoms in the guide due to evaporative cooling. The increase of the slope for a tilted guide compared to a horizontal

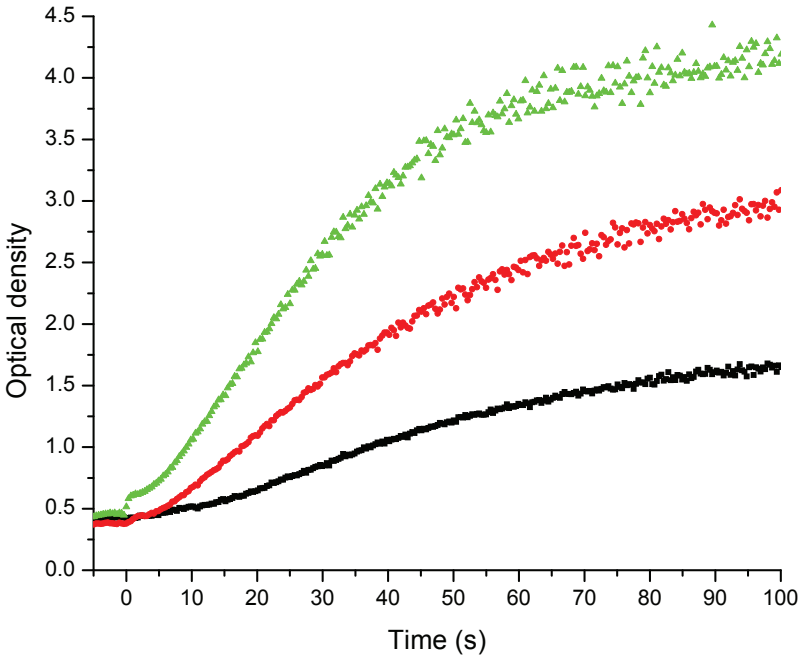

Figure 5.5: Growth of optical density on resonance after the barrier is turned on at $t = 0$ for different positions in the guide with a downward slope of 5 mrad. Positions: point A (black squares), point B (red circles) and point C (green triangles). Due to the gravitational compression there is an increase in the density by nearly a factor of 3 at the lowest point (point C) compared to the highest point (point A).

guide is due to the larger number of atoms in a tilted guide and not by a higher loss rate, which we have confirmed by carefully analyzing the data. Figure 5.4 is a clear signature for the hydrodynamic behavior of our atoms in the guide and together with the results of Figs. 5.2 and 5.3 striking evidence for the appearance of a shock wave. Roos *et al.* [42] discuss a theoretical model for the loading of a non-dissipative trap using collisions between incoming atoms and atoms already present in the trap. Although they obtain similar results as presented here, their results depend on the use of different evaporation thresholds in the axial and radial direction and do not rely on the use of a shock wave. Their approach will not lead to compression in the horizontal guide.

One of the issues that remains to be discussed is the stabilization of the shock wave, which is evident from the experimental results. Under normal conditions the shock wave is expelled from the guide in a converging geometry like ours. This behavior, which is referred to as inlet unstart, relieves the kinetic pressure on the atoms in the guide and all subsonic atoms will flow back to the MOT region. This does not play a role in our experiment, as is evident from the continuous increase in the density in Fig. 5.3 even after the shock wave has reached the beginning of the guide. We think that inlet unstart is not happening in our guide, because the mean free path at the entrance of the guide exceeds the distance to the MOT, causing excess atoms to leak back to the MOT.

This stabilizes the shock wave and thus maintains the kinetic pressure on the atoms in the guide. One of the key properties here is the fact that our beam is guided using a conservative potential and that the beam in the guide is radially collisionless, which allows for rapid transition from hydrodynamic behavior in the guide to collisionless behavior at the entrance of the guide in the axial direction.

The use of a shock wave in our experiment yields several advantages for the cooling of the beam. First of all, the beam is reduced to subsonic speeds, which increases the traversal time considerably. The densities are increased, which leads to a higher collision rate. But, what is most important, the shock wave allows us to exploit gravitational compression, which further increases the density. In Fig. 5.5 the optical density is shown at different positions in the guide. The density increases towards the end of the guide, which is another sign of gravitational compression, whereas the density gradient is small in a horizontal guide. Note that the optical density is approximately proportional to the collision rate of the atoms (see Supplementary information), which grows at the end of the guide by more than an order of magnitude. Tilting the guide leads to an increase of the accumulation time of the guide (as seen from Fig. 5.4) and thus to an increase of the number of atoms in the guide. Under these conditions we have accumulated 5×10^{11} cold atoms in the guide, which is more than an order of magnitude larger than the traditional way of loading a magnetic trap [15]. Shock wave assisted loading thus also is a promising route for continuous loading of a conservative trap without the use of nearly resonant light [43] or the use of atom specific dark states [44], where the loading times are limited by light scattering to below a second.

Converting the beam to subsonic speeds completely changes the paradigm in the requirements and achievable performance of a continuous atom laser. For cooling a supersonic atom beam a guide length of hundreds of mean free paths is required, but for a subsonic atom beam strictly only the width of a shock wave (a couple of mean free paths) is needed. For a subsonic beam there is no longer a direct proportionality between the distance traveled and the collision rate so the length of the cooling region can be neglected. The use of gravitational compression is only achievable due to the low temperatures in our setup. The limits of gravitational compression are not clear, as a larger slope should always result in higher densities. Our experimental results show that this is not true in practice.

To show that the conditions in the guide are sufficient to cool the beam down to degeneracy, we have employed rf-induced evaporative cooling on the atoms in the guide. Cooling all the atoms in the beam down simultaneously using different rf-stages [39] is a challenge for a subsonic beam. First of all, the cooling has to be performed on an upward slope to compensate for the decreasing number of atoms, since the behavior of the subsonic beam is dominated by hydrodynamic pressures. Secondly, the heat conduction through the beam can be prohibitively large [45], which limits the temperature gradient in the guide. Heat conduction in subsonic beams has a large influence on the attainable temperature gradient, whereas it does not play a significant role for supersonic beams. To circumvent these problems, we have extracted about 20% of the atoms from the reservoir by temporarily lowering the first barrier and trapping them between the first and second barrier (see Fig. 5.1). These atoms are evaporatively cooled for 95 s to degeneracy and subsequently released further into the guide, leading

to a pulsed atom laser [1]. A long evaporation time is used, since our guide is not optimized for evaporation using a single rf-frequency. The procedure of extracting atoms is repeated and this way we have created a pulsed atom laser with each packet containing 10^7 atoms. This method can be further optimized by using *several* moving barriers, in which the evaporation can take place, thus effectively creating a conveyor belt scheme, which allows for the creation of a continuous atom laser [46]. Note that the complications and limitations for loading the conveyor belt using a supersonic beam, as identified in that work, are not present if a subsonic beam is used. Based on our loading flux of the guide and usual evaporation efficiencies [15, 47] the expected flux of the atom laser will be 2×10^7 atoms/s, which is about two orders of magnitude increase compared to the "traditional" way of producing Bose-condensed atoms. Such an atom laser beam can be adjusted to be either supersonic or subsonic, pulsed or continuous and thus can be considered as a "universal" atom laser. A transition from the subsonic to the supersonic regime constitutes a black hole for the elementary excitations (phonons), and as such generates a version of Hawking radiation [48]. Phenomena to be studied are cosmological inflation [49], trans-Planckian physics [50] and black hole lasers [51].

In conclusion, we have created a shock wave that allows for the conversion of an incoming supersonic beam to a dense, subsonic beam. Due to the shock wave the collision rate in the beam can be increased dramatically using gravitational compression and evaporative cooling. We have used magnetic barriers to repetitively split off part of the beam and cool it to degeneracy in a very short distance to create atom laser pulses. In combination with a conveyor belt the present setup can be used to generate a continuous atom laser with a flux rate of condensed atoms as high as 2×10^7 atoms/s. The use of a shock wave makes the atom laser robust, reproducible, and stable. The large increase in the number of collisions due to the shock wave makes the production of a sustainable continuous atom laser viable.

Supplementary information

Setup – Our primary atom source is a recirculating oven [47] heated to a temperature of 430 K with an aperture with a diameter of 6 mm, which generates a flux of 8×10^{12} atoms/s through a hole with a diameter of 36 mm close to the MOT chamber. A Zeeman slower slows atoms down to a velocity of 30 m/s for loading into the MOT. The MOT capture rate is 4×10^{11} atoms/s, which is a factor of 20 higher compared to Ref. [36]. During a period of 80 ms we capture about 3×10^{10} atoms. The atoms are launched in packets with a frequency of 6 Hz into the guide. The cloud is pre-shaped into an elongated cloud before launching for 30 ms and accelerated in upward direction for 10 ms to 2.4 m/s using a moving molasses. The magnetic field is switched off and the detuning of the cooling lasers is increased to -60 MHz leading to a temperature of the cloud is 0.09 mK. A transient two-dimensional quadrupole field is mode-matched at 0.6 T/m to the cloud and ramped up in 44 ms to 1.7 T/m forcing the atoms into the guide. In this procedure we manage to compress, launch, cool, and spin polarize about 6×10^9 atoms per packet.
The four meter long guide consists of four rods of copper tubing with a diameter of 6 mm with a spacing of 2 mm. The tubes are cooled by water pumped with a pressure of 10 bar through the core with a diameter of 4 mm. The maximum gradient of the guide is 20 T/m at a current of 800 A, but we typically operate at a current of 550 A leading to a gradient of 13 T/m. To avoid spin-flips in the center of the guide a longitudinal bias field of 0.7 mT is used. The guide in a Corning 7740 Pyrex tube is pumped by ion pumps of 50 l/s at both ends. In the tube a SAES st707 NEG strip is used to lower the pressure. The lifetime due to background collisions is ∼400 s, indicating a pressure below 5×10^{-12} mbar in the guide. Two barrier coils at the end of the guide can provide a bias field of 40 mT.
To adiabatically transfer the atoms from the pre-guide into the guide, the gradient at the entrance of the guide is slowly increased from 1 T/m to 13 T/m. To achieve this the four rods in the guide are partially shorted in the beginning using twelve segments. Furthermore, in the beginning the spacing between the rods is 10 mm, which is reduced to 2 mm after 30 cm. After launching vertically for 15 cm the trajectory of the atoms is bent to horizontal in a 5 cm radius. The final velocity is 0.7 m/s and the temperature in the guide is 1.1 mK. We find a loading efficiency of 1/3 for the atoms launched towards the guide. In a guided beam the speed of sound is given by $c = \sqrt{9k_BT/7M}$, which is 0.4 m/s under our conditions.
Cooling to degeneracy – The collision rate of the shock wave assisted loading is ∼70 Hz, which is high enough to cool the atoms to degeneracy. However, there is a trade-off between loading and evaporative cooling. For optimal evaporative cooling the gradient should be reduced during the cooling cycle from 8 T/m to 2 T/m, which reduces the three-body decay. At the end of the cycle the atoms are trapped in an harmonic trap with trap frequencies of 0.6 x 70 x 70 Hz. Although this trap is not optimal for the evaporation, we are able in 95 s to generate nearly pure condensates of 2×10^7 atoms, which is to our knowledge comparable to the largest rubidium Bose-Einstein condensates [15]. Our current flux of condensed atoms is around 10^5 atoms/s. Limitations are the compromise for the gradient between the loading and the evaporation, and the propagation of the rf-signal along the guide or the NEG strip. These limitations should be

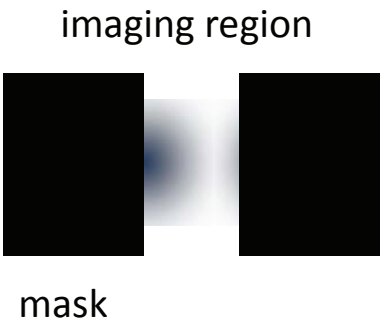

Figure 5.6: Setup for the detection of the velocity distribution.

taken into account in the design of future atom lasers.

Probing the velocity distribution – The velocity distribution in Figs. 5.2 and 5.4 is determined by depleting atoms in a 4 mm region (see Fig. 5.6) by illumination for 1 ms with light detuned -8 MHz from the $5^2\mathrm{S}_{1/2}(F_g = 1)$ to $5^2\mathrm{P}_{3/2}(F_e = 2)$ transition. This pumps all the atoms to an untrapped state. Atoms flowing into this region during 3 ms are imaged using the same light beam. The image is simulated using a Gaussian distribution and the center yields the beam velocity and the width is a measure of the temperature. Potential limits in the accuracy of the method are incomplete depumping, atoms in the high velocity tail of the distribution, and the exact position of the measurement area. Note that the depletion region is much smaller than the guide length and thus that this probing technique does not affect the distribution of atoms in the guide significantly.

Probing the density and temperature – To measure the linear density and temperature of the beam in Fig. 5.3 we detect the absorption of nearly resonant light by the atoms. To obtain sufficient accuracy using this technique the detuning of the light is varied over a large range from -30 to $+10$ MHz. The absorption of the atoms in the inhomogeneous magnetic field is modeled using the cross section for transitions to different upper states, which are Zeeman shifted [19] (see also Ref. [52]). The absorption for different positions and detunings are fitted, where the only two relevant fit parameters are the temperature and the linear density. The method is repeated for different linear polarizations of the light and the results are consistent. The probing is effectively non-destructive due to the low probing repetition rate, and the small illuminated area.

Probing the optical density – In Fig. 5.5 the optical density is measured directly by observing the absorption of a light beam at a detuning of -8 MHz from the $5^2\mathrm{S}_{1/2}(F_g = 1)$ to $5^2\mathrm{P}_{3/2}(F_e = 2)$ transition. Under these conditions, the optical density is highly correlated to the collision rate, like in a harmonic guide at low temperatures, For a harmonic guide one obtains the collision rate $\gamma_{\mathrm{col}} \propto n_{3\mathrm{D}} v_{\mathrm{th}}$ and the optical density $OD \propto n_{3\mathrm{D}}\sigma$, where $n_{3\mathrm{D}}$ is the density, v_{th} the thermal velocity and σ the width of beam. The last two are proportional to each other by the relation $v_{\mathrm{th}} = \omega\sigma$ with ω the guide frequency. The effects of non-harmonicity of the trap and of Zeeman broadening largely cancel each other for different temperatures, as we have deduced from our model described above.

Within the temperature of the experiment (1.1–1.8 mK) an optical density of one corresponds to a collision rate of 16 Hz.
Simulations – The experimental evidence of the shock wave has been corroborated by simulations based on the hydrodynamic equations [53] including evaporative cooling. The cooling is effectively two-dimensional instead of three-dimensional as discussed in Ref. [54]. In the simulations also viscosity and thermal conductivity [45] are taken into account. The partial differential equations are solved with boundary conditions for the flux, temperature and speed of the incoming beam. These are supplemented with von Neumann boundary conditions on the temperature and velocity gradients on the downstream side the barrier. These equations are only valid under local thermal equilibrium, which is not fully met at three places: at the barrier, which is not wide enough, in the shock wave, since it is rapid transition, and at the entrance of the guide, where the behavior is largely collisionless due to the weaker confinement. The results can therefore only qualitatively be compared to the experimental results. An important parameter in the evaporative cooling, viscosity and thermal conductivity is the collisional cross section. The atoms in our system collide at energies larger than the s-wave regime, and also exceed the d-wave resonance [55, 56]. The scattering becomes dominated by d-waves, g-waves and i-waves. Moreover, the scattering becomes non-isotropic, and many of the scattering events are glancing causing only a small velocity change. In our simulations these complications are taking into account by assuming an isotropic cross section reduced by 30% from the zero-energy s-wave cross section.

CHAPTER 6

Bose-Einstein condensation in a magnetic guide

Direct evaporative cooling of a supersonic beam is more difficult than cooling a trapped cloud of atoms. First, the pulsed injection results in a longitudinal dilution of the atom packets and the resulting decrease in the atomic density results in a low initial collision rate γ. Second, the time available for evaporation is limited by the guide length and the mean velocity of the beam. Third, the collision rate and thus the phase-space density scales less favorably in a 2D confinement than for a 3D trap.
The subsonic beam is a continuous source of ultra-cold atoms ready for evaporative cooling. The subsonic beam is not diluted but hold a large density (8×10^{10} atoms/m). With the subsonic beam loaded into the 4 meter long conservative trap it is possible to make BEC. Loading a part of the beam into a 3D trap and apply normal 3D evaporative cooling.
In this chapter it is first shown, that surface evaporation on the guide tubes is present and can be evaluated by the hydrodynamical equations. Second it is shown, how the number of collisions are dependent on the trap potential that the atoms are evaporated in. Both 3D traps and 2D traps are analyzed with 3D evaporative cooling. Third, it is shown that it is possible to make a large BEC ($\gg 1 \times 10^7$ atoms) from the subsonic beam. Lastly it is shown that it is possible to make a BEC, while the guide is being loaded continuously.

6.1 Evaporation on the guide tubes

From the experiment we can see that there is an extra gain in density and an extra lowering of the temperature as the subsonic beam propagates down the guide (see fig. 5.3). This is a contribution from evaporative cooling on the guide tubes. In order to evaluated the evaporation on the guide the loss rate

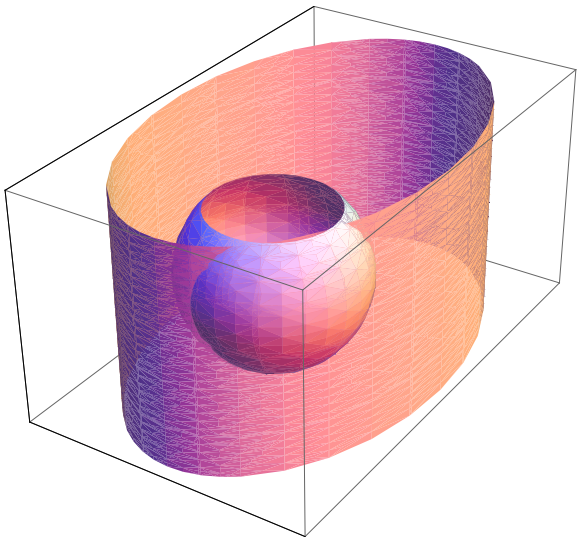

Figure 6.1: The integration space. The cylinder represent the guide. The sphere represent the collision sphere. If the sphere extends the cylinder an atom is evaporated away.

is estimated by using the hydrodynamical equations (4.15)-(4.17) with an extra loss parameter for the evaporation Ref. [53].

$$\ldots = -\Gamma_1 n - \Gamma_2(\eta)\, n \tag{6.1}$$

$$\ldots = -M\Gamma_1 nu - M\Gamma_2(\eta)\, nu \tag{6.2}$$

$$\ldots = -\Gamma_1 nE - \Gamma_2(\eta)\, n\left(\frac{1}{2}Mu^2 + V\right) - \Gamma_3(\eta)\, nk_B T \tag{6.3}$$

Here Γ_2 is the evaporative-induced particle loss rate and Γ_3 is the energy loss rate. They are proportional to the elastic collision rate γ and depend on the evaporation parameter η Ref. [53]. Calculating the evaporation space in momentum space allows for an evaluation of the decrease of temperature and the increase of density in the atom beam. Figure 6.1 shows the elliptical cylinder representing the momentum of the particles trapped in the magnetic field of the guide. The shorter axis represents the radial velocity needed to escape the trap and the other axes represents the tangential velocity. In the axial direction the velocity is infinite, since all velocities are trapped in the longitudinal direction of the guide. The region outside the elliptical cylinder represents all the momenta for which the particle can escape the trap.
The relative velocity of two colliding particles can be represented by a sphere, since momentum and energy is conserved and all angles for the collision are allowed. Depending on the relative velocity of the collision the outcome of the collision may lead to a loos of a particle, if one particle gains momentum in the radial direction larger than the trap can contain. The other particle will then have a smaller momentum and thereby cooled down, which decreases the average temperature. This is evaporative cooling and data strongly indicates that we have evaporative cooling on the guide tubes.

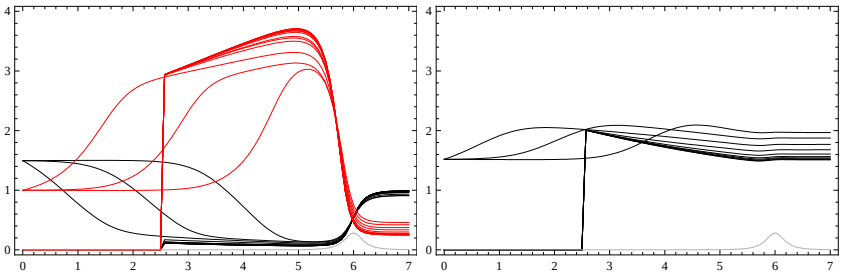

(a) Density increase (b) Temperature decrease

Figure 6.2: The effect on the density and the temperature of the evaporative cooling on the guide tubes.

Figure 6.2(a) shows the effect of evaporative cooling until a new equilibrium is reached. It is clear that additional increase of the density due to evaporative cooling is present after the shock wave. The guide is horizontal and the shock wave develops without evaporative losses until a time t, where the evaporative losses are added. The end barrier has been moved to 6 meter. This is done to ensure that the shock wave has developed but not reached the beginning of the guide, so that the increase due to the evaporation loss is clear. After the shock wave the beam velocity is close to zero and to maintain a constant force in the guide the density must increase, when the temperature decreases. Figure 6.2(b) shows the decrease of temperature. Notice that the decrease of temperature is larger the further down the guide the beam is. This simulation corresponds to the tendencies in the measurement of Fig. 5.3. When applying a downward slope in this situation, the evaporative cooling and gravitational compression can be mutually enhancing. In simulations at high fluxes, it can even lead to an instability towards Bose-Einstein condensation or three body decay. This physical situation discussed here is quite similar to the situation discussed in Ref. [57]

Discussion

We have corroborated the additional increase of density and decrease of temperature in the subsonic beam. This is from evaporation of the hot spiraling atoms circulating the atomic beam.

6.2 BEC

BEC can not be reached by laser cooling alone. Even though laser cooling of atoms can reach temperatures of μK, the achievable phase-space density is limited. Laser cooled atoms effectively repel each other through radiation pressure, limiting the achievable density. Light from one atom is reabsorbed by another causing a repulsion between them, when the cloud becomes optical thick. Furthermore, when the density increases, so does the collision rate. Inelastic collisions lead to the loss of atoms. The dominant process is light assisted collisions between atoms in the atomic ground state S and atoms in the excited state P.

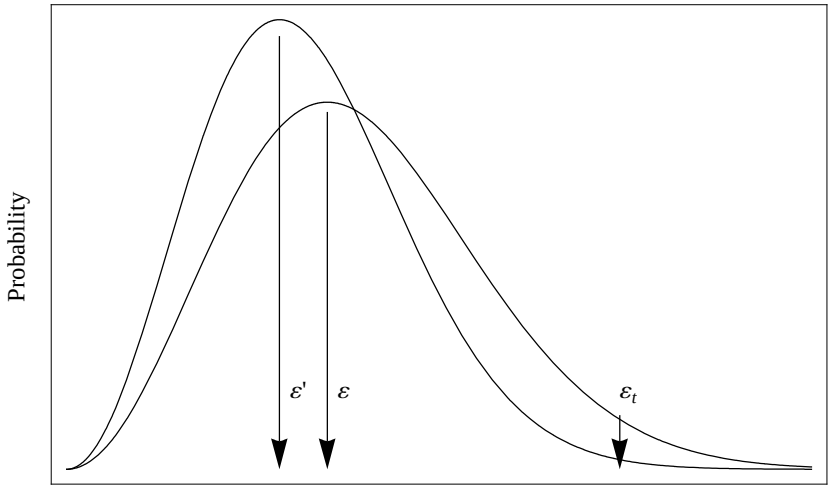

Figure 6.3: Truncated Maxwell-Boltzmann distribution at two energies $\varepsilon' < \varepsilon$ and ε_t is the cut-off energy.

A cold gas contained in a conservative trap has a specific energy distribution $f(\varepsilon)$ (see figure 6.3). A good way of removing the energetic atoms is by evaporative cooling in a conservative trap. Evaporative cooling is performed by letting two particle collide producing a low energy particle and a high energy particle. Efficiently removing the highest energy particles causing the cloud to cool down. Evaporative cooling can be done in two ways: either by a solid surface or by an RF knife. The idea is the same. The atoms with the highest energy travel further out to the periphery of the cloud. Moving a solid surface close to an atom cloud will then remove the most energetic atoms, leaving the colder atoms and letting them rethermalize through collisions. With an RF-knife, atom at a certain threshold energy ε_t are spin flipped to a high field seeking state and therefore removed from the confining potential. The threshold energy is continuously lowered with the temperature. The process is continued until the atoms reach BEC. To describe the evaporation process the truncation parameter is defined

$$\eta = \frac{\varepsilon_t}{k_B T} \tag{6.4}$$

where T is the temperature of the system. The parameter η is a measure of the trap depth. For low η a large evaporation rate occurs, but the average temperature drop per evaporated atom is low. For large η the temperature drop per evaporated atom is large, but only few atoms will have an energy high enough to get evaporated. Using a constant η means lowering the energy ε_t, since the temperature is lowered per evaporation step.
Usually a BEC experiment starts with a phase-space density of 10^{-9}, which can be brought to unity and thus BEC by losing up to 3 orders of magnitude in atoms.

6.3 Cooling in different trap configurations

Here we study the 3D and 2D evaporative cooling in different trap configurations. We want to explain the difference between evaporative cooling in a guide, a Ioffe-Pritchard trap and all 2D or 3D combinations in between.
At the end of our guide two coils are placed. One of the coils is used to create a shock wave and the other is placed 40 cm below. These two coils in combination with the guide create a combination of linear and harmonic 3D trap (a hybrid trap) where RF-evaporative cooling is applied. As the evaporation continues the trap eventually becomes a 3D harmonic trap, before we reach degeneracy. The guide is a 2D trap, where at high temperatures it is linear, while at lower temperatures it is harmonic due to the presence of a small longitudinal bias field. All 5 trap configurations are investigated for the efficiency of evaporative cooling.

The evaporative cooling process is limited by the rate at which atoms scatter into high energy states that are non-trapped. However, in Ref. [24] it is shown, that this rate is reduced due to depletion of energy states just below the threshold. It is found that as soon as high energy particles collide and some are evaporated, it takes time until the high energy states are refilled. This causes a limited availability of high energy particles that can be evaporated, thereby slowing down the evaporation process. The distribution function at lower energies is barely affected by this process and thus corresponds to a Boltzmann distribution. In Ref. [24] only two cases are discussed, the 3D harmonic and linear trap, but here we report on all different trap geometries.
The purpose of the model Ref. [24] is to determine the time t_0 to reach degeneracy. This can be done by monitoring the evolution of the collision rate, density and temperature. The distribution function and the collision rate can be described by self-similarity. The distribution function will reshape itself through the thermalization process into a shape identical for all temperatures, (see Fig. 6.3). When the temperature gets colder the distance between the atoms in a trap decreases thereby increasing the collision rate γ.
For the collision rate γ the time derivative depends quadratically on γ, since if the collision rate increases the time between each collision t will decrease. Thus $d\gamma/dt = \gamma^2/N_c$. The solution is

$$\gamma = \gamma_0 \left(1 - \frac{t}{t_0}\right)^{-1}. \tag{6.5}$$

Note that this shows the behavior of runaway evaporative cooling, where the collision rate goes to infinity for $t = t_0$, indicating BEC is reached in a finite time. In a similar way the time-dependence of temperature T and number of particles N can be written [58]

$$T = T_0 \left(1 - \frac{t}{t_0}\right)^{\alpha_T} \tag{6.6}$$

$$N = N_0 \left(1 - \frac{t}{t_0}\right)^{\alpha_N} \tag{6.7}$$

where T_0 and N_0 are the initial temperature and number of particles respectively, and α_T and α_N can be determined by the minimum number of collisions. The

relation between α_N and α_T is

$$\alpha_N = \alpha_T \left(\delta - \frac{1}{2}\right) - 1, \tag{6.8}$$

where δ is a number determine by the potential (see Tab. 6.1). Depending on the potential the density of state, and the number of collisions will change. All numbers presented in Tab. 6.1 is for 3D cooling. The sequence of the potential are determined by the energy per particle. Notice that the density of states follows this order as well.
Here the transverse and longitudinal directions can not be separated due to collisions and the density of state is calculated for the 3D case. With the initial collision rate $\gamma_0 = n_0 \sigma v_{rel}$ and the time t_0 it takes to reach degeneracy the critical number of collision is given by $N_c = \gamma_0 t_0$. The critical number of collisions is constant for a given trap and evaporation efficiency. Only the time it takes to reach degeneracy is determined by the initial conditions.

Figure 6.4 shows the number of collisions N_c in a potential for 3D cooling and 2D cooling. The effective evaporation efficiency $k_B T \eta_{eff} \equiv \frac{dE}{dN}$ is the effective amount of energy that is cut off per evaporated particle. It is the energy of the atoms that are leaving the trap, instead of the energy above which atoms can leave the trap. The dashed line is the truncated Boltzmann distribution where the solid line is the model of Ref. [24]. The dotted line is 2D cooling and is determined from Eq. (6.1)-(6.3). The 2D cooling is shown for the 2D traps where this is relevant. In all cases the truncated Boltzmann underestimates N_c. The result shows that the evaporation process is definitely slower than can be expected Ref. [59] due to the lack of high energy particles.
The potential configuration with smallest N_c is the quadrupole trap. This is clear since there are more relative energetic particles, thus the cloud shrinks faster as a function of temperature. The energy per particle removed decreases in each trap resulting in a larger number of collisions per trap and a higher α_T is needed per trap for effectively cooling. It is seen that the 2D cooling is a factor of two less effective than 3D cooling. The effective minimum is still the same and the α_T is the same as for 3D cooling. This shows that cooling directly on the guide is a very difficult task.

In our experiment we start with a hybrid radially linear and axially harmonic trap. About halfway in the evaporation sequence the atoms become so cold that the trap is effectively harmonic. At this time, the collision rate usually will have increased by only a factor of 2 in all three directions, following Eq. (6.5).
Throughout the sequence of the RF-knife an $\alpha_T = 3$ is chosen to have an effective evaporative cooling, both in the hybrid and 3D harmonic trap. Hence the temperature follows a $(1 - t/t_0)^3$ curve. For the RF-knife this curve is followed with respect to the resonance frequency for atoms at the center of the trap.

Discussion

The number of collisions are investigated for all possible trap configurations spanning from the quadropole trap to the 2D harmonic guide. It can be seen that the least number of collisions is needed in the quadropole trap whereas the

Definition	Symbol	Quadrupole trap (3D)	Hybrid (3D)	Linear guide (2D)	Harmonic trap (3D)	Harmonic guide (2D)
Potential trap	$U(r)$	λr	$\frac{1}{2}m\omega^2 z^2 + \lambda r$	λr	$\frac{1}{2}m\omega^2 r^2$	$\frac{1}{2}m\omega^2 r^2$
	δ	3	$\frac{5}{2}$	2	$\frac{3}{2}$	1
Density of states	$\rho(\varepsilon)$	$\frac{32\sqrt{2}m^{3/2}\varepsilon^{7/2}}{105\pi\lambda^3\hbar^3}$	$\frac{m\varepsilon^3\pi}{6\pi\lambda^2\omega\hbar^3}$	$\frac{\sqrt{32}m^{3/2}\varepsilon^{5/2}}{15\pi\lambda^2\hbar^3}$	$\frac{\varepsilon^2}{2\omega^3\hbar^3}$	$\frac{\sqrt{8}\sqrt{m}\varepsilon^{3/2}}{3\pi\omega^2\hbar^3}$
Collision rate	γ	$N\frac{\sigma\lambda^3}{16k_B^3\sqrt{m}\pi^{3/2}T_0^{5/2}}$	$N\frac{\lambda^2\omega\sigma}{4\pi^2T_0^2}$	$N\frac{\lambda^2\sigma}{2\pi^{3/2}\sqrt{mT_0^3}}$	$N\frac{m\sigma\omega^3}{2\pi^2k_B^{3/2}T_0}$	$N\frac{\sqrt{\frac{m}{T_0}}\omega^2\sigma}{\pi^{3/2}}$
Energy per particle	E	$\frac{9}{2}nk_BT$	$4nk_BT$	$\frac{7}{2}nk_BT$	$3nk_BT$	$\frac{5}{2}nk_BT$
Effective evaporation efficiency	η_{eff}	$\frac{-18+63\alpha_T}{-4+10\alpha_T}$	$\frac{4-12\alpha_T}{1-2\alpha_T}$	$\frac{-14+35\alpha_T}{-4+6\alpha_T}$	$\frac{-3+6\alpha_T}{-1+\alpha_T}$	$\frac{-10+15\alpha_T}{-4+2\alpha_T}$

Table 6.1: Parameters defining the harmonic and linear potential trap.

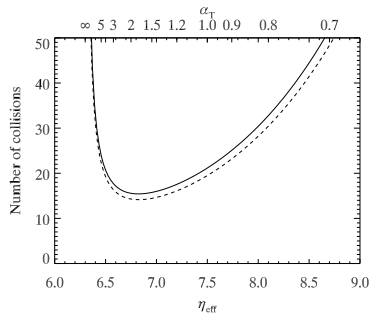

(a) Number of collision in a quadrupole trap.

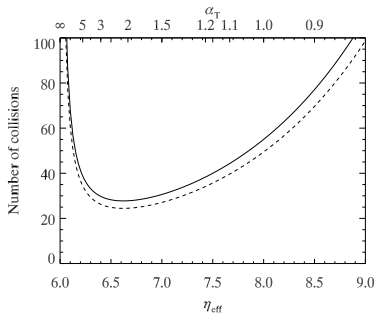

(b) Number of collision in a hybrid trap.

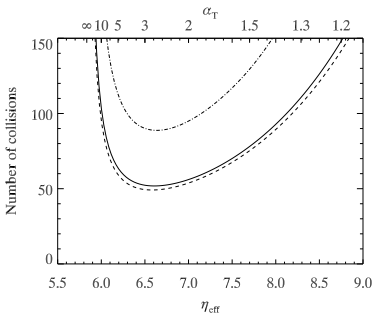

(c) Number of collision in a 2D linear guide.

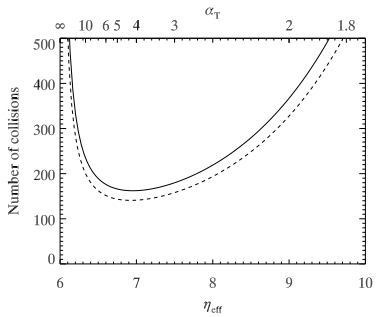

(d) Number of collision in a 3D harmonic trap.

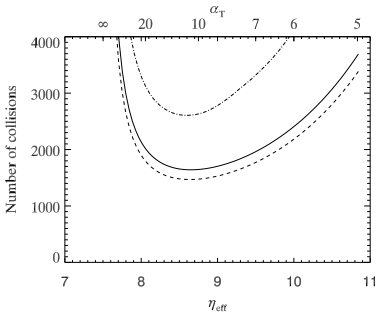

(e) Number of collision in a 2D harmonic guide.

Figure 6.4: Number of collision N_c in different trap configurations as a function of the evaporation efficiency η_{eff}

largest number of collisions is needed in the 2D harmonic guide. It is shown that the lack of high energetic particles increases the number of collisions needed and that cooling in 2D is a very difficult task.

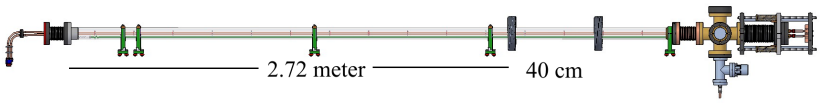

Figure 6.5: The 4 meter guide with the two coils

6.4 BEC in the guide

The previous section lead us to understand that direct evaporative cooling in the guide is an almost impossible task and that the best approach is to load the atoms into a 3D trap for evaporative cooling. This is described here.

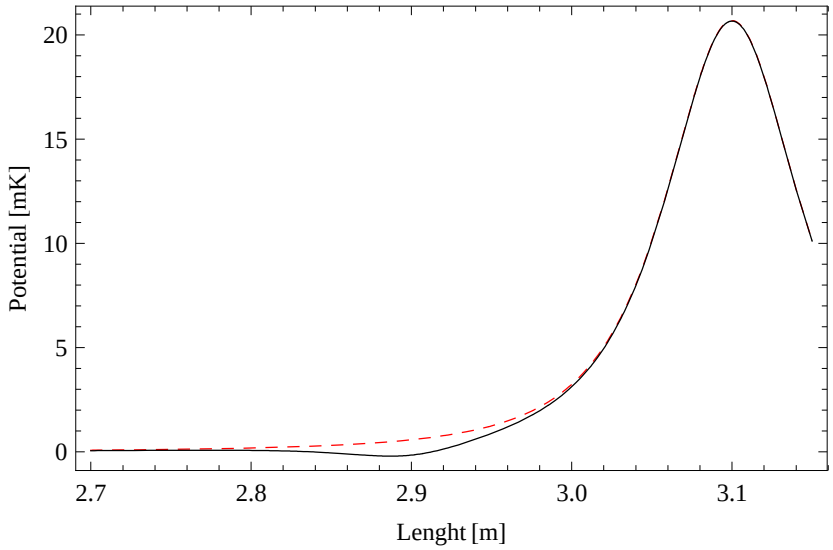

Figure 6.6: The trap potential made by second coil and the half coils shows the potential the atoms flow into when the first coil is lowered. Red curve is without the anti bias coil the black curve is with.

The guide is tilted down 2 cm over 4 meters. After 3.7 m two coils are placed with a distance of 40 cm in between. These will act as pinch coils. The coils are identical and have 7×8 windings with a mean diameter of 15 cm. For the first coil the maximum current is 120A, since at a higher current the cooling water can not effectively cool the coil down. The second coil is attached to two ZUP power supplies in parallel with a maximum of 70A each. The two coils in combination with the guide is a standard Ioffe-Pritchard trap. Since the guide is tilted downwards the atoms sag to the end of the guide, causing asymmetrical evaporative cooling. To counteract the repulsive force of the end coil at the position of the trap during loading, another anti-bias coil with 2 winding in series with the second coil is placed 20 cm before the second coil. This levels the potential out (see Fig. 6.6), but does not counteract the sag. Between the two coils a butterfly wounded RF antenna is placed on the outside of the vacuum glass. The RF-power is up to 4W, which creates an oscillating field of 52 mG.

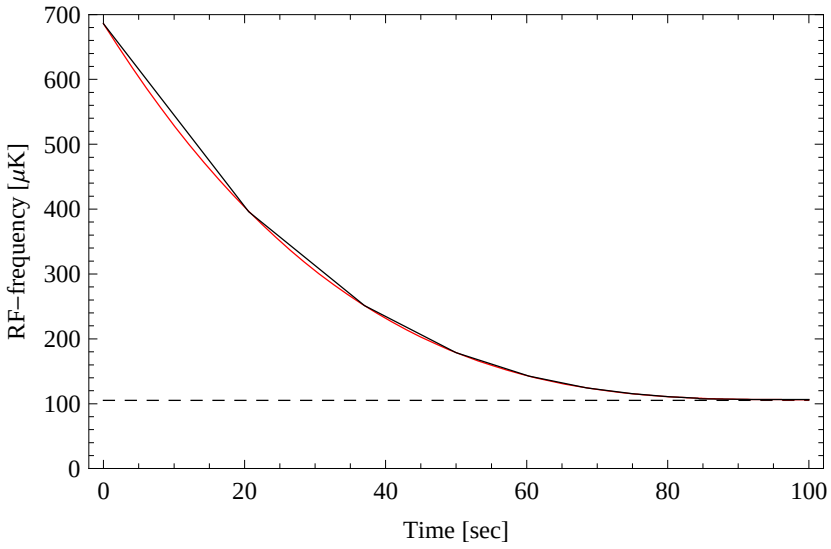

Figure 6.7: Frequency ramp used in the evaporation process as a function of time. The black curve is the RF-frequency and the red curve is Eq. (6.6) for $\alpha_T = 3$. The dashed line is the bottom of the trap.

In the last 20 s of the evaporation sequence this is lowered to 37 mG.

The guide is loaded on the last coil with 400 packets creating a shockwave and subsequent a dense subsonic beam. The lifetime in the guide is up to 400 s, limited by the vacuum pressure. The first coil is raised in 1 s and the guide magnetic field gradient is reduced from 13.5 T/m to 9.64 T/m. A part of the subsonic beam is now in a 3D hybrid trap and settles down in a 4 second equilibrium period. The current through the coils is held constant creating a axial trap frequency of $\omega_l/2\pi = 0.67$ Hz. Figure 6.7 shows the evaporation curve as a function of time. The dashed line indicates the bottom of the trap and the black curve the radio-frequency ramp. The red curve is Eq.(6.6) at a chosen $\alpha_T = 3$. Evaporative cooling is performed for 92 seconds. At the same time the magnetic gradient from the guide is lowered from 9.64 T/m to 4.82 T/m decompressing the trap to a trap frequency of $\omega_r/2\pi = 98$ Hz. After the evaporation we decompress again for 60 ms in the radial direction to a trap frequency of $\omega_r/2\pi = 24.5$ Hz, before applying time of flight, by releasing the atoms.

In general, 3D adiabatic decompression leads to a conservation of phase-space density

$$\rho \quad = \quad N\left(\frac{\hbar\overline{\omega}}{k_B T}\right)^3 \tag{6.9}$$

and the ratio $\frac{\hbar\overline{\omega}}{k_B T}$ remains constant. We can assume that when the cloud is released in TOF it only expands radially, since $\omega_l \tau_{TOF} \ll 1$. The radial decompression of the trap frequency ω_{rad} by a factor of 4 leads to a reduction

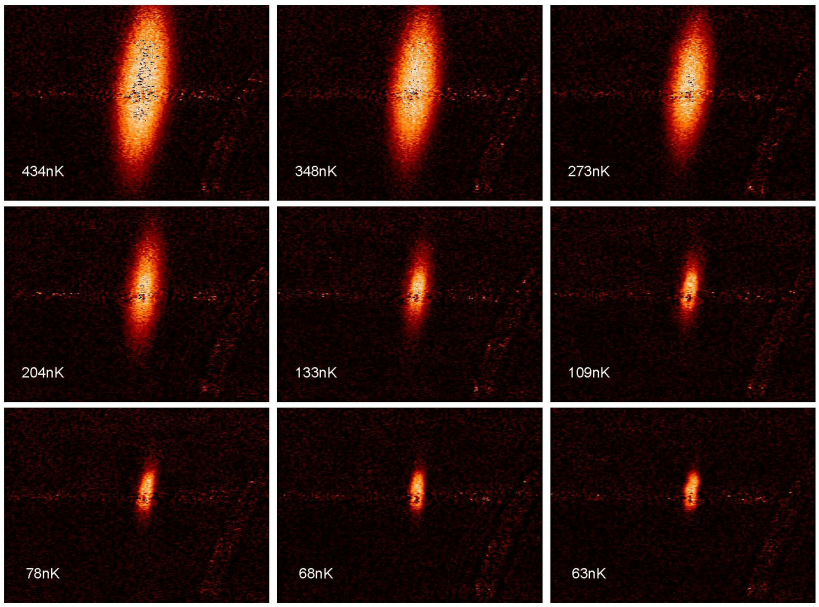

Figure 6.8: Image sequence of the BEC forming out of a thermal cloud

of the temperature in the radial direction with a factor of 4, $T_{rad}^{int} = 4T_{rad}^{final}$. BEC is reached at a rf-frequency 200 kHz above the bottom of the trap.
The pixel size is measured to be 16.9 μm with the chosen lens and by measuring the width in both the axial and the radial direction the size of both the BEC and the thermal cloud can be determined. The images are observed after an expansion time $\tau = 45$ ms. The width of the cloud will expand according to equation (2.13). The BEC shown in the last pictures of Fig. 6.8 is 0.96 mm long and 70 μm wide holding 1×10^7 condensed atoms.

The number of atoms are determined by absorption Eq. (2.14) and Fig 6.9 show the result. This is the last 20 s of the evaporation process. At condensation temperature $T_c = 162$ nK we have 10^8 thermal atoms. Degeneracy is reached in the last 10 s and the BEC grows out of the thermal cloud as a bimodal distribution reaching a pure BEC with 1×10^7 condensed atoms. Figure 6.10 shows the axial temperature and the radial temperature. They drop from 500 μK down the 50 μK in unison, indicating that good rethermalization is present. It must be noted that this trap does not produce the largest condensates. We have made a BEC with $3{\times}10^7$ condensed atoms in a under weaker trap frequency conditions.

Discussion

A BEC of 1×10^7 condensed atoms is created in a weak axial and strong radial 3D trap with the source of the cold atoms from the subsonic beam with a density of 10^{10} atoms/m. This BEC is a record for ^{87}Rb BEC Ref.[15].

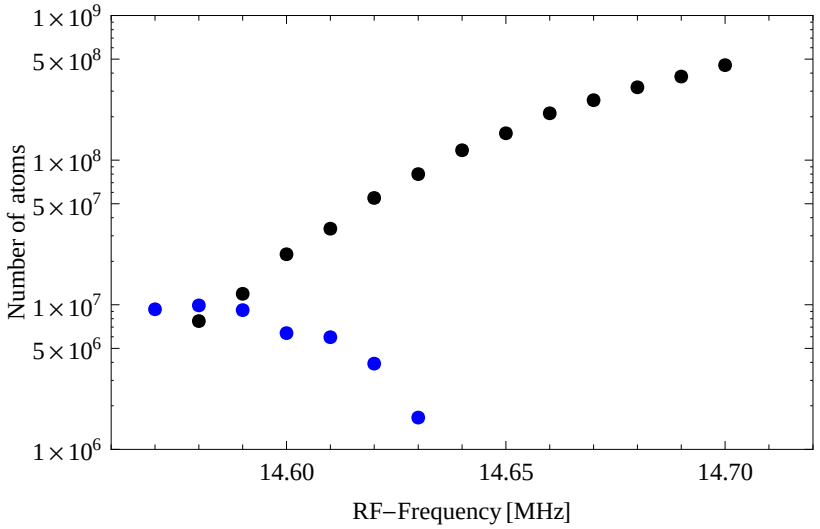

Figure 6.9: Number of atoms for the thermal atoms (black dots) and the condensed atoms (blue dots) as a function of the rf-frequency for evaporative cooling.

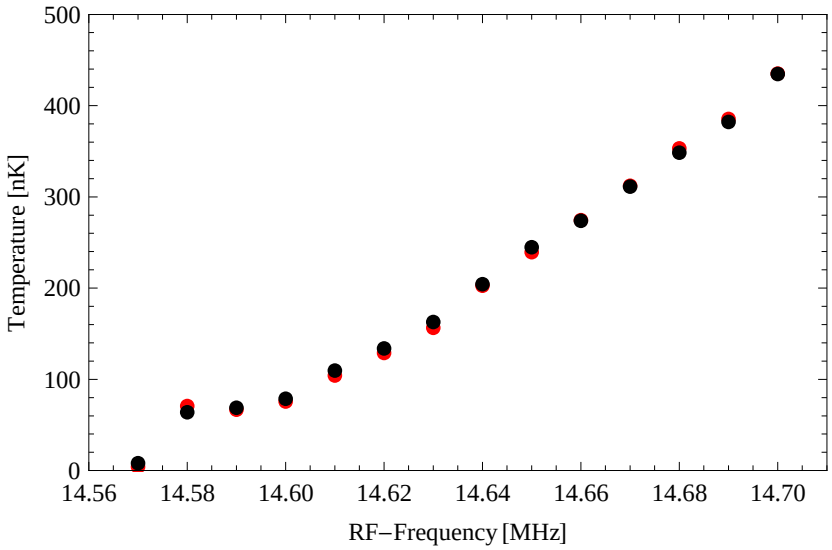

Figure 6.10: Temperature for the condensed atoms in the radial direction (black dots) and axial direction (red dots.)

6.5 BEC in the guide while loading the guide

It is relatively straight forward to load the beginning of the guide while at the end of the guide evaporative cooling is performed. Here we will create a BEC as previous described, but while RF-cooling we continue to load the guide on the first coil. Remember that while loading the next bit of the subsonic beam, the guide current is lower so that effective evaporative cooling is made in the 3D trap between the two coils, this will give a less effective loading of the guide and the next BEC is expected smaller. The first BEC is discarded and the trap is loaded again from the subsonic beam that have been affected by the creation of the previous BEC. This cloud is cooled to degeneracy and observed.
In total 400 packets are loaded into the guide on the second coil. The second coil is held at a constant current. The first coil is lowered for 1 s to zero and the subsonic beam flows along the guide until stopped at the second coil. The first coil is raised again and the now 3D trapped beam is left for 4 s to settle. The guide current is lowered from 13.5 T/m to 9.64 T/m and 92 s of evaporation is conducted. At the same time the guide is loaded again on the first coil to continue adding atoms to the subsonic beam. A BEC is created with the same numbers in Sec. 6.4. The new BEC is then discarded and the first coil is lowered. Again part of the subsonic atom beam flows along the guide until the second coils is reached and is trapped in the 3D trap. This scheme can be set at a repetition of 10.5 mHz. For observation the guide is lowered to 0.3 T/m in 200 ms and then turned off giving a TOF time of 43 ms before the BEC is observed underneath the guide tubes.

Figure 6.11 shows the number of atoms as determined by Eq. (2.14). This is the last 20 s of the evaporation process. Because the trap is stronger than the previous BEC the bottom of the trap is raised with an additional 5 MHz, hence the evaporation curve is raised 5 MHz higher than in Fig. 6.7. Degeneracy is reached in the last 10 s from a thermal cloud of 10^7 atoms into BEC with 5.3×10^6 condensed atoms. Figure 6.12 shows the axial temperature and the radial temperature relative to the bottom of the trap. It is not until we have reached a pure BEC that there is effective rethermalization.

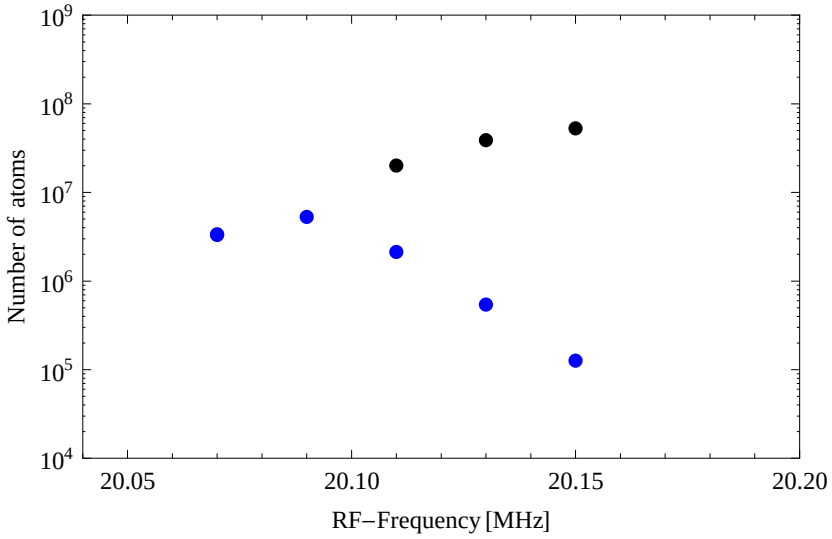

Figure 6.11: Number of atoms. The black dots are the thermal cloud and the blue dots are the BEC.

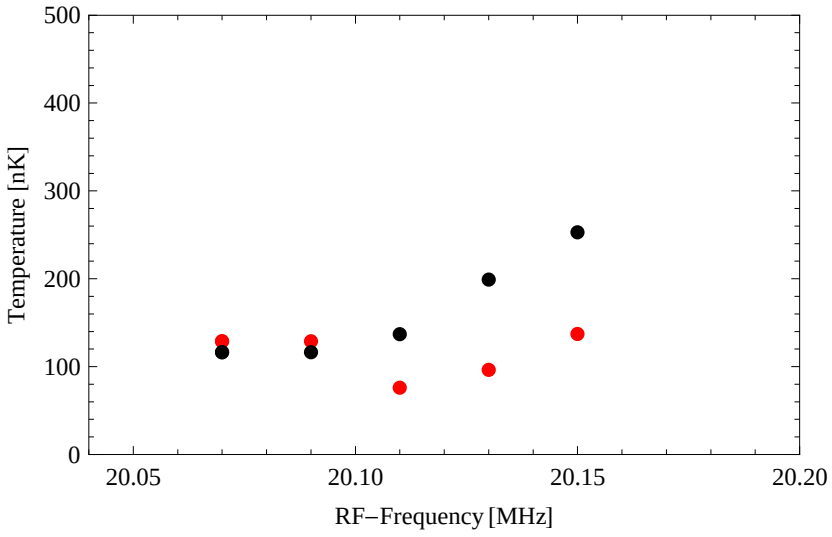

Figure 6.12: Temperature for the condensed atoms in the radial direction (black dots) and axial direction (red dots).

Discussion

The number of condensed atoms in second BEC is 50% of the first BEC made. We believe that there can be three reasons for this: The magnetic gradient of the guide is lowered and will have an effect on the loading of the guide, and thus on the creation of a subsonic beam. Second, large condensates are produced under the condition that the radial trap frequency is lowered. But the second BEC is created in a stronger trap than the first BEC. Third, the RF-signal leaks over the confining barrier removing atoms in the subsonic beam.

That the BEC is created from the affected subsonic beam shows that we are on the right track to a continuous BEC machine. The capability of cooling atoms while loading the guide creates the possibility of loading a conveyor belt, which will replace our trap. The loading of a conveyor belt is even more efficient, since the loss of phase-space density when the first coil is opened does not occur. From atoms cooled in such a conveyor belt a continuous atom laser can be generated. Our demonstration of reaching Bose-Einstein condensation shows that it is in principle possible to reach degeneracy in a conveyor belt.

6.6 Resume

We have investigated evaporative cooling in all different trap configurations and can show that the lack of atoms with a large energy add to an increase of number of collisions before reaching degeneracy. Moreover, the trap configuration is very important, as can be seen from Fig. 6.4. The least number of collisions is needed in a quadropole trap and the largest number of collisions is needed in the 2D harmonic guide. With 2D evaporative cooling it becomes even more difficult. This shows that even without the thermal conductivity direct evaporative 2D cooling in the magnetic guide is impossible, and another approach to evaporative cooling in a magnetic guide should be used.
The dense subsonic beam is used to load a hybrid trap between two coils at the end of the guide. In this trap we have created large ^{87}Rb BEC of 1×10^7 condensed atoms. We have also created a BEC of 5.3×10^6 condensed atoms, while the guide is loaded at the same time. This shows that we have successfully designed, constructed and tested an experimental setup, where a continuously dense source of ultra cold atoms is produced and ready to cool to degeneracy.

CHAPTER 7

Future perspective and summary

7.1 Future perspective

We have shown that it is possible to cool a part of the subsonic beam to degeneracy while loading the guide. One option to obtain an atom laser is to continuously outcouple part of the BEC. This has been done before [3, 32] but only leads to a low flux quasi-continuous atom laser. In order to have a high flux atom laser we must provide a continuous evaporative cooling of a cold atom beam. This is hard due to the thermal conductivity. To archive the continuous Bose-Einstein condensate beam we have to perform evaporative cooling while the atoms are moving in the magnetic guide.
We suggest to suppress thermal conductivity, by placing a co-moving barriers or conveyor belt in such a beam (see Fig. 7.1). This would enable efficient initial evaporative cooling of a very slow beam with a roughly constant beam velocity. The evaporative cooling can occur completely analogous to the proven evaporative cooling in a Ioffe-Pritchard trap.

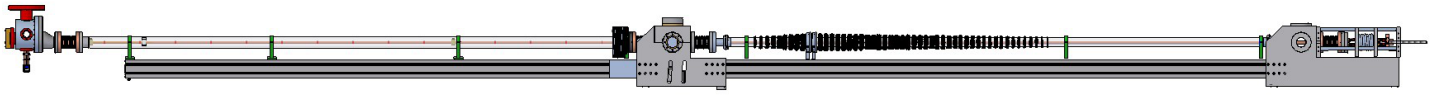

Figure 7.1: The experimental setup for the atom laser. The magnetic guide is 8 meter.

As a practical example, we will discuss a plausible scenario for our system. The magnetic guide is extended into an 8 meter guide. A conveyor belt with 52 coils can be build. Each 3th coil is connected in series and by alternating the current in the coils the bottom of the traps can move from the left to the right. With a lifetime of 400 s, and a cooling section of 4 m, a suitable beam velocity would be around 4 m/400 s = 1 cm/s. This would be the slowest velocity of the conveyor belt. With an initial collision rate of 70/s, as demonstrated in Sec. 6.3, the number of collisions along the guide would be about 70/s $\times$ 400 s = 28000, an order of magnitude over what is required in the worst possible scenario. This conveyor belt can move at an arbitrary velocity. The conveyor belt providing multiple standard Ioffe Pritchard traps, which are hybrid at high temperature, but 3D-harmonic at low temperature. Adding multiple RF antennas along the conveyor belt, each with a decreasing frequency from the previous and activated when an atom cloud passes by, the atoms in the trap will be evaporatively cooled while moving in the co-moving frame. By decreasing the amount of windings on each coil the potential of each barrier between each trap is lowered and follows the dropping of the temperature (see Fig. 7.2). Due to lowering of the barrier the axial decompression vanishes and the scenario of standard Ioffe Pritchard traps (Fig. 6.4(b) and Fig. 6.4(d)) are no longer valid. Instead the evaporative cooling closely resembles the scenario of cooling in a guide (Fig. 6.4(c) and Fig. 6.4(e)).

Two possible scenarios can be used to reach a degenerate atomic beam. Either cooling to degeneracy in the conveyor belt or not. If the choose is made to cool to degeneracy in the conveyor belt effectively a pulsed atom laser is created when the atoms leave the conveyor belt. Here each BEC while have a different phase. A continuous degenerated beam will form since the BEC's will merge together in the longitudinal direction due to expansion. This will happen as long as the condensation temperature T_c will not drop below the expansion energy. The condensation temperature T_c drops due to the dilution of the density in the longitudinal direction. For each merger one soliton will be emitted ensuring the same phase for the degenerated atomic beam [60, 61], which could decay into quantized vortices.

The other option is to not cool all the way down to T_c in the conveyor belt. As the temperature drops and hence the mach number becomes high, the thermal conductivity becomes inconsequential, at which point the barriers can be removed completely. The reason why the thermal conductivity becomes inconsequential is that the diffusion process causing thermal conductivity, is much slower than the evaporative cooling rate. Again the atom packets will form a continuous atomic beam in a decelerating potential. At this point, the final stretch of evaporative cooling to degeneracy can be performed in the guide in two ways. The first way is to continue evaporative cooling to degeneracy following Fig. 6.4(e). Alternatively, the mach number can be kept constant by using an upward sloped guide. This will result in an evaporation scenario resembling fig. 6.4(d).

Note that not only is there the flexibility in the scheme to generate supersonic or subsonic atom laser, there is also the advantage of either a pulsed or a continuous atom laser.

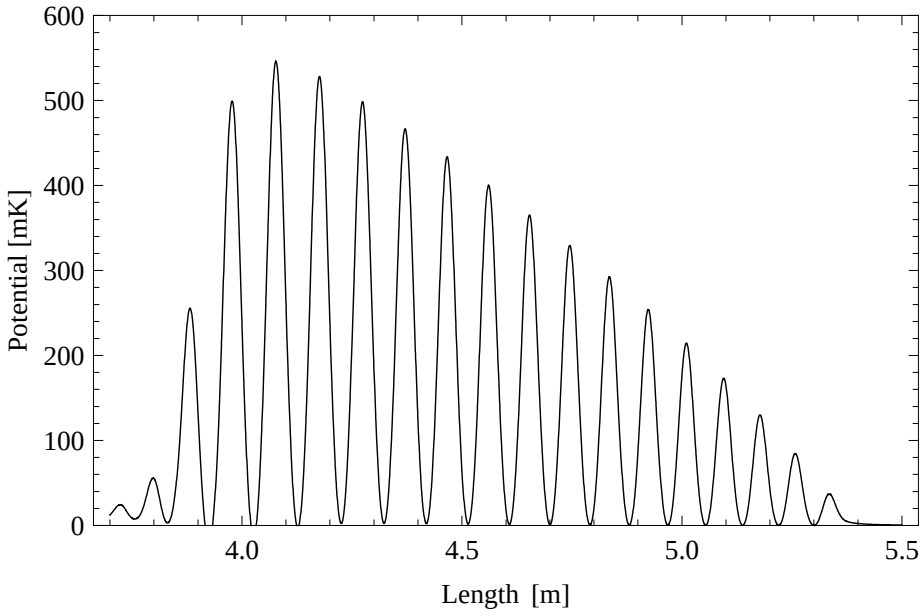

Figure 7.2: The potential from the conveyor belt of 52 coils, where every 3th coils is in series. By alternating the current in the coils the bottom of the traps can move from the left to the right.

7.2 The black hole laser.

The atom laser can be used to create an artificial event horizon and thereby the ability to study the equivalence of Hawking radiation in this system.
Hawking predicted that an event horizon should spontaneously emit quantum pairs of particles, where one particle of each pair falls into the hole and the other escapes into space, constituting the radiation of the horizon know as the Hawking temperature.

Picture the atom laser flowing from right to left at subsonic velocities (See Fig. 7.3 [62]). Inserting a Laval nozzle will accelerate the beam to supersonic velocities. Consider the fate of a sound wave propagating against the current of the atom laser beam. In the subsonic region sound wave can travel against the flow, but in the supersonic region it can not. No sound can escape the point where the flows turns supersonic. This is the sonic horizon.
The sonic horizon acts as an acoustic equivalent of an event horizon. Travelling from subsonic to supersonic is the equivalent of a black hole horizon and travelling from supersonic to subsonic is the equivalent of a white hole horizon. Both horizons emits quanta of phonons. However, for the black horizon phonons can propagate against the flow on the right side of the black horizon. Just to the left of the horizon phonons can only travel with the atom laser flow and the phonos from the subsonic region will be swept into the supersonic region. For the white horizon phonons can propagate on the left side of the white horizon but not on the right side.

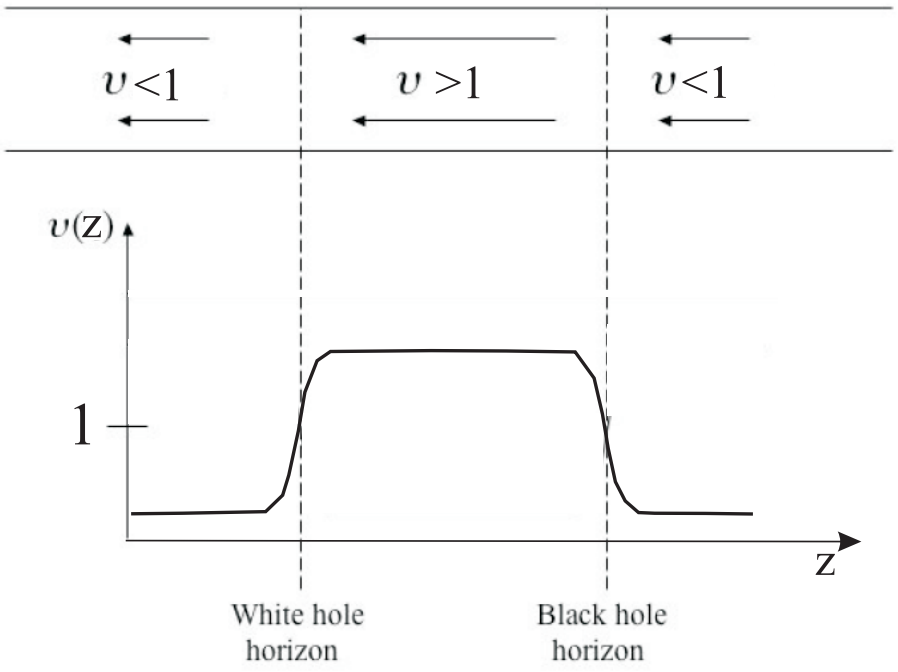

Figure 7.3: Sonic horizon in a atom laser, in which the speed of sound is 1. The velocity profile of the fluid attends the value 1 at two values for z. These are the horizons for the sound waves that are moving towards the right with respect to the flow of the atoms laser beam. At the right hand horizon right moving waves are trapped, with waves just to the left of the horizon being swept into the supersonic flow region $v > 1$. No sound can emerge from the region through the horizon and is equivalent to a black hole horizon. At the left hand horizon the situation is reversed and this is equivalent to a white hole horizon.

This means that the horizons combined works as a cavity and that all phonos propagating in the supersonic region will leave though the white horizon. Adding multiple alternating horizons will lead to a continuous flow of phonos propagating from the right to the left thus creating, what is know to be, a black hole laser.
The phonos emitted from the black hole laser will have the equivalent of a Hawking temperature. In the sonic case this is given by the velocity gradient at the horizon [50], which corresponds to 1.2 nK/phonon. This is an effect that is possible to study in a high flux atom laser.

7.3 Summary

In 1925 Einstein predicted a new state of matter. Einstein was heavily influence by the statistical work done by Satyendra Nath Bose. Bose worked with the statistical properties of light particles, called photons, which Einstein expanded to atoms. When the temperature is lowered to absolute zero, bosonic atoms show strong "social" behavior and allowed to share the same quantum state namely, the one with the lowest energy. This is known as Bose-Einstein condensation (BEC). When the temperature of the atoms is lowered the atoms behaves as waves instead off as particles. In a BEC all the atoms merge together and form one large wave. This wave has one phase and one wavelength.
An atom laser is a coherent beam of atoms with one phase. De Broglie wavelength of the atoms is much smaller than the wavelength of light. An atom laser provides a tool for high precision interferometry and holographic images. So far all atom lasers have been made by outcoupling condensed atoms from an already existing BEC. The flux and lifetime of these atom lasers are restricted by the initial size of the BEC. A typical atom laser has a lifetime of 100 ms and is of low flux. The continuous high flux atom laser is a holy grail for atom physicist. This work describes our experimental setup for the high flux atom laser.
The kinetic energy of an ensemble of atoms is a measure of the temperature, so by lowering the kinetic energy of the atoms is equivalent to cooling the atoms. The most effective way for lowering the kinetic energy of the atoms is by Doppler cooling. If an atom is excited, it will experience a momentum loss equal to the momentum of the photon. On average this does lead to a change of the momentum of the atom. Repeating this process many times will lead to a lowering of the kinetic energy. The Doppler cooling has a minimum temperature due to the random recoil of the emitted photons. To further decrease the temperature evaporative cooling is used. Evaporative cooling is a slow process that much resembles the cooling of a cup of coffee. The atoms are put in a trap where they will collide. The most energetic atoms will leave the trap and the least energetic stays behind, which must thermalize through collisions to a lower temperature.
In **chapter two** the experimental setup is described. The experiment consists of a rubidium oven, where a beam of rubidium atoms is formed. The atoms are slowed using laser light and collected and cooled using optical molasses. The atoms are loaded into a 4 meter magnetic guide acts as a outlet for the atom laser. The entire experiment is kept at ultra high vacuum. In order to cool the atoms we use Doppler cooling, which cools atoms from hundred of degrees to milli Kelvin temperatures in a matter of milli seconds. We have built five lasers, two for slowing the atoms, two for cooling the atoms and one for observing the atoms. All lasers are at 780 nm, the wavelength used to manipulate rubidium atoms. In the cooling chamber we produce a collection of 10^{10} ultra cold atom in 80 ms, which is a very large number.
In **chapter three** the launching procedure is described. The large packet of atoms that was made in the previous chapter is transferred into the magnetic guide. The lasers that are used for cooling also push the atoms into the guide. The magnetic guide confines the atoms in the transverse direction but the atoms are free to travel in the axial direction. Where new atoms are launched into the guide every 166 ms the atom beam become continuous 50 cm into the guide. This beam has a velocity that is larger than the speed of sound and therefor

supersonic. Unfortunately the density of this beam is not large enough to have effective evaporative cooling. By changing the beam into a subsonic beam the density of the beam will increase. The beam velocity is changed by reflecting the beam on a magnetic barrier and colliding the returning beam with the incoming beam. This creates many collisions that result in a shock wave.
In **chapter four** the theoretical understanding of the creation of the shock wave is described. The creation of the shock wave is best described by an analogous situation. Take a high pressure hose that is used to clean tiles in the garden and aim it into a bucket. When the high pressure water beam hits the bottom of the bucket the water do not spray over the bucket edges and stays behind. This is because the water molecules collide with each other. After the collision the velocity of the water molecules has lowered and the water remains in the bucket, thus creating a water mirror. Any additional water from the high pressure beam that hits this water mirror is slowed down to slow velocities as well and raises the water level. This is how the shock wave is created and affects the supersonic atomic beam in our experiment, even though the guide is horizontal. The shock wave have an additional feature: the only way that the supersonic beam can become subsonic beam is through a large density increase. This hydrodynamical phenomenon is used in the creation of a dense subsonic atomic beam. This dense subsonic atomic beam has an internal collision rate large enough for effective evaporative cooling. With a subsonic beam an additional density increasing effect can be used: gravitational compression. The theory shows that if the guide has a downward slope the density of the subsonic beam at the end of the guide will increase due the weight of the upstream atoms.
In **chapter five** the experimental prof of the shock wave is described. At a distance of 3 meter from the entrance of the guide is a magnetic coil, which acts as an impenetrable barrier for the atomic beam. The supersonic beam returns on the coil and collides with the incoming beam. This creates a shock wave between the supersonic beam and the subsonic beam. The change of beam velocity is directly observed by looking at the flow of atoms passing by a specific point in the guide. In the experiment the shock wave is identified by a density increase and a velocity decrease that travels upstream. The shock wave is observed for different fluxes of the supersonic beam and it shows that the lower the flux the larger the width of the shock wave becomes. It is also observed that the density increases significantly when the guide is tilted on a downward slope. In the experiment a subsonic dense atomic beam ready for evaporative cooling has been created.
The dense subsonic beam is to be cooled to Bose-Einstein condensation. However, there are two problems. Direct cooling on a beam is not as effective as cooling atoms in a trap. Second, thermal conductivity by high energetic atoms spiralling the atomic beam produces an unavoidable heating of already cooled atoms. In **chapter six** the difference in trap configurations for evaporative cooling is described. The critical number of collision for BEC is investigated for different trap configurations and it is found that in a trap 2 orders of magnitude less collisions are needed than in a guide. After the magnetic barrier a second magnetic coil is placed. These two coils together with the guide act as a three-dimensional trap into which part of the subsonic beam is loaded. In this trap evaporative cooling is preformed, producing the largest rubidium condensate, as far as we know.
In the last chapter **(chapter seven)** the future prospect of the experiment is

described. In principle atoms from the large BEC can be outcoupled to form an atom laser, but this still only leads to a low flux atom laser, with a lifetime determined by the initial size of the BEC. We strive for a continuous high flux atom laser. This can be done by loading the subsonic beam into a conveyor belt and perform evaporative cooling of the packets in the conveyor belt. This leads to very cold packets of atoms that can be merged together again after of the conveyor belt and cooled to BEC with evaporative cooling. This scheme leads to a high flux atom laser.

7.4 Sammenvatting

In 1925 voorspelde Einstein een nieuwe toestand van materie. Einstein was sterk beïnvloed door het statistische werk van Satyendra Nath Bose. Bose werkte aan de statistische eigenschappen van elementaire lichtdeeltjes, fotonen genaamd, en Einstein breidde het werk uit voor atomen. Wanneer de temperatuur verlaagd wordt tot het absolute nulpunt, gaan een bepaald soort atomen, bosonen genaamd, zich "sociaal" gedragen en is het toegestaan, dat ze dezelfde toestand bezetten, namelijk degene met de laagste energie. Dit is sindsdien bekend geworden als Bose-Einstein condensatie. Bij lage temperaturen gedragen de atomen zich als golven in plaats van deeltjes. In het condensaat smelten de atomen samen en vormen één grote golf met één fase en één golflengte.
Een atoomlaser is een coherente bundel van atomen met een welbepaalde fase. De golflengte van ene atoomlaser is veel kleiner dan de golflengte van licht. Een atoomlaser is een apparaat, dat gebruikt kan worden voor hoge-precisie interferometrie en holografische beelden. Alle atoomlasers, die tot dusver ontwikkeld zijn, maken gebruik van het uitkoppelen van gecondenseerde atomen van een bestaande Bose-Einstein condensaat. De flux en levensduur van deze atoomlasers worden beperkt door de oorspronkelijke grootte van het condensaat. Typisch is de levensduur in de orde van 100 milli-seconde. De constructie van een continue hoge-flux atoomlaser is een heilige graal voor atoomfysici. Dit proefschrift beschrijft onze inspanningen voor de constructie van een hoge-flux atoomlaser.

De kinetische energie van een verzameling van atomen is een maat voor de temperatuur, dus door het verlagen van de kinetische energie kan de temperatuur verlaagd worden. De meest effectieve manier voor het verlagen van de kinetische energie van atomen is door Doppler koelen. Als een atoom aangeslagen wordt, dan zal de impuls verlaagd worden gelijk aan de impuls van het foton. Na korte tijd zal het atoom vervallen naar de grondtoestand door spontaan verval, waarbij het foton in een willekeurige richting uitgezonden wordt. Daarbij blijft na vele spontane verval processen gemiddeld de impuls in de richting van de waarnemer onveranderd, zodat in het gehele proces, absorptie gevolgd door spontane emissie, de impuls in de richting van de waarnemer afneemt. Door het veelvuldig herhalen van dit proces, zal de kinetische energie afnemen. Doppler koelen heeft een minimale temperatuur door de willekeurige terugstoot van de uitgezonden fotonen. Om de temperatuur verder te verlagen wordt verdampingskoeling gebruikt. Verdampingskoeling is een traag proces dat lijkt op het koelen van een kop koffie. Door de meest energetische atomen uit de val te verwijderen, kunnen de overgebleven atomen door middel van botsingen ther-

maliseren naar een lagere temperatuur. Het is daarom van groot belang, dat de dichtheid van de atomen en daarmee de botsingssnelheid voldoende hoog zijn.

De experimentele opstelling is beschreven in **Hoofdstuk 2**. Het experiment bestaat uit een rubidium bron, waarmee een bundel van rubidium atomen geproduceerd wordt. De atomen worden vertraagd door een laserbundel, die tegen de richting van de atoombundel ingeschoten wordt. Daarna worden de atomen ingesloten in een web van laserlicht, die de atomen verzamelt en afkoelt. Daarna worden de atomen geschoten in een magnetische geleider van vier meter, die gebruikt wordt als uitlaatstuk voor de atoomlaser. Het gehele experiment word uitgevoerd in metalen ketels, die onder ultra-hoge vacuüm condities gehouden worden. De atomen worden met laserlicht in een korte tijd van enkele milliseconden gekoeld van honderden graden Kelvin naar enkele milli-Kelvins. Voor het produceren van licht hebben we vijf lasers gebouwd: twee voor het vertragen van de atomen, twee voor het koelen van de atomen en één voor het detecteren van de dichtheid van de atomen. Alle lasers hebben een golflengte van 780 nm, de resonantie golflengte voor de rubidium atomen. In de opstelling produceren we 10^{10} ultra-koude atomen in 80 milli-seconde: een bijzonder groot aantal.

De lanceer-procedure is beschreven in **Hoofdstuk 3**. Het grote aantal ultra-koude atomen, zoals beschreven in het vorige hoofdstuk, worden verplaats naar de magnetische geleider. De lasers, die eerst gebruikt werden voor het afkoelen van de atomen, worden nu gebruikt om de atomen in de geleider te duwen. De magnetische geleider van vier meter sluit de atomen op in de transversale richting, maar laat de atomen vrijelijk bewegen in de axiale richting. Na een periode van 166 milli-seconde wordt er weer een nieuw pakket ultra-koude atomen in de geleider geschoten, en na 50 centimeter in de geleider vormen de pakketten een aaneengesloten bundel. De snelheid van de bundel is groter dan de geluidssnelheid en we noemen de bundel daardoor supersoon. Helaas is de dichtheid van de atomen in de bundel onvoldoende om verdampingskoeling toe te passen. Door de bundel te vertragen tot subsone snelheden, waarbij de bundelsnelheid onder de geluidssnelheid komt te liggen, zal de dichtheid van de atomen toenemen. De bundelsnelheid wordt verlaagd door de bundel aan het eind van de geleider op een magnetische barrière te laten reflecteren en te laten botsen met de inkomende bundel. Door de vele botsingen ontstaat er een schokgolf, waardoor atomen met subsone snelheden geproduceerd worden.

Het theoretische begrip van het ontstaan van een schokgolf is beschreven in **Hoofdstuk 4**. Beschouw voor het gemak een hoge drukspuit, die gebruikt wordt om de tegels in de tuin schoon te maken. Richt de spuit op een gat tussen de tegels. Als de waterstraal met hoge druk de bodem van het gat bereikt, dan loopt het water niet over de rand van het gat: het water blijft achter. Dit komt omdat de water moleculen met elkaar botsen en na de botsing is de snelheid van het water molecuul verlaagd. Het water blijft in het gat staan en vormt een water spiegel. Het water van de waterstraal dat de water spiegel raakt wordt vertraagd en dit laat het waterpeil stijgen. Dit is de manier waarop de schokgolf werkt voor de supersone bundel in ons experiment, ook al staat onze geleider vlak. De schokgolf heeft een extra voordeel: de enige manier waarop een supersone bundel subsoon kan worden is door middel van een sterke toename in de dichtheid van de atomen. Dit hydrodynamische fenomeen is waar we gebruik

van maken voor het construeren van een dichte, atomaire bundel. De dichte, subsone bundel heeft een interne botsingssnelheid, die voldoende hoog is voor effectieve verdampingskoeling. Door het toepassen van de schokgolf kunnen we gebruik maken van nog een ander fenomeen: compressie door middel van de zwaartekracht. Onze theorie laat zien, dat als de geleider omlaag gekanteld is, dan neemt de dichtheid aan het eind van de geleider toe door het gewicht van de atomen, die zich daarboven bevinden.

Het experimentele bewijs van een schokgolf in onze opstelling is geleverd in **Hoofdstuk 5**. Op drie meter van de ingang van de geleider is een ondoordringbare barrière gecreëerd door een magnetische spoel. De supersonische bundel reflecteert aan deze barrière en botst met de inkomende bundel en dit veroorzaakt de schokgolf. De verandering van de bundelsnelheid wordt direct waargenomen door de flux van de atomen op een specifiek punt in de geleider waar te nemen. Tegelijkertijd kunnen we de schokgolf waarnemen, die van het eind van de geleider zich verplaatst naar het begin van de geleider. Verder kunnen we waarnemen dat de schokgolf breder wordt naarmate de inkomende flux lager wordt. Door het naar beneden kantelen van de geleider hebben we waargenomen, dat de dichtheid van de atomen aan het eind van de geleider sterk toeneemt. Hierdoor hebben we in het experiment een dichte, subsone atomaire bundel geproduceerd, die geschikt is voor verdampingskoeling.

We hebben daarmee een subsone bundel verkregen, die we verder kunnen afkoelen naar temperaturen, waarbij Bose-Einstein condensatie optreedt. Er blijven echter twee problemen over. Ten eerste is het verdampen van een bundel atomen niet zo effectief als het verdampen van atomen in een val. Ten tweede is de thermische geleiding in een subsone bundel sterk vergroot ten gevolge van atomen, die om de bundel heen spiraliseren. In **Hoofdstuk 6** is de invloed beschreven, die de vorm van een val heeft op het verdampingskoelen. Het kritieke aantal botsingen voor Bose-Einstein condensatie is bestudeerd en we vinden, dat voor een drie-dimensionale val 100 keer minder botsingen nodig zijn dan voor een twee-dimensionale geleider. Na de magnetische barrière is een tweede spoel geplaatst en tussen de twee spoelen ontstaat een drie-dimensionale val, waar een deel van de subsone bundel geladen kan worden. In deze val is verdampingskoeling uitgevoerd, waarbij het grootste rubidium condensaat van de wereld geproduceerd is, voor zover wij weten.

In het laatste hoofstuk (**Hoofdstuk 7**) is de toekomst van het experiment besproken. In principe kunnen we van het grote condensaat atomen uitkoppelen om een gepulste atoom laser te maken, maar dit zal leiden tot een lage flux atoomlaser met een levensduur, die beperkt wordt door de grootte van het condensaat. We willen echter een continue, hoge flux atoomlaser. Dit kunnen we bereiken door de subsone bundel te laden in een transportband voor koude atomen en de atomen op de transportband verder te koelen door verdamping. Dit leidt dan tot pakketjes van atomen die zeer koud zijn, die na de transportband samengevoegd kunnen worden en uiteindelijk verder gekoeld kunnen worden naar Bose-Einstein condensatie door verdampingskoeling. Een dergelijk schema leidt tot een continue, hoge flux atoomlaser.

Bibliography

[1] M.-O. Mewes, M. R. Andrews, D. M. Kurn, D. S. Durfee, C. G. Townsend, and W. Ketterle. Output coupler for bose-einstein condensed atoms. *Phys. Rev. Lett.*, 78:582–585, Jan 1997.

[2] Immanuel Bloch, Theodor W. Hänsch, and Tilman Esslinger. Atom laser with a cw output coupler. *Phys. Rev. Lett.*, 82:3008–3011, Apr 1999.

[3] W. Guerin, J.-F. Riou, J. P. Gaebler, V. Josse, P. Bouyer, and A. Aspect. Guided quasicontinuous atom laser. *Phys. Rev. Lett.*, 97(20):200402, Nov 2006.

[4] A. Bernard, W. Guerin, J. Billy, F. Jendrzejewski, P. Cheinet, A. Aspect, V. Josse, and P. Bouyer. Quasi-continuous horizontally guided atom laser: coupling spectrum and flux limits. *New Journal of Physics*, 13(6), June 2011.

[5] J. E. Debs, P. A. Altin, T. H. Barter, D. Döring, G. R. Dennis, G. McDonald, R. P. Anderson, N. P. Robins, and J. D. Close. Comparing thermal and lasing atomic sources for precision inertial measurement. *ArXiv e-prints*, November 2010.

[6] C. F. Roos, P. Cren, T. Lahaye, J. Dalibard, and D. Guéry-Odelin. Injection of a cold atomic beam into a magnetic guide. *ArXiv Condensed Matter e-prints*, December 2002.

[7] G. Reinaudi, Z. Wang, A. Couvert, T. Lahaye, and D. Guéry-Odelin. A moving magnetic mirror to slow down a bunch of atoms. *European Physical Journal D*, 40:405–410, December 2006.

[8] H.Metcalf and P. van der Straten. *Laser cooling and trapping*. Springer, 1999.

[9] C. Slowe, L. Vernac, and L. V. Hau. High flux source of cold rubidium atoms. *Review of Scientific Instruments*, 76(10):103101, October 2005.

[10] A. Marchant, S Haendel, T. Wiles, S. Hopkins, and S. Cornish. Guided transport of ultracold gases of rubidium up to a room-temperature dielectric surface. *ArXiv e-prints*, August 2011.

[11] Daniel A. Steck. Rubidium 87 d line data. 2003.

[12] Dorthe Madsen. *Experimental sutdies of cold Magnesium atoms.* PhD thesis, Niels Bohr Instituet, 2001.

[13] C. Pethick and H. Smith. *Bose-Einstein condensation in dilute gases.* Cambridge University Press, 2002.

[14] Erik van Oijen. *Realization and Illumination of Bose-condensed Sodium Atoms.* PhD thesis, Utrecht University, 2005.

[15] E.W. Streed, A. P. Chikkatur, T.L. Gustavson, M. Boyd, Y. Torii, D. Schneble, G.K. Campbell, D.E. Pritchard, and W. Ketterle. Large atom number bose-einstein condensate machines. *Review of Scientific Instruments*, 77:023106, 2006.

[16] Xi Chen and J. G. Muga. Transient energy excitation in shortcuts to adiabaticity for the time-dependent harmonic oscillator. *Phys. Rev. A*, 82(5):053403, Nov 2010.

[17] P. W. H. Pinkse, A. Mosk, M. Weidemüller, M. W. Reynolds, T. W. Hijmans, and J. T. M. Walraven. Adiabatically changing the phase-space density of a trapped bose gas. *Phys. Rev. Lett.*, 78(6):990–993, Feb 1997.

[18] J. M. Vogels, T. Lahaye, C. Roos, J. Dalibard, and D. Guéry-Odelin. How to reach the collisional regime on a magnetically guided atomic beam. *J. Phys. IV France*, 116:259–264, 2004.

[19] Koen van Aken. Observation of a shockwave in ultra cold guided atoms using zeeman imaging. Master's thesis, Utrecht University, 2010.

[20] Robert Meppelink. *Hydrodynamic excitations in a Bose-Einstein condensate.* PhD thesis, Utrecht University, 2009.

[21] Pieter Bons. Characteristics of a shockwave in a thermal cloud of ultra cold atoms trapped in a magnetic guide. Master's thesis, Utrecht University, 2010.

[22] P. van der Straten and J.M. Vogels. Hydrodynamic damping in the transverse collisionless limit. *Submitted to Phys. Rev. Lett.*, 2011.

[23] Rob van Rooij. Heat conduction in an ultra-cold quantum gas. Master's thesis, Utrecht University, 2007.

[24] J.M. Vogels J. van de Groep, P. van der Straten. The rate of runaway evaporative cooling. *Phys. Rev. A (accepted)*, 2011.

[25] S. L. Rolston and W. D. Phillips. Nonlinear and quantum atom optics. *Nature*, 416:219–224, 2002.

[26] S. A. Diddams, J. C. Bergquist, S. R. Jefferts, and C. W. Oates. Standards of time and frequency at the outset of the 21st century. *Science*, 306:1318 – 1324, 2004.

[27] Hendrick L. Bethlem and Wim Ubachs. Testing the time-invariance of fundamental constants using microwave spectroscopy on cold diatomic radicals. *Faraday Discuss.*, 142:25 – 36, 2009.

[28] J. B. Fixler, G. T. Foster, J. M. McGuirk, and M. A. Kasevich. Atom interferometer measurement of the newtonian constant of gravity. *Science*, 315(5808):74–77, 2007.

[29] B. E. Sauer M. R. Tarbutt, J. J. Hudson and E. A. Hinds. Prospects for measuring the electric dipole moment of the electron using electrically trapped polar molecules. *Faraday Discuss.*, 142:37 – 56, 2009.

[30] K. S. Johnson, J. H. Thywissen, N. H. Dekker, K. K. Berggren, A. P. Chu, R. Younkin, and M. Prentiss. Localization of Metastable Atom Beams with Optical Standing Waves: Nanolithography at the Heisenberg Limit. *Science*, 280(5369):1583–1586, 1998.

[31] B. P. Anderson and M. A. Kasevich. Macroscopic quantum interference from atomic tunnel arrays. *Science*, 282(5394):1686–1689, 1998.

[32] E. W. Hagley, L. Deng, M. Kozuma, J. Wen, K. Helmerson, S. L. Rolston, and W. D. Phillips. A well-collimated quasi-continuous atom laser. *Science*, 283(5408):1706–1709, 1999.

[33] A. P. Chikkatur, Y. Shin, A. E. Leanhardt, D. Kielpinski, E. Tsikata, T. L. Gustavson, D. E. Pritchard, and W. Ketterle. A continuous source of bose-einstein condensed atoms. *Science*, 296(5576):2193–2195, 2002.

[34] Nicholas P. Robins, Cristina Figl, Matthew Jeppesen, Graham R. Dennis, and John D. Close. A pumped atom laser. *Nature Physics*, 4:731–736, 2008.

[35] E. Mandonnet, A. Minguzi, R. Dum, I. Carusotto, Y. Castin, and J. Dalibard. Evaporative cooling of an atomic beam. *EUR.PHYS.J.D*, 10:9, 2000.

[36] T. Lahaye, J. M. Vogels, K. J. Günter, Z. Wang, J. Dalibard, and D. Guéry-Odelin. Realization of a magnetically guided atomic beam in the collisional regime. *Phys. Rev. Lett.*, 93(9):093003, Aug 2004.

[37] Spencer E. Olson, Rahul R. Mhaskar, and Georg Raithel. Continuous propagation and energy filtering of a cold atomic beam in a long high-gradient magnetic atom guide. *Phys. Rev. A*, 73(3):033622, Mar 2006.

[38] A. Aghajani-Talesh, M. Falkenau, V. V. Volchkov, L. E. Trafford, T. Pfau, and A. Griesmaier. Laser cooling of a magnetically guided ultracold atom beam. *New J. Phys.*, 12:065018, 2010.

[39] T. Lahaye, Z. Wang, G. Reinaudi, S. P. Rath, J. Dalibard, and D. Guéry-Odelin. Evaporative cooling of a guided rubidium atomic beam. *Phys. Rev. A*, 72(3):033411, Sep 2005.

[40] M. A. Hoefer, M. J. Ablowitz, I. Coddington, E. A. Cornell, P. Engels, and V. Schweikhard. Dispersive and classical shock waves in bose-einstein condensates and gas dynamics. *Phys. Rev. A*, 74(2):023623, Aug 2006.

[41] R. Meppelink, S. B. Koller, J. M. Vogels, P. van der Straten, E. D. van Ooijen, N. R. Heckenberg, H. Rubinsztein-Dunlop, S. A. Haine, and M. J. Davis. Observation of shock waves in a large bose-einstein condensate. *Phys. Rev. A*, 80(4):043606, Oct 2009.

[42] C.F. Roos, P. Cren, D. Guéry-Odelin, and J. Dalibard. Continuous loading of a non-dissipative atom trap. *Europhys. Lett.*, 61:187, 2003.

[43] V. S. Bagnato, G. P. Lafyatis, A. G. Martin, E. L. Raab, R. N. Ahmad-Bitar, and D. E. Pritchard. Continuous stopping and trapping of neutral atoms. *Phys. Rev. Lett.*, 58(21):2194–2197, May 1987.

[44] J. Stuhler, P. O. Schmidt, S. Hensler, J. Werner, J. Mlynek, and T. Pfau. Continuous loading of a magnetic trap. *Phys. Rev. A*, 64(3):031405, Aug 2001.

[45] R. Meppelink, R. van Rooij, J. M. Vogels, and P. van der Straten. Enhanced heat flow in the hydrodynamic collisionless regime. *Physical Review Letters*, 103, 2009.

[46] T. Lahaye, G. Reinaudi, Z. Wang, A. Couvert, and D. Guéry-Odelin. Transport of atom packets in a train of ioffe-pritchard traps. *Physical Review A*, 74:033622, 2006.

[47] K. M. R. van der Stam, E. D. van Ooijen, R. Meppelink, J. M. Vogels, and P. van der Straten. Large atom number bose-einstein condensate of sodium. *Rev. Sci. Instrum.*, 78:013102, 2007.

[48] W. G. Unruh. Experimental black-hole evaporation? *Phys. Rev. Lett.*, 46(21):1351–1353, May 1981.

[49] M. Uhlmann, Y. Xu, and R. Schtzhold. Aspects of cosmic inflation in expanding bose-einstein condensates. *New Journal of Physics*, 7(1):248, 2005.

[50] U. Leonhardt, T. Kiss, and P. hberg. Bogoliubov theory of the hawking effect in boseeinstein condensates. *Journal of Optics B: Quantum and Semiclassical Optics*, 5(2):S42, 2003.

[51] Steven Corley and Ted Jacobson. Black hole lasers. *Phys. Rev. D*, 59(12):124011, May 1999.

[52] C. V. Nielsen, J. K. Lyngsø, A. Thorseth, M. Galouzis, K. T. Therkildsen, E. D. van Ooijen, and J. W. Thomsen. Characterization of a magnetic trap by polarization dependent zeeman spectroscopy. *European Physical Journal D. Atomic, Molecular and Optical Physics*, 48(1):111–119, 2008.

[53] Thierry Lahaye and David Guéry-Odelin. Kinetics of the evaporative cooling of an atomic beam. *Phys. Rev. A*, 73(6):063622, Jun 2006.

[54] W. Ketterle and N.J. van Druten. Evaporative cooling of trapped atoms. *Adv. Atom. Mol. Opt. Phys.*, 37:181–236, 1996.

[55] Nicholas R. Thomas, Niels Kjærgaard, Paul S. Julienne, and Andrew C. Wilson. Imaging of s and d partial-wave interference in quantum scattering of identical bosonic atoms. *Phys. Rev. Lett.*, 93(17):173201, Oct 2004.

[56] Ch. Buggle, J. Léonard, W. von Klitzing, and J. T. M. Walraven. Interferometric determination of the s and d-wave scattering amplitudes in ^{87}rb. *Phys. Rev. Lett.*, 93(17):173202, Oct 2004.

[57] T. Lahaye and D. Guéry-Odelin. Discrete-step evaporation of an atomic beam. *European Physical Journal D*, 33:67–75, April 2005.

[58] E. Mandonnet, A. Minguzzi, R. Dum, I. Carusotto, Y.Castin, and J. Dalibard. Evaporative cooling of an atomic beam. *The European Physical Journal D. 10, p.9-18*, 2000.

[59] O. J. Luiten, M. W. Reynolds, and J. T. M. Walraven. Kinetic theory of the evaporative cooling of a trapped gas. *Phys. Rev. A*, 53(1):381–389, Jan 1996.

[60] R. G. Scott, T. E. Judd, and T. M. Fromhold. Exploiting soliton decay and phase fluctuations in atom chip interferometry of bose-einstein condensates. *Phys. Rev. Lett.*, 100(10):100402, Mar 2008.

[61] C. N. Weiler, T. W. Neely, D. R. Scherer, A. S. Bradley, M. J. Davis, and B. P. Anderson. Spontaneous vortices in the formation of bose-einstein condensates. 455:948–951, October 2008.

[62] U. Leonhardt and T. G. Philbin. Black Hole Lasers Revisited. *ArXiv e-prints*, March 2008.

Louise Kindt

Academic interest

Both during my master of science degree and my Ph.D degree I primarily worked as an experimental physicist. In my masters I started on an already existing experiment of which I redeveloped. I gained a large expertise in building an experiment and data analyzing. In my Ph.D degree I build an atom laser experiment up from the ground. I started with an empty lab and three years later I had my first "new physics" measurement. The experience of building something up from the ground and making it work has been ecstatic. My machine made new physics within the field of ultra cold atom physics. I made the largest known Bose-Einstein-condensate in Rubidium and a shock wave in a 4 meter long thermal cloud.

Education

2007–2011	**Ph.D thesis**, *Utrecht University*, Utrecht, Netherland.
2004–2006	**Master thesis**, *Niels Bohr Institute*, Copenhagen, Denmark.
Summer 2004	**Experimental work**, *Graz University of Technology*, Gratz, Austria.
Spring 2003	**Undergraduate project**, *Niels Bohr Institute*, Copenhagen, Denmark.

Ph.D thesis

title	*Shock wave loading in a magnetic guide*
supervisors	Dr. ir. Johnny M.Volges and Professor Peter van der Straten
description	Building a continues source of BEC.

Master thesis

title	*Ultra cold magnesium 25 atoms*
supervisors	Associate Professor Jan Thomsen
description	Experimental investigation of the possibility for sub-Doppler cooling on magnesium 25 at the Copenhagen magnesium setup.

Experimental work

title	*Helium scanning microscope*
supervisors	Professor Bodil Holst
description	Investigation of flow through membranes

Bachelor thesis

title	*Photometry of Gamma Ray Bursts*
supervisors	Professor Jens Hjort
description	Participated of the investigation of GRB030329, which was the burst that proved that GRB's and supernova's are connected.

Conferences

Oudkerkhof 19A – 3512GH Utrecht, Netherland
+31(0)6 33 87 30 94 • ✉ *louise.kindt@gmail.com* • *Danish*

2007-2011	Presentation of Ph.D project at various international conferences through both presentations and poster.
Feb. 2006	Road trip across USA visiting ultra cold atom physics groups and presenting my master thesis
2-3-2005	Poster at DFS annual meeting
title	"New two photon cooling scheme on 24Mg and sub-Doppler cooling of 25Mg"
20-4-2004	Poster at the CAUAC network meeting, Pourquerolle, Nice
title	"Study of two level atom dynamics by release and recapture experiments"

Social activities

2000-2006	Producer of the Physics cabaret
	Annual cabaret of sketches, music and lots of laughter. I was the woman making sure that it was possible.
2001-2004	First year tutor

Teaching

2007-2011	Supervisor of 8 bachelor projects and 2 master projects
2006	Teaching assistant in the course "Introduction to atomic physics"
2003-2006	Teacher at Kopernikursus, the only physics summer school for Danish high school student.

Languages

Danish	Native Language
English	Fluent
Dutch	Spoken

Computer skills

Platforms	Linux, Windows
Languages	MatLab
Scientific	Mathematica, Origin, Igor, Corel, Microsoft Office
Makeup Languages	HTML and LaTeX.

Interests

I find that playing music and cooking is a nice way of concentrating on something else. I play the accordion on a entertaining level and ring with church bells. I can make the most delicious, light pasta and the juiciest steak. On top of that I swim and have a keen interest in photography.

Oudkerkhof 19A – 3512GH Utrecht, Netherland
+31(0)6 33 87 30 94 • ✉ *louise.kindt@gmail.com* • *Danish*